SOME MEASUREMENTS

IN

SYNTHETIC TURBULENT BOUNDARY LAYERS

Thesis by

Ömer Savaş

In Partial Fulfillment of the Requirements

for the Degree of

Doctor of Philosophy

California Institute of Technology

Pasadena, California

1979

(Submitted May 21, 1979)

PERSONAL ACKNOWLEDGEMENTS

Many have contributed.

My advisor, Prof. Donald Coles, has been the prime mover.

Central Engineering Services personnel, Aero Shop personnel, Aero Services personnel, Kathy Franson, Marcia Clark, the Inmates, and GALCIT will be vividly remembered.

I thank all.

I am very grateful to my mentors and protectors,

Coles and Liepmann.

ACKNOWLEDGEMENTS

The research described in this thesis was supported by the National Science Foundation under Grants ENG 75-03694 and ENG 77-23541. During the period from September, 1974 to September, 1978, the author was the recipient of a NATO Fellowship through the Scientific and Technical Research Council of Turkey.

ABSTRACT

Synthetic turbulent boundary layers were constructed on a flat plate by generating systematic moving patterns of turbulent spots in a laminar flow. The experiments were carried out in a wind tunnel at a Reynolds number based on plate length of 1.7×10^6. Spots were generated periodically in space and time near the leading edge to form a regular hexagonal pattern. The disturbance mechanism was a camshaft which displaced small pins momentarily into the laminar flow at frequencies up to 80 Hz. The main instrumentation was a rake of 24 hot wires placed across the flow in a line parallel to the surface. The main measured variable was local intermittency; i.e., the probability of observing turbulent flow at a particular point in space and time. The results are reported in numerous x-t diagrams showing the evolution of various synthetic flows along the plate. The celerity or phase velocity of the large eddies was found to be 0.88, independent of eddy scale. All patterns with sufficiently small scales eventually showed loss of coherence as they moved downstream. A novel phenomenon called eddy transposition was observed in several flows which contained appreciable laminar regions. The large eddies shifted in formation to new positions, intermediate to their original ones, while preserving their hexagonal pattern. The present results, together with some empirical properties of a turbulent spot, were used to estimate the best choice of scales for constructing a synthetic boundary layer suitable for detailed study. The values recommended are: spanwise period/thickness ≈ 3.2, streamwise period/thickness ≈ 11.

TABLE OF CONTENTS

LIST OF SYMBOLS

c	celerity of coherent structures in boundary layer; dx/dt at constant phase
Cp	pressure coefficient, $(p-p_{ref})/q_\infty$
f	frequency of disturbance cycle (Hz)
N	divisor for 2 MHz clock signal, set by thumbwheel switches on preset counter
p	pressure
P	dimensionless pressure difference Δp for surface tube (defined on p. 9 of text)
p_{ref}	reference pressure used in claculation of Cp; taken from pitot-static probe for Figure 4, from plate surface for Figures 28 and 29
q_∞	local dynamic pressure, $\frac{1}{2}\rho u_\infty^2$
Re_x	streamwise Reynolds number, Ux/ν
U	nominal tunnel velocity (1000 cm/s)
u_∞	local free-stream velocity (1013 cm/s)
x	streamwise coordinate, measured from plate leading edge at upstream end of test section (cm)
y	normal coordinate, measured from plate surface (cm)
z	spanwise coordinate, measured from plate centerline (cm)
α	polar angle centered at leading edge of flow shield (degrees) (see Figure 2)
γ	intermittency (0 or 1); $\langle\gamma\rangle$ is probability of turbulent flow
δ	boundary layer thickness (cm)
Δ	value of y corresponding to standard intermittency; taken as distance of hot-wire rake from plate surface (cm)
δ^*	boundary layer displacement thickness, $\int_0^\infty (1-\frac{u}{u_\infty})\,dy$
ζ	spanwise period of disturbance pattern (cm)

ν	kinematic viscosity (0.161 cm^2/s at 27^oC and 74.3 cm Hg)
ρ	density ($1.19 \times 10^{-3} gr/cm^3$)
τ	temporal period of disturbance pattern (s)
$< >$	ensemble average

I INTRODUCTION

The contemporary view of turbulent fluid motion is that turbulent shear flows are not as random as was once thought, but contain organized eddy structures which represent characteristic concentrations of vorticity at the largest scale of the flow. In any attempt to find and study such coherent motions in the turbulent boundary layer, it is a serious difficulty that the eddies occur in various stages of development at random places and times. Presumably the eddies have a typical signature in terms (say) of surface pressure, surface friction, local turbulent intensity, interface geometry, large-scale vorticity, and the like. However, this signature cannot be determined until the eddy has been found, and the eddy cannot readily be found unless its signature is known.

Another difficulty is that many measurements of structure in boundary layers have been made using single fixed probes. Such measurements are not well suited for describing the properties of an irregular pattern of three-dimensional large eddies being convected past the probe, because no information is available about the lateral position of these eddies. Hence their properties cannot be sharply defined.

As a possible means for bypassing these difficulties, Coles and Barker (1975) proposed the concept of a synthetic turbulent boundary layer and made a few preliminary measurements in one such flow. Their point of departure was the fact that transition from laminar to turbulent flow in a boundary layer is characterized by the appearance

of turbulent spots. The turbulent spot, first discovered by Emmons (1951) and first documented experimentally by Schubauer and Klebanoff (1955), is an arrowhead-shaped region of turbulence which appears in a laminar boundary layer (when there is a suitable natural or artificial disturbance) and moves downstream, growing in size nearly linearly in all directions. The spot has been identified as essentially a large horseshoe vortex by the work of Coles and Barker (1975), Wygnanski, Sokolov, and Friedman (1976), and Cantwell, Coles and Dimotakis (1978). Consequently, in the context of the coherent-structure formulation, the spot suggests itself as a possible prototype large eddy for the turbulent boundary layer. Cantwell et al. end by viewing the spot not as a prototype large eddy, but as an alternative flow to the boundary layer, primarily because of the eventual discrepancy in scale. Nevertheless, they expect the isolated spot to have important structural features in common with characteristic large-scale vorticity concentrations in the turbulent boundary layer. Zilberman, Wygnanski, and Kaplan (1977) and Haritonidis, Kaplan, and Wygnanski (1977) have recently followed an artificially generated spot into a turbulent boundary layer for very large distances. They find that the growth of the spot is severely inhibited in the streamwise and spanwise directions, but not in the normal direction. The characteristic celerity of the spot in the boundary layer is found to be about $0.9u_\infty$. On the basis of these experiments, Wygnanski (1978) refers to the turbulent spot as an orderly structure which may be viewed as the basic module for the turbulent boundary layer.

The first major investigation of outer structure in the turbulent boundary layer was carried out by Kovasznay, Kibens, and Blackwelder (1970) and by Blackwelder and Kovasznay (1972). Their results of greatest interest for the present research include space-time correlations which suggest a celerity of $0.93\,u_\infty$ for the outer turbulent regions. There is strong persistence of the large eddies over distances $\Delta x/\delta$ of 15 or more. A set of correlation maps in (z,t) have zero-correlation contours indicating a streamwise scale $u_\infty \Delta t/\delta$ of about 2.5 and a spanwise scale $\Delta z/\delta$ of about 1.2 for the typical large eddy at the half-intermittency level. Later triple-correlation measurements by Fulachier, Arzoumanian, and Dumas (1977), using heat as a passive contaminant, support these estimates of scale. Blackwelder and Kovasznay (1972) infer a qualitative picture of the mean motion in a moving reference frame which shows large-scale rotation in the same sense as the general vorticity in the flow. These authors approach, but do not quite reach, the conclusion that the large-scale mean motion is a transverse vortex. Praturi and Brodkey (1978), using a combination of dye and tracer particles and a moving camera for flow visualization, frequently observe large, persistent transverse vortices, but do not observe the swept-back structure which would be characteristic of the main vortex in a turbulent spot. Finally, Brown and Thomas (1977) find that the active region at the rear of a large eddy is oriented at an angle of about 18 degrees to the wall and terminates at the wall in a zone where both friction and fluctuations in friction are larger than the average. The scale of the

large eddy is estimated to be about 2δ.

The experiment carried out by Coles and Barker (1975) was to generate a regular hexagonal pattern of turbulent spots in the laminar boundary layer near the leading edge of a flat plate and to sample the flow farther downstream at times locked to the phase of the disturbance generator. They found that periodicity in space and time persisted downstream, and that the average velocity profile was close to that which would be expected in a natural turbulent boundary layer at the same Reynolds number. Figure 1 (courtesy of D. Coles) shows a photograph of a single spot in water, using surface dye for flow visualization, together with a photograph of a synthetic turbulent boundary layer under the same conditions in the same channel.

The present research continues the work begun by Coles and Barker. Their measurements were made in water, using momentary jets to create the turbulent spots and using a single-channel laser-Doppler velocimeter as main instrumentation. Because of insufficient width for the channel and insufficient flow rate for the pump, the Reynolds number was relatively low, and the useful region of the plate surface was severely limited by transverse contamination from the side walls. There was also a substantial acceleration of the free stream along the plate.

The present experiments were carried out under conditions which avoid these problems, particularly the problem of transverse contamination. The main difference is that the present measurements were made in a wind tunnel, requiring a shift to the hot-wire anemometer as main instrumentation, and requiring also a shift to a disturbance

mechanism capable of operating at much higher frequencies. A relatively large range of scales in space and time is explored, in an attempt to determine which patterns are most comfortable at certain stations in the flow. A few measurements are also reported for the turbulent spot, for completeness and to connect the present study with earlier work on transition. The emphasis is on pattern and scale, as revealed by measurements of intermittency in the outer part of the layer. Except for some preliminary work with surface pressure, there are as yet no measurements of velocity, surface stress, turbulence intensity, or other variables involved in the problem of signatures and eventually in the problem of dynamics. The task of the present exploratory research is to define one or more synthetic flows which are best in some sense, and detailed measurements are not required for this purpose.

II MODEL AND INSTRUMENTATION

2.1 Wind Tunnel

The experiments were carried out in the Merrill wind tunnel at GALCIT (Graduate Aeronautical Laboratories, California Institute of Technology). The test section is 265 cm long. The width increases from 114.5 cm at the entrance to 117.4 cm at the exit, and the height increases from 81.6 cm to 82.8 cm. The contraction ratio is 9:1. The tunnel is of closed-circuit type, with a vent to atmosphere around the entire perimeter at the exit of the test section. Two screens are provided, but no honeycomb. A 75-Hp 1200-rpm synchronous electric motor drives a three-bladed variable-pitch propellor. Rotation is removed by an eight-bladed stator. With the present model installed, free stream speeds up to 50 m/s could be achieved for short periods. However, there is no provision for cooling, and the experiments were conducted at 10 m/s to avoid overheating as well as to obtain a maximum region of laminar flow. For continuous operation at this speed, the temperature increased at a rate of about 3.5° C per hour.

In several recent experiments carried out in the Merrill tunnel, vibration of the tunnel structure has sometimes been a problem. Before the present experiments were begun, therefore, an existing structural connection between the test-section frame and the diffuser was cut, and the test-section frame was braced to the building. The model supports were also located so that low-order vibration modes of the flat-plate model would be inhibited.

The tunnel was carefully cleaned before the experiments began.

Experience with numerous hot wires was that the life expectancy was at least several hundred hours of tunnel operation.

2.2 Flat-Plate Model

The flat-plate model was made from two sections of aluminum-alloy plate, as shown in Figure 2. The front section is 30.5 cm long, 114.0 cm wide, and 1.9 cm thick. The rear section is 233.7 cm long and 1.27 cm thick; the width increases from 114.0 cm at the joint to 117.2 cm at the trailing edge. Both sections were heat treated to improve dimensional stability during manufacture. The working surface of the assembled model was smoothed and polished.

Two 12.7-cm diameter plugs are provided on the centerline of the plate at $x = 57.8$ cm and $x = 114.9$ cm, and one 20.3-cm diameter plug is provided at $x = 187.3$ cm. These plugs are intended for eventual installation of surface instrumentation.

The leading edge of the plate is a 10:1 ellipse, chosen to prevent large positive pressure gradients which could cause separation and/or premature transition near the leading edge.

The plate was installed in the test section with the working (top) surface approximately 41 cm from the tunnel ceiling. The leading edge was located at the beginning of the test section, which was partitioned by the flat plate model along its entire length. The plate was supported from below by six streamlined struts whose height could be individually adjusted. Narrow gaps between the plate and the side walls of the tunnel were sealed by inflated latex tubing.

Throughout this paper, a right-handed rectangular coordinate

system, oriented as shown in Figure 2, is used. The streamwise coordinate x is measured from the leading edge of the plate; the spanwise coordinate z is measured from the plate centerline; and the normal coordinate y is measured from the plate surface.

2.3 Flow Control

Figure 3 is a photograph of the test section looking downstream. To obtain a good approximation to uniform flow, various flow-control techniques were used. These included:

(1) Six individually adjustable supports capable of bending the plate substantially.

(2) Two extruded-angle metal shields extending from $x = 31$ cm to $x = 275$ cm at $z = \pm 48.3$ cm. These shields were 12.7 cm high and were intended to isolate the flow over the plate from the boundary layers developing on the tunnel side walls. The shields were also used to locate and support the hot-wire rake.

(3) A two-dimensional blister to modify the ceiling contour of the tunnel at the entrance to the test section. The maximum thickness of the blister was about 0.8 cm at $x \approx 20$ cm.

(4) A screen of 20-percent solidity installed across the upper half of the test section at the trailing edge of the plate, just before the peripheral vent. The purpose was to match the pressure loss caused by the presence of the supporting struts and other excrescences under the plate. The test section pressure at a speed of 10 m/s was about 0.08 mm Hg above atmospheric pressure.

Various types of small trailing-edge flaps were also tried for positioning the leading-edge stagnation line, but were abandoned in favor of the screen.

The final pressure distribution over the plate is shown in Figure 4. The pressure coefficient was constant within ±.01 over most of the working surface. These measurements were taken when the hot wire rake was not in the tunnel. Later measurements, also shown in the figure, established that the presence of the rake had no significant upstream effect on the pressure distribution.

2.4 Undisturbed Flow

With no artificial disturbances, the boundary layer on the plate centerline was laminar along the total length of the plate ($Re_x = 1.7 \times 10^6$ at 10 m/s at the trailing edge). The edge-contamination regions emanating from the two boundary layer shields were mapped by surface-tube measurements. The pressure differential Δp between a surface tube (1.65 mm OD x 1.19 mm ID) and a static-pressure tap located 2.5 cm upstream was used to deduce the regime of flow. The difference Δp was made dimensionless in the particular form

$$P \equiv \frac{\rho^{1/2} \nu}{d^2} \cdot \frac{x \, \Delta p}{q_\infty^{3/2}}$$

which is expected to be constant in a laminar (Blasius) boundary layer.

In Figure 5, P is plotted against polar angle (centered at the leading edge of the shields) to demonstrate that the edge contamination regions were growing conically at the accepted angle of about 10 degrees. The edge of the contaminated region is indicated by the

dashed lines in Figure 2 above.

2.5 Disturbance-Generating Mechanism

Disturbance-generating mechanisms used by previous investigators include electrical, fluidic, and mechanical methods. The electrical method (spark) has usually been employed when working in air and the fluidic method (jet) when working in water. The mechanical method has previously been used only for qualitative experiments in water (Elder 1960).

The objectives of the present research required a disturbance generator capable of operating reliably over a range of frequencies from a few Hz to 100 Hz or more. Multiple spark gaps were not considered suitable because of probable severe electrical interference with the data-acquisition system. Fluidic methods were not considered suitable because of unavoidable frequency limitations for solenoid devices. A mechanical method was therefore adopted.

The disturbances were generated by momentarily displacing small cylindrical pins into the laminar boundary layer. Figure 6 shows some geometrical details of the mechanism. The basic element is a nylon pin which is embedded in the front section of the plate. Normally, a compression spring keeps the pin retracted and in contact with a retaining plate, as shown at the left, so that the plate surface is uninterrupted. The pin is displaced into the boundary layer, as shown at the right, by a rotating nylon cam (impregnated with molybdenum disulfide to reduce friction). A beryllium-copper leaf spring between each pin and the associated cam guarantees smooth and non-destructive

contact between the two moving elements and also removes heat generated during operation.

The camshaft is 127 cm long and is mounted on the lower side of the front section of the plate, as shown in Figure 7. It is supported at seven locations in needle bearings. One end of the camshaft is clamped in a ball-bearing assembly to prevent axial motion. The other end extends out of the wind tunnel (through a 2.5-cm diameter hole in the side wall) and is connected to an electric motor by a flexible coupling. The camshaft assembly is shielded from the air flow by a curved shield which extends from side wall to side wall. Cooling air introduced into the camshaft cavity is discharged through the clearance gap around the shaft at the motor end. The life of the cam-pin assembly was found to be critically dependent on the amount of cooling provided.

The cam mechanism has a 1.2-cm diameter steel shaft fitted with six nylon cam sleeves separated by needle bearings. The sleeves were carefully aligned, with an individual four-lobe cam corresponding to each pin in the plate. Any cam lobes which were not wanted were machined off the sleeves. Figure 8 shows the appearance of a cam sleeve before and after final machining. Normally two lobes, 180 degrees apart, were retained at each pin location. Alternate cams along the length of the camshaft were displaced by 90 degrees. Thus, the disturbance generator produced a close-packed hexagonal pattern in a (z, t) plane when the shaft was rotating, as indicated in Figure 9. The period ζ in the z direction was fixed by the cam in use. The

period τ in time was half the period of shaft rotation. For convenience, the temporal frequency f, where $f\tau = 1$, will sometimes be cited instead of the corresponding period τ.

A total of 201 pins are installed in the model at a station 22.9 cm from the leading edge. The pins are spaced 0.508 cm (0.2 in) apart. At several lateral positions, two adjacent pins are omitted to make room for the bearings used to support the camshaft. The minimum uniform pin spacing is therefore 1.524 cm (0.6 in). This spacing can be increased in increments of 0.508 cm (0.2 in) up to the full width of the plate. With a hexagonal disturbance pattern, the minimum spanwise pitch or wave length ζ is therefore 3.048 cm (1.2 in). The three values actually used in the present tests were 6.10, 9.14 and 12.19 cm (2.4, 3.6, and 4.8 in).

Considerable development work was required to settle various details of the cam mechanism. During bench tests, the thickness of the leaf spring and the clearances of the cam-spring-pin geometry were varied, and strobe lighting was used to observe the motion of the various elements. Satisfactory smooth, bounce-free operation on the bench was achieved at pin frequencies up to 200 Hz (6000 rpm for the cam shaft, with two cam lobes 180 degrees apart). A life test was discontinued after about seventy million cycles (270 hours at 70 Hz) when no problems were encountered except for slight wear of the pins and cam lobes.

In the tunnel, one factor limiting maximum speed was heat removal; another was bandwidth and maximum voltage available in the

servo amplifier driving the cam shaft. One failure occurred early in the experiments when high temperature for a few of the leaf springs led to premature fatigue fracture. The leaf thickness was increased from 0.025 cm to 0.038 cm, and a procedure was adopted of running the disturbance generator for the minimum possible time required to achieve lock and record data.

Figure 10 shows typical records of static pin displacement plotted against camshaft angle (measured from the encoder index pulse). There were slight inadvertent variations in cam radius and pin length, amounting to ± 0.005 cm; these variations were sometimes detectable in the data as variations in size and strength of the turbulent spots.

Figure 10 also shows pin position at maximum displacement relative to the estimated (not measured) laminar boundary layer profile at the pin station.

2.6 Cam Drive System

The phase-locked loop servo system built by Cantwell (1975) was modified to drive the camshaft. In the present application, the feedback signal originated at a 200-line optical encoder (Renco Corporation Model KT-23A-200-3D). The inertial load was 11,000 gr-cm^2. At speeds in the range of 120-2400 rpm, the required torque varied between essentially zero and one Newton-meter four times per revolution.

The pulse train from the encoder was divided by 4 before it was fed into the phase-frequency comparator, in order to remain within

the bandwidth of the power amplifier (Control Systems Research, Inc. Model 800 PRA) at all cam-rotation rates, without having to make any adjustments except for loop gain. The command frequency was also divided by 4 before being fed into the camparator. To the instrumentation, therefore, the phase-locked servo system appeared to be running on a 200 lines/revolution encoder.

The cam drive system performed satisfactorily at all running conditions. Some minor gain adjustments were necessary to maintain lock at extreme shaft speeds. It was found that if the system were simply switched on, the servo would hunt for a time before locking to the command pulse train. To avoid possible damage to mechanical components of the system at high speeds, therefore, system gain was first set to zero and then increased to a suitable value, thus allowing smooth locking to the command signal.

2.7 Hot-Wire Rake

Twenty four hot-wire probes (TSI-1276V-T1.0) were mounted in a rake configuration transverse to the flow and parallel to the plate surface. The rake was suspended from a full-span bridge by three struts, as shown in Figure 3 and in a closer view in Figure 11. The rake and struts were made from streamlined brass tubing (0.66 cm chord, 0.33 cm thick). The bridge itself was made from elliptical stainless steel tubing (3.00 cm chord, 0.84 cm thick). The rake was 14.5 cm below the bridge. All electrical wiring except for connections at the probes was contained within the rake, struts and bridge. The probes had no common electrical connection. The entire rake and

bridge structure was filled with epoxy resin (Stycast 1264) for increased stiffness. When the tunnel was running, there was some vibration of the bridge in the vertical direction in the fundamental mode at a frequency of about 11 Hz. The amplitude was not large, and vibration was not a problem during the intermittency measurements in steady flow. However, the transient motion when the tunnel was started was large enough so that it has so far prevented mounting the rake very close to the plate surface.

A slotted end plate at each end of the bridge tied the rake assembly to the two boundary layer shields. Each end plate had a carefully machined horizontal reference plate. These reference plates were used to position the sensors in the flow, as indicated in Figure 12. The vertical distance between the reference plates and the hot wire sensors was known. By stacking shims, the rake could be located at any specified distance from the plate surface up to about 8 cm. After positioning, the slotted end plates were bolted to the shields to secure the bridge. Slots on the end plates provided continuous variability in vertical rake position. Holes in the shields were located 7.62 cm (3.0 in) apart. These holes are sometimes referred to by station number; the relation between station number and the location x of the hot wires in cm is given by

$$x(\text{cm}) = 26.4 + 7.62\,(\text{STA})$$

Six of the available stations (4, 8, 12, 16, 20, 24) were used in the present experiments (see Table I).

Temperature rise during the experiments introduced a slight

uncertainty in the vertical position of the rake. The use of different materials for the plate, the bridge and the filling (aluminum alloy, stainless steel, and epoxy resin, respectively) led to thermal stresses in the bridge structure when the tunnel temperature changed. The extreme vertical displacement of the rake from this cause was estimated to be less than 0.1 cm.

The 24 hot-wire probes were located symmetrically about the plate center and were spaced 0.762 cm (0.3 in) apart. The span of the rake was therefore 17.5 cm (6.9 in). The hot-wire sensors were parallel to the plate surface and hence responded mainly to the streamwise component of velocity. The sensors were 2.5 μm in diameter and about 0.15 cm in length. They were made of platinum-plated tungsten wire and were operated at a constant temperature of 250° C. All of the results reported here have been obtained from the same 24 wires. No wire failure occurred during the experiments, which required several hundred hours of tunnel running time.

2.8 Pressure Instrumentation

The tunnel dynamic head was constantly monitored by a pitot-static probe (United Sensor PDC-12-G-10-KL) mounted from the tunnel ceiling (this probe is visible in Figure 3). The tip of the probe was at $x = 61$ cm, $y = 21$ cm, $z = 0$. The probe was connected to a 100-mm Hg differential electronic manometer (Datametrics Barocel Pressure Sensor 511-11 and Electronic Manometer 1014A). To measure the free-stream velocity near the hot wires, a second pitot-static probe (modified United Sensor PDA-12-F-10-KL) was installed

on the hot-wire rake. This probe was connected to a 10-mm Hg differential electronic manometer (Datametrics Barocel Pressure Sensor 511-10 and Electronic Manometer 1015-S2). The tip of this pitot-static probe was about 8.7 cm above the sensors of the hot-wire probes.

Altogether, 44 surface-pressure taps were provided on the flat plate. Of these, 16 were on the centerline and 14 were on each of the lines $z = \pm 30.5$ cm. Static pressure at these taps was also measured using a 10-mm Hg differential electronic manometer.

2.9 Hot-Wire Anemometers

Twenty four constant-temperature hot-wire anemometer circuits were fabricated for these experiments. The design was based on that of Perry and Morrison (1971). Each circuit included an intermittency meter consisting of a passive bandpass filter, a rectifier, a level detector, and a retriggerable monostable multivibrator, or one-shot. A circuit diagram is shown in Figure 13. Each anemometer with its associated intermittency meter was contained on a single printed-circuit board. In the same enclosure was provided a digital multiplexer for coding of the 24 bits of intermittency data. The multiplexer was interfaced to the data-acquisition system as an input device on channel 22_8. The 24 bits of intermittency information were latched at read time and later transferred to the computer in two 12-bit sections. Two other bits identified the section and the occurrence, once per revolution, of the encoder index pulse.

2.10 Intermittency

Intermittency was the primary measured variable in the present research. Turbulent flow was distinguished from laminar flow in terms of energy content at high frequencies. After some preliminary measurements, the cut-off frequencies of the single-pole RC band-pass filter in Figure 13 were set at 2.7 KHz and 7.0 KHz and were left fixed throughout the course of the experiments. The threshold levels on individual channels varied slightly with differences in the particular wires and components in the units. The pulse lengths of the one-shots were set to 1 ms; no attempt was made to correct the data for the associated time lag at the end of a turbulent region.

Adjustment of the intermittency meters was essentially a subjective process. All twenty-four circuits were tuned in a turbulent boundary layer flow generated by taping the tripping device shown in Figure 14 onto the plate surface at $x \approx 23$ cm (slightly upstream of pins, pins retracted). The trip extended from wall to wall. The rake was placed well downstream at a suitable distance from the plate surface. After considerable adjustment of probe height and circuit parameters, the average intermittency factor seen by the 24 wires at $x = 118$ cm, $y = 2.02$ cm, $U = 10$ m/s was 0.50, with extreme individual readings being 0.48 and 0.53. Figure 15 shows some typical analog outputs from the anemometers under these conditions, together with the associated intermittency signals. The intermittency function was also measured at a few points across the tripped boundary layer, with the result shown in Figure 16. The data seem entirely compatible

with similar curves previously reported in the literature (e.g., Klebanoff 1954).

III DATA PROCESSING

3.1 Solo System

The experiments used the GALCIT mobile computer-controlled data-acquisition system, known as the Solo System. The main system component is an HP-2100 computer having 32K (32, 768) 16-bit words of core memory. As of March, 1979, peripherals include CRT terminal, cartridge disc, phase-encoded magnetic tape transport, line printer, plotter, and analog-to-digital converter. A general-purpose 16-bit digital I/O channel (channel 22_8) is also available. The operating system is the real-time executive RTE-II.

The data system includes a preset counter used as a master clock. The output, called PACER, is a 2-MHz crystal-controlled pulse train which can be divided by any desired integer N set on front-panel switches. By coincidence, the number N had a special significance for the present data. The reason is that the pulse frequency 2, 000, 000/N was again divided by 200 in a 200-line encoder which controlled the phase-lock camshaft drive. Hence the period of the camshaft was N/10, 000 sec. Since the nominal free-stream velocity in the present experiments was 10 m/s or 10, 000 mm/s (actually 10, 130 mm/s, on the average), the number N was for practical purposes the distance in millimeters travelled by the free-stream flow during two cycles of the periodic disturbance pattern, or during one camshaft revolution.

3.2 Timing

The time base for the experiment was the PACER pulse train. The PLL camshaft drive was locked to this pulse train (with both command

and feedback frequencies divided by 4). The motor rotation speed was 10,000/N revolutions/sec, and the pin frequency in the synthetic boundary-layer experiments was 20,000/N Hz. The timing of data acquisition is explained in Figure 17. An index pulse (E) was provided once per revolution by the optical encoder. A stretched copy (I) of this index pulse was generated at the leading edge of the first PACER pulse following the true index pulse. The stretched pulse was 125 μs long and was monitored by the data system as the least significant bit of input 22_8. The data-acquisition program detected the leading edge of the stretched index pulse, cleared the intermittency multiplexer, and initiated data acquisition at the next PACER pulse. "FIRST" and "LAST" on signal trace (C) in Figure 17 indicate the relative positions of the first and last samples of a run.

Intermittency data were recorded as a continuous time series on magnetic tape. One data file was written for each run. Files were numbered in chronological order throughout the experiments. A typical file contains one identification record and 400 data records, each of which corresponds to 5 camshaft revolutions. Data were recorded at each PACER pulse on trace (C) in Figure 17. At each pulse, 5 16-bit words were read into the computer. The first two words were intermittency data on channel 22_8 and were transferred automatically under DMA (direct memory access) control. The first word contained the intermittency bits for wires 1-12, the second for wires 13-24. All 24 intermittency readings were simultaneous, having been previously latched by the clock pulse (C) that commanded the multiplexer. The

remaining three words were three analog signals digitized by the AD converter. The first was a general-purpose signal (used,for example, for surface-pressure measurements) and the other two were the ceiling and rake pitot-static readings. After some processing, a 3020-word record was written on magnetic tape. The first 2000 words were intermittency data; the next 1000 words were the general-purpose signal; and the last 20 words were the two channels of pitot-static data in the form of averages over each of the 10 cycles of the record.

The index pulse was checked by the data system after every 200 samples (every other pin cycle). Absence of the index pulse, presumably due to loss of lock in the camshaft drive, caused the run to be aborted. In effect, a position control was the requirement, not a speed control. A phase-locked servo system was a tailored answer to this requirement.

3.3 Filtering

A filtering operation was applied to the intermittency data before ensemble averages at constant phase were computed. There were two reasons. One was to sharpen the classification of the flow into laminar and turbulent regimes. The other was to provide a means for communication between adjacent wires, which sometimes had slightly different responses in the same flow.

After some experimenting, the filtering method chosen was to center a rectangular window, 3 wires wide and 5 samples long, over each bit of the pattern. If the sum of the 15 bits was 8 or more, the center bit was replaced by a one; if the sum of the 15 bits was 7 or

less, the center bit was replaced by a zero. The data from wires 1 and 24, at the ends of the rake, retained their original values. Because the same 3 x 5 filter window was used for all of the data processing, the effect of filtering was uniform for different probe stations but not for different cam speeds. The time interval corresponding to 5 samples was directly proportional to N, so that the affected frequencies in the signal $\gamma(t)$ varied inversely with N. This non-uniformity is not considered important for the purposes of the present research.

Figure 18 shows short segments of typical intermittency data, before and after filtering, for three flows. These are the turbulent spot (Run 538), the synthetic boundary layer (Run 117), and the natural boundary layer (i.e., a flow tripped by the serrated tape trip shown in Figure 14 above).

The filtered data were ensemble averaged over the 4000 cycles of a file as a 24 x 200 array, covering one camshaft revolution. In principle, the two cycles of a revolution should be identical and could be combined. In practice, however, slight variations in maximum pin displacement were sometimes detectable as variations in peak intermittency within a turbulent region. For this reason, the fundamental period of the experiments was usually taken as one revolution rather than one cycle.

Two characteristic values for overall intermittency were also calculated and can be found listed in Table IV below. One is the global mean intermittency; i.e., the value obtained by averaging over one

revolution and over the number of wires corresponding to one spanwise period of the pin disturbance. This value is usually a little lower than the global mean value chosen during the experiment to set the probe height (the target value was a global mean of 0.40 for N = 800). The reason is that the probe was set with the aid of a quick-look program (IBALL) which did not filter the intermittency data. The second characteristic overall intermittency was the value midway between the largest and smallest values occurring in the filtered 24 x 200 array. This value, called the median value in Table IV, identifies the contour which is shaded to indicate regions of turbulence in Figures 21-23 and 33-63 below. The median was preferable to the mean for this purpose because it did not decrease toward zero in flows with low inherent intermittency, such as the low-frequency spot data of Figure 21.

IV TURBULENT SPOT

4.1 Disturbance Margin

The disturbance mechanism described in Section II was designed on the premise that it could always be made to work by increasing the tunnel speed sufficiently. Higher speed increases the Reynolds number at the disturbance station (i.e., increases the margin with respect to the small-disturbance stability boundary), and also thins the boundary layer, so that the pins seem to be larger and to extend farther into the flow. The normal pin displacement was 0.165 cm, although it could be increased if necessary to 0.2 cm at the cost of a substantial increase in the loads on the cam mechanism.

A test was carried out to determine experimentally the relation between free-stream speed and the probability of generating a spot. One single-lobe cam was used to drive the center pin, which was displaced into the laminar boundary layer every 80 ms (N = 800). A close-up photograph of the pin at maximum displacement is shown in Figure 19. The duty cycle was about 20 percent (cf. Figure 10). The hot wire rake was at x = 148.3 cm, y = 1.57 cm. Figure 20 shows the maximum ensemble-averaged intermittency seen by the rake, the value plotted being typical of data near the center of the spot and the center of the rake. That this value was in fact the probability of generating a spot was checked by an examination of raw intermittency records. All spots were found to be essentially the same size. Only the number of spots seen at the rake was changing. Virtually no spots were generated for speeds less than about 9 m/s. The normal tunnel

speed of 10 m/s is indicated by the arrow in Figure 20; the operating margin for the disturbance generator is small but probably sufficient. Factors which argued strongly for the lowest possible tunnel speed were the lower plate Reynolds number, the lower operating speed for the disturbance-generating mechanism (for a given eddy spacing in the streamwise direction), and the lower heating rate for the tunnel.

4.2 Celerity

Turbulent spots were studied during the present experiments mostly for the purpose of proving the instrumentation. Spots were generated once per camshaft revolution by the center pin of the disturbance-generating mechanism, as in the test just described. Three camshaft speeds were used; N = 1991, 800, and 386; thus spots were produced at intervals of 199.1 ms, 80.0 ms, and 38.6 ms, respectively. Intermittency measurements were made at six equally-spaced downstream stations, with the Reynolds number based on distance from the leading edge varying from 0.36×10^6 to 1.32×10^6. At each station, the rake was first positioned at a distance from the wall such that spots would only occasionally register at the rake (i.e., very small but non-zero maximum intermittency) for N = 800. The rake was then lowered half way to the wall, and intermittency measurements were made at the three cam speeds mentioned.

The results of the spot measurements at half-height are displayed in Figures 21, 22, and 23 for N = 1991, 800, and 386. These figures anticipate and illustrate the problem of presenting measurements of one dependent variable, which is here $\langle\gamma\rangle$ (ensemble-averaged

intermittency) as a function of four independent variables, which are here N, x, z, and t (disturbance period, streamwise distance, spanwise distance, and time, or more properly phase). The synthetic boundary layer also involves the spanwise period, ζ, and if the objective were a more complete study of a single flow, rather than a survey, the quantity y (distance from the wall) would become an additional independent variable.

The main coordinates in each figure define the (x, t) plane. The origin in time is the index pulse, which for these spot measurements very nearly coincides with the point of maximum pin displacement. At each x corresponding to one of the six probe stations, a centered strip of data shows contours of constant ensemble-averaged intermittency $<\gamma>$ in coordinates (z, t); i.e., in coordinates representing a plan view of activity in a narrow strip symmetrical about the plate centerline. These are filtered data, so that the two end wires are not used directly. The effective width of the rake is 16.0 cm (6.3 in). The contour interval in $<\gamma>$ is 0.1. The pattern in each strip is periodic with period $Ut = 2U\tau$, where 2τ is the time required for one camshaft revolution. The figures therefore depict the progress downstream of an average spot. To assist in visualization, the region inside the median contour (see Section 3.3) is shaded for the particular spot which was generated at t = 0 at the pin station. The solid horizontal line and the small circle at the pin station indicate the time during which the flow is disturbed and the moment when the pin is at top dead center.

In Figure 21, at the lowest frequency (N = 1991), the spot shape

is distorted at least at the first two stations, presumably because of the relatively longer time the pin is displaced into the flow. In Figure 23, at the highest frequency (N = 386), the spots interact rapidly in the streamwise direction and soon cease to be recognizable as individual spots. In Figure 22 (N = 800), there is some interaction at the last station, but the behavior of the spot elsewhere is unexceptionable. In particular, the nearly identical intermittency data at the first two stations for N = 800 and N = 386 suggest that the spot shape is no longer dependent on details of the driving disturbance.

The celerities of the leading and trailing edges of the spot in Figure 22 can be determined by measuring the time of arrival and departure of the median contour (usually $\langle\gamma\rangle = 0.5$) at the various rake stations. These times are shown in Figure 24. The growth of the spot is closely linear, at least in the range of x-Reynolds numbers from 0.4 to 1.3 million. The celerities of the leading and trailing edges are $0.82\,u_\infty$ and $0.69\,u_\infty$, respectively.

The virtual origin of the spot in x and t is marked in Figure 24 at $x_o = -30$ cm and $t_o = -63$ ms. Since the distance of the rake from the wall is a measure of spot thickness in the plane of symmetry, a plot of y against x should also admit $x_o = -30$ cm as virtual origin. That this is indeed the case is shown in Figure 25.

The results just obtained support the similarity argument made by Cantwell et al. (1978). To compare the two sets of data directly, it is necessary to consider conical similarity coordinates $\xi = (x-x_o)/u_\infty(t-t_o)$, $\eta = y/u_\infty(t-t_o)$, where from Figure 24 $x_o = -30$ cm

and $t_o = -63$ ms. Figure 26, taken from Cantwell et al., shows the spot cross section inferred by a different method, using ensemble-averaged velocity traces. Provided that turbulent fluctuations define the same boundary, the location of the hot-wire rake can be marked on the figure by the two rays through the origin in the (ξ, η) plane. The upper ray represents the trajectory of the rake at the crest of the spot. The lower ray represents the trajectory of the rake during the intermittency measurements of Figure 22, at half height in the spot. The rake should enter the spot studied by Cantwell et al. at $(\xi, \eta) = (0.83, 0.0064)$ and leave at $(\xi, \eta) = (0.62, 0.0047)$. Now in Figure 25, the straight line is $y/(x-x_o) = 0.0088 = \eta/\xi$. Hence the present measurements have the rake entering the spot at $(\xi, \eta) = (0.82, 0.0072)$ and leaving at $(\xi, \eta) = (0.69, 0.0060)$.

4.3 Pressure Signature

The long-range task of the present research program is first to prove and eventually to exploit the concept of a synthetic turbulent boundary layer by measuring various interesting, useful, and accessible properties of large or coherent eddies in a suitable synthetic layer. So far, one such measurement has been attempted, but only in a preliminary way, and only for the turbulent spot. This is measurement of the pressure signature at the wall in the plane of symmetry of the spot. The low free-stream velocity in the present experiments makes such a measurement an extremely delicate operation which depends critically on the use of ensemble averaging to improve the signal-to-noise ratio. The sensor used was a Pitran

pressure transducer (Stow Laboratories Inc. Model PT-M2M01). The Pitran is a silicon NPN planar transistor whose emitter-base junction is mechanically coupled to a diaphragm. A differential pressure applied to the diaphragm produces a large, reversible change in the gain of the transistor. The sensor was calibrated against a 10-mm Hg differential electronic manometer and found to have a sensitivity (with 2.0 volts bias) of 220 mV/mm Hg.

The signal port of the Pitran was connected to a surface-pressure tap on the plate centerline at $x = 86.4$ cm, $z = 0.0$ cm. The reference port was connected to an off-center surface-pressure tap at $x = 86.4$ cm, $z = 30.5$ cm, where the boundary layer was always laminar even when spots were being generated along the centerline of the plate. The sensor assembly was suspended underneath the plate by a soft helical spring, as shown in Figure 27, and was not shielded against the air flow.

The most difficult step was tuning the sensor to minimize the effect of speed changes and substantial acoustic disturbances in the tunnel. A differential transducer can be considered as two transducers in tandem. In order to measure differential pressure, both transducers must have the same time constant and hence the same phase response. If the sensor is idealized as a large cavity of volume V connected to a tap by thin tubing of length L, the time constant of the unit should be proportional to LV. The sensor was mounted with matched values for L. The volume on the reference side was fixed, but the volume on the signal side could be adjusted using the piston and syringe which are

visible in Figure 27. Final tuning was done with the tunnel running at 10 m/s and the spot generating mechanism turned off. The volume ahead of the diaphragm was adjusted until the sensor output was reasonably quiet.

Figure 28 displays a typical ensemble-averaged pressure signature in the plane of symmetry of the turbulent spot. The data are an average for 2000 spots, generated every 80 msec (N = 800; one lobe on the camshaft). Intermittency data at half height obtained at the second station in Figure 22, with the hot-wire rake at x = 87.3 cm, y = 1.02 cm, are also shown in Figure 28 (the spot at half height is considerably smaller than at the wall). A small pressure rise at the leading edge of the spot is followed by a low pressure region (where the vortex is thought to be), by a subsequent sharp pressure rise, and finally by a decay in the wake of the spot. Note that the peak-to-peak amplitude is about 0.03 in C_p, corresponding to a pressure amplitude of about 12 μm Hg, or 0.17 mm H_2O, or 2.7 mV of electrical signal.

Figure 29 uses similarity coordinates to compare the present measurement with an indirect measurement by Cantwell et al., who inferred the pressure signature in the free stream from the conical property of the spot, the nonsteady Bernoulli equation, and the measured velocity perturbation in the free stream caused by passage of the spot. If both measurements are correct, there is a noticeable pressure difference across the spot. In fact, because the spot is relatively thin, values of dp/dx at the surface ($\Delta C_p \sim 0.030$ in 20 cm in Figure 28) are appreciably smaller than values of dp/dy

($\Delta C_p \sim 0.015$ in 2 cm in Figure 29).

The shape of the pressure signature in Figure 28 does not agree with the experience of DeMetz and Casarella (1973). These investigators were interested in natural transition, and their surface-pressure signals were ordinarily high-pass filtered and interpreted in terms of intermittency. Their Figure 26 is a brief record of unfiltered signals obtained in a flow with a substantial negative pressure gradient (made necessary by an unfortunate leading-edge geometry), at an unknown distance from the spot centerline, using instrumentation with highly non-uniform system gain in the important frequency range. The cause of the discrepancy is unclear; we can say only that we have considerable confidence in our own measurements.

Two investigations have recently been published concerning pressure signatures in natural turbulent boundary layers. Dinkelacker, Hessel, Meier, and Schewe (1977) have manually reduced a small fraction of data obtained by an ingenious and ambitious interferometric technique involving multiple elastic surface membranes. Both the scale and the celerity of the observed patterns seem too small to be characteristic of large-eddy structure. Thomas (1978) has obtained time correlations of surface pressure centered on the local occurrence of large, high-frequency fluctuations in surface pressure or surface shearing stress. The typical result is an anti-symmetric pressure correlation which is first positive and then negative; i.e., opposite to the signature for a spot in Figure 28. The scale is large enough, but the celerity seems low. The only hope of reconciling his result

with the present one is the possibility (suggested by the location of Thomas' detection event with respect to his picture of the large structure) that Thomas may be associating the last half of the pressure signature from one structure with the first half of the pressure signature from the next.

V SYNTHETIC BOUNDARY LAYERS

5.1 Scope of Experiments

The main parameters of the various synthetic flows studied during the present research are listed in several tables. Table I gives the distance from the leading edge of the plate to the pin station and to the six rake stations. Table II gives the rake height from the surface for the various measurements. Table III translates the cam-speed parameter N into disturbance period τ and lists the various combinations of spanwise and streamwise periods which were studied. A number entered into Table III indicates the figure in which the intermittency data may be found; an asterisk indicates that data were obtained at all six stations but are not presented in a figure. Finally, Table IV summarizes most of the parameters of interest for all runs involved in either preliminary or final measurements.

For the synthetic flows, a systematic method was wanted for setting the hot-wire rake at a suitable distance from the plate surface. During some preliminary runs with the 12.2-cm cam, it became apparent that a disturbance frequency of 25 Hz (N = 800) produced a very regular, coherent flow over the full length of the plate (see Figure 39). Some experimenting showed that a good rake position for this flow was one where the global intermittency (for unfiltered data averaged over all 24 wires; IBALL program) was about 0.4. This value was therefore adopted as a standard to be set at each station for the particular cam speed N = 800 for each cam, and the probe position was left unchanged for all other runs with the same cam. As

an example of the experimental experience, Figure 30 shows analog signals obtained from two of the hot wires (13 and 21), with their associated intermittency signals, when the rake was at the most upstream station and the 12.2-cm cam was running at N = 1991 (Run 190).

Because of changes in spot size and density with frequency, and also changes in apparent origin for spot growth, one consequence of the method just described was that the global intermittency changed significantly with x for fixed N (for $N \neq 800$), as shown in Figure 31, and also changed with N for fixed x, as shown in Figure 32. The values plotted in these figures are mean intermittency for filtered data, averaged over one revolution and one spanwise period, and are taken from Table IV.

The primary experimental results of the present research are shown in Figures 33-63. The presentation is the same as in Figures 21-23 for the turbulent spot, and all of the remarks in Section 4.2 apply to Figures 33-63 also. The scheme used at the pin station to indicate pin displacement is the same, and the shaded regions are again the regions inside the median contour line for intermittency, half way from the smallest to the largest value of $\langle \gamma \rangle$. The unit of data is one camshaft revolution, repeated as many times as necessary to fill the figures. Note that the coordinates x, z, and Ut are all in cm and have the same scales, so that the intermittency data in Figures 33-63 show the various flow patterns without distortion except for the small difference between celerity and reference velocity.

5.2 General Conclusions

During the study of synthetic boundary layers, the two main parameters, pin spacing and cam speed, were varied over a range which we hoped would include one or more synthetic flows giving good cause for eventual closer study. This hope was realized in full.

Figure 33, which is not part of the main sequence of experiments (cf. Table III), shows the result obtained when the 6.1-cm cam was run at quite slow speed, the object being to investigate the feasibiltiy of generating turbulent strips, or two-dimensional spots. The result is inconclusive, since the intermittency data in the figure retain a slight spanwise modulation even at the most downstream station. Another attempt should perhaps be made with the closest possible pin spacing, which is four times smaller than the one used here.

Figures 34-63, taken as a whole, establish the important conclusion that the downstream large-eddy structure always develops directly from the original disturbance pattern, with an explicit correspondence between spots and large eddies. In this sense, at least, the turbulent spot can certainly serve as a prototype large eddy. The data also confirm a related finding by Zilberman et al. (1977). There is an enormous reduction in the growth rate of each spot, in both the spanwise and streamwise directions, as it moves downstream in a crowd of neighboring spots. The growth rate normal to the surface, however, is almost unaffected (cf. Table II). The data do not support the conclusion by Elder (1960) that spots grow independently of each other and can be treated by superposition. Elder studied only the case

of two spots side by side, and then only at an x-Reynolds number of about 0.4×10^6. The present data deal with large arrays of spots and with the range of x-Reynolds numbers from 0.4×10^6 to 1.3×10^6.

Another important result, apparently new, concerns an interaction phenomenon which we propose to call eddy transposition. This phenomenon is conspicuous in Figures 34-36, 44-47, and 54-59. It involves the appearance and rapid growth of regions of new turbulence to the rear of the original spots and in the gaps between them. The original spots then decay and disappear. In the middle of the transposition process (for example, at the last station in Figure 36), the number of large eddies is twice the normal value, and these eddies form a honeycomb pattern of hexagons with empty centers. When the transposition process is complete, the original hexagonal pattern is restored with a substantial phase shift.

It may be that eddy transposition in the synthetic boundary layer is connected with the appearance of wave packets and new breakdowns to turbulence at the wings of a single spot, as observed by Wygnanski, Haritonidis, and Kaplan (1979). The evidence is not clear. In most but not all cases (cf. Figure 59), at least the early stages of the transposition process involve configurations with substantial regions free or almost free of turbulence (see in particular the strip pattern in Figure 33, which shows evidence of transposition). If so, transposition should probably be classified as part of the transition process and

should not be expected to be conspicuous in a fully turbulent flow. Examination of the raw intermittency data of the present experiments might shed more light on the matter, and should be undertaken.

Another question is raised by the disappearance of the original eddies in the late stages of transposition. Our conjecture at the moment is based on the position taken by Cantwell et al. (1977) regarding the process which supplies energy to a turbulent spot. In their view, free-stream fluid overtakes the spot and is entrained and slowed by friction on the wall at the rear of the spot, where the surface friction is large (the large friction may be thought of as either a cause or an effect of the deceleration). The rear of the spot, incidentally, is also the region of high surface pressure in Figure 28. It may be that during transposition the rear eddies shield the front ones and reduce their energy supply to such a level that they are obliged to decay and disappear. This conjecture, if it is correct, implies that a configuration with large eddies following in line, one behind the other, might be quite unstable. Hence a rectangular pattern would be a poor choice for a synthetic flow, whereas a hexagonal pattern would be a good one. It should be admitted that our original reasons for choosing a hexagonal pattern, following Coles and Barker, were aesthetic rather than scientific. In any event, an experimental test of the conjecture in these terms is clearly feasible.

5.3 Celerity

In any flow configuration where the large eddies remain intact as they move downstream, their celerity can be easily measured as the slope Udx/dUt in Figures 34-63. Such a measurement, corrected

for the small difference between U = 1000 cm/s and u_∞ = 1013 cm/s, and with strong emphasis on the data at the more downstream stations, shows a constant celerity of 0.88 ($\pm$0.02) u_∞ . The dispersion is a measure of experimental scatter rather than of any systematic dependence of celerity on either of the two scales of the hexagonal eddy pattern. The phenomenon of eddy transposition, in particular, affects the position but not the celerity of the large eddies.

5.4 Coherence Diagram

A study of the results in Figures 34-63 suggests that there might be a way to collapse the results for different cams, different cam speeds, and different stations into a map or diagram showing the kinds of interactions and evolutions which can occur. On the reasonable assumption that the flow is not much affected by viscosity, variables which suggest themselves for this purpose are the spanwise and streamwise periods normalized by the local layer thickness. Because the patterns vary from open and highly regular (Figure 34) to closed and nearly incoherent (Figure 63), it is not a simple matter to define a layer thickness consistently. The nearest available variable is the rake height, which was adjusted at each station to obtain a global unfiltered intermittency close to 0.4 for the particular cam speed N = 800, and was left unchanged for other cam speeds. Values obtained for global or mean intermittency for the filtered data are listed in Table IV and have been plotted for part of the data in Figures 31 and 32. The values in question vary from 0.2 to 0.7 for the last five data stations. The variation could have been avoided by adjusting the probe height for each x and N, but the

additional experimental effort would have been enormous and the additional benefit small. For the present, we have chosen simply to ignore variations in intermittency and to make the periods nondimensional using the probe height, now denoted by Δ, directly.

The results are shown in Figure 64, which is the main product of the present research. The various data strips in Figures 34-63 were first classified, more or less subjectively, into various categories; e.g., coherent pattern, transposing pattern, and disintegrating pattern, (i.e., a pattern showing marked loss of coherence). These categories are indicated by open, slashed, and solid symbols, respectively, in Figure 64. There is also a further differentiation by symbol shape for the various cams; squares, circles, and triangles are used for the 12.2-, 9.1-, and 6.1-cm cams respectively.

Logarithmic scales have been used for both coordinates in Figure 64. Consequently, the trajectory of a given synthetic flow as the layer thickness increases is downward and to the left along a line of slope + 1. Several regions and processes can be identified in the figure. For large pin spacing (large ζ) and fast cam speed (small τ), evolution of the flow is uneventful until the pattern eventually begins to lose coherence. For the same pin spacing but for slower cam speeds, the flow can pass into or through the transposition region and emerge as a displaced but still coherent pattern.

The scaling in Figure 64 is successful in establishing a connection between flows which are formally quite different. For example, the group of three points near $U\tau/\Delta = 14$, $\zeta/\Delta = 4.2$ rep-

resents Runs 163, 446, and 253 (Figure 39, station 24; Figure 51, station 16; and Figure 63, station 8). The flow patterns are geometrically quite similar. The group of two points near $U\tau/\Delta = 33$, $\zeta/\Delta = 5$, in the transposition region, represents Runs 148 and 389 (Figure 35, station 20 and Figure 47, station 12). Again there is reasonable similarity; both flows show the honeycomb pattern already mentioned.

The original synthetic flow studied by Coles and Barker (1975) can be placed in Figure 64 once an estimate is made for the boundary layer thickness. The flow apparently falls in the late transposition region, as indicated by the star at the point $\zeta/\Delta = 3.8$, $U\tau/\Delta = 24$. The present indication of transposition may account for the observation by Coles and Barker that the region of ensemble-averaged velocity defect passed the probe with its blunt end forward, rather than its narrow end.

5.5 Scales

It is now possible to reconsider the question of scales raised in the Introduction. The correlation measurements by Kovasznay et al. (1970) revealed an average large eddy about 1.2 δ wide and 2.5 δ long at the half-intermittency level. Such an eddy would command an area about 1.5 δ wide and 3.0 δ long. Other investigators have used counting methods, measuring the frequency of various events which are believed to be related to the large-scale motion. For example, Kovasznay et al. (1970) counted interface crossings and found a maximum frequency $u_\infty/f\delta$ of about 1.3 at the half-intermittency

level. This value was later confirmed by Chen and Blackwelder (1978), who used heat as a passive contaminant and counted temperature-interface crossings. Various results obtained from the position of zero crossings in time correlations have been summarized, with new data at higher Reynolds numbers, by Badri Narayanan and Marvin (1978). They recommend the value $u_\infty \tau/\delta = 5$ to 6.

These experimental estimates of scale give values which are at variance with each other and are all appreciably smaller than the scales which characterize the coherent region in Figure 64. We now propose a conceptual estimate based on a return to the idea, discussed at some length in the Introduction, that the large eddy can be explicitly identified with the turbulent spot.

In dye photographs of spots (see Figure 4 of Cantwell et al. 1978), the vortex position is usually quite well defined by a strong concentration of dye. The included angle between the two legs of the vortex in a plan view is close to 40 degrees. The same angle can be inferred from the angle of the dye concentrations in the regions of transverse contamination, as well as from the aluminum photographs in the same paper. Consider therefore the hexagonal cross-hatched pattern shown in the sketch, in which the diagonal lines represent vortex cores aligned in a regular way. The geometry of the sketch implies $\tan \theta/2 = \zeta/c\tau$. For $\theta = 40$ degrees and $c = 0.88\, u_\infty$, it follows that $\zeta/u_\infty \tau = 0.32$. This condition is shown in Figure 64 by the dashed line. For $u_\infty =$ 1013 cm/s and for $\zeta = 12.2$, 9.1, and 6.1 cm, the appropriate values for τ are 0.038, 0.028, and 0.019 seconds. The corresponding flows,

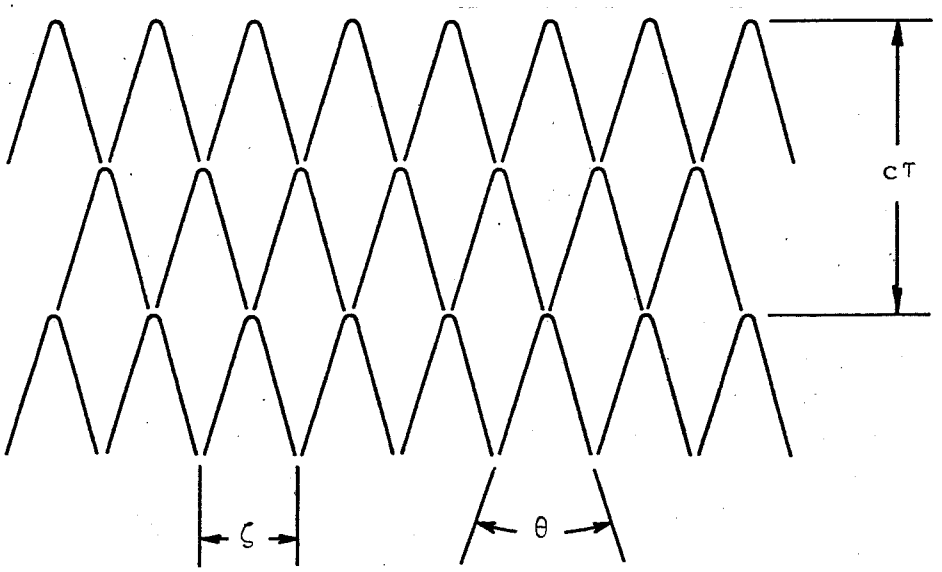

according to Table III, are those described by Figures 39, 51, and 63. These flows show loss of coherence in Figure 64 at about $\zeta/\Delta = 4.0$, $U\tau/\Delta = 13.5$. If $\Delta/\delta = 0.8$, therefore, the flow in the sketch should be marginally stable when

$$\frac{\zeta}{\delta} \approx 3.2 \quad , \quad \frac{u_\infty \tau}{\delta} \approx 11$$

Both values are close to the scales reported by Zilberman et al. (1977) and Haritonides et al. (1977) for a spot immersed in a natural (i.e., tripped) turbulent boundary layer. Their streamwise scale, however, should properly be doubled before the comparison is made.

At this point, a combination of scales can be specified for constructing a synthetic boundary layer suitable for work on the signature problem discussed in the Introduction. To operate in a marginal state at a given station and a given speed, it is only necessary to know (or guess) the layer thickness. The required cam spacing and cam speed

then follow from the numerical estimates just derived. Because the boundary of the disintegration region in the left center of Figure 64 has a negative slope, slightly different combinations of cam spacing and cam speed might also serve, within limits, as long as an increase in one is compensated by a decrease in the other.

5.6 Eddy Coalescence

What is missing from the measurements so far is any quantitative measure of the dispersion or loss of coherence which is observed to occur as the synthetic flows move downstream. It is reasonable to suppose that this loss of coherence is associated with an insupportable geometrical distortion of the three-dimensional large-eddy structure. As a synthetic flow develops in what we have called the coherent region, the spanwise and streamwise scales do not change, but the thickness increases almost linearly with time or distance. Eventually, a phenomenon like the vortex pairing or coalescence observed in the plane mixing layer by Brown and Roshko (1974) and Winant and Browand (1974) must occur. To fix the ideas, suppose that eddies in the boundary layer normally coalesce in pairs, and coalesce rapidly enough so that the volume of turbulent fluid does not change.* During the pairing process, the spanwise and streamwise scales must then increase by a factor $\sqrt{2}$, while the thickness remains unchanged. The main effect of the pairing process must therefore be to reduce the relative thickness of the large eddies, and the situation should remain stable until the

*That the volume of turbulent fluid is almost constant during pairing in the mixing layer has been established by computer analysis of high-speed shadowgraph movies taken by L. Bernal in the Brown-Roshko apparatus at GALCIT (J. Jimenez, private communication).

thickness has again grown by a factor $\sqrt{2}$. This argument implies that the most comfortable synthetic eddy for a given combination of spanwise and streamwise scales is one for which the thickness Δ or δ is about 20 percent less than the value at which loss of coherence becomes apparent in Figure 64. This conclusion should be taken into account in any selection of scales for a synthetic boundary layer, as should the likely proposition that coalescence might occur more naturally for vortex fours than for vortex pairs.

The present data have not yet been examined in detail on the question of eddy coalescence. Whatever the results may be, it is interesting to speculate about the properties of a hypothetical synthetic flow so perfectly constructed that loss of coherence is itself a deterministic process. What should happen, once the flow reaches the boundary of the shaded region in Figure 64, deserves to be called planned coalescence. The trajectory should reverse direction and then resume its normal evolution with new scales. Since there is considerable design freedom in the method used for generating disturbances during the present research, such an experiment is probably within reach.

REFERENCES

Badri Narayanan, M.A. and Marvin, J.G. 1978 On the period of the coherent structure in boundary layers at large Reynolds numbers. In "Coherent Structure of Turbulent Boundary Layers" (C.R. Smith and D.E. Abbott, eds.), AFOSR/Lehigh Workshop, 380-385.

Blackwelder, R.F. and Kovasznay, L.S.G. 1972 Time scales and correlations in a turbulent boundary layer. Phys. Fluids 15, 1545-1554.

Brown, G.L. and Roshko, A. 1974 On density effects and large structure in turbulent mixing layers. J. Fluid Mech. 64, 775-816.

Brown, G.L. and Thomas, A.S.W. 1977 Large structure in a turbulent boundary layer. Phys. Fluids 20, No. 10, Part II, S243 - S252.

Cantwell, B. 1975 A flying-hot-wire study of the turbulent near wake of a circular cylinder at a Reynolds number of 140,000. Ph.D. Thesis, California Institute of Technology.

Cantwell, B., Coles, D., and Dimotakis, P. 1978 Structure and entrainment in the plane of symmetry of a turbulent spot. J. Fluid Mech. 87, 641-672.

Chen, C.-H.P. and Blackwelder, R.F. 1978 Large-scale motion in a turbulent boundary layer: a study using temperature contamination. J. Fluid Mech. 89, 1 - 31.

Coles, D. and Barker, S.J. 1975 Some remarks on a synthetic turbulent boundary layer. In "Turbulent Mixing in Nonreactive and Reactive Flows" (S.N.B. Murthy, ed.), Plenum, 285-292.

DeMetz, F.C. and Casarella, M.J. 1973 An experimental study of the intermittent properties of the boundary layer pressure field during transition on a flat plate. NSRDC Rep. 4140.

Dinkelacker, A., Hessel, M., Meier, G.E.A., and Schewe, G. 1977 Investigation of pressure fluctuations beneath a turbulent boundary layer by means of an optical method. Phys. Fluids 20, No. 10, Part II, S216-S224.

Elder, J.W. 1960 An experimental investigation of turbulent spots and breakdown to turbulence. J. Fluid Mech. 9, 235-246.

Emmons, H.W. 1951 The laminar-turbulent transition in a boundary layer. Part I. J. Aeron. Sci. 18, 490-498.

Fulachier, L., Arzoumanian, E., and Dumas, R. 1977 Experimental investigation of a turbulent field from temperature fluctuations. In "Structure and Mechanisms of Turbulence II" (H. Fiedler, ed.), Lecture Notes in Physics No. 76, Springer-Verlag, 46 - 57.

Haritonides, J.H., Kaplan, R.E., and Wygnanski, I. 1977 Interaction of a turbulent spot with a turbulent boundary layer. In "Structure and Mechanisms of Turbulence I" (H. Fiedler, ed.), Lecture Notes in Physics No. 75, Springer-Verlag, 234-247.

Klebanoff, P.S. 1954 Characteristics of turbulence in a boundary layer with zero pressure gradient. NACA Tech. Note 3178; also, NACA Tech. Rep. 1247, 1955.

Kovasznay, L.S.G., Kibens, V., and Blackwelder, R.F. 1970 Large-scale motion in the intermittent region of a turbulent boundary layer. J. Fluid Mech. 41, 283-325.

Perry, A. and Morrison, G. 1971 A study of the constant-temperature hot-wire anemometer. J. Fluid Mech. 47, 577-599.

Praturi, A.K. and Brodkey, R.S. 1978 A stereoscopic visual study of coherent structures in turbulent shear flow. J. Fluid Mech. 89, 251-272.

Schubauer, G.B. and Klebanoff, P.S. 1955 Contributions on the mechanics of boundary-layer transition. NACA Tech. Note 3489: also NACA Tech. Rep. 1289, 1956.

Thomas, A.S.W. 1978 Conditionally sampled measurements of the fluctuating pressure at the wall beneath a turbulent boundary layer. AIAA Paper 78-1157.

Winant, C.D. and Browand, F.K. 1974 Vortex pairing: the mechanism of turbulent mixing-layer growth at moderate Reynolds number. J. Fluid Mech. 63, 237 - 255.

Wygnanski, I., Sokolov, N., and Friedman, D. 1976 On the turbulent 'spot' in a boundary layer undergoing transition. J. Fluid Mech. 78, 785 - 819.

Wygnanski, I. 1978 On the possible relationship between the transition process and the large coherent structures in turbulent boundary layers. In "Coherent Structure of Turbulent Boundary Layers" (C.R. Smith and D.E. Abbott, eds.), AFOSR/Lehigh Workshop, 168-193.

Wygnanski, I., Haritonidis, J.H., and Kaplan, R.E. 1979 On a Tollmien-Schlichting wave packet produced by a turbulent spot. (Submitted to J. Fluid Mech.; see Wygnanski 1978.)

Zilberman, M., Wygnanski, I., and Kaplan, R.E. 1977 Transitional boundary layer spot in a fully turbulent environment. Phys. Fluids 20, No. 10, Part II, S258 - S271.

TABLE I

STREAMWISE STATIONS (cm)

Leading Edge		0
Pins		22.9
Station	4	56.9
	8	87.3
	12	117.8
	16	148.3
	20	178.8
	24	209.3
Trailing Edge		264.2

TABLE II

DISTANCE OF HOT-WIRE RAKE

FROM PLATE SURFACE (cm)

Station	4	8	12	16	20	24
x(cm)	56.9	87.3	117.8	148.3	178.8	209.3
Crest of spot	1.34	2.03	2.57	3.13	3.68	4.10
Center of spot	.67	1.02	1.29	1.57	1.84	2.06
12.2-cm cam	.63	1.36	1.76	2.18	2.52	2.89
9.1-cm cam	.73	1.36	1.78	2.18	2.52	2.89
6.1-cm cam	.89	1.43	1.86	2.25	2.57	2.95

TABLE III

SCOPE OF EXPERIMENTS

N	τ(s)	ζ(cm)		
		12.2	9.1	6.1
		See Figure:		
4953	.248		*	33
2867	.143	*	*	*
2389	.119		*	
1991	.100	34	44	54
1659	.083	35	45	55
1382	.069	36	46	56
1152	.058	37	47	57
960	.048	38	48	58
800	.040	39	49	59
667	.033	40	50	60
556	.028	41	51	61
463	.023	42	52	62
386	.019	43	53	63
322	.016		*	*
268	.013		*	

TABLE IV

RUN NO	CAM	ZETA (CM)	N	TAU (S)	STA	X (CM)	Y (CM)	U (CM/S)	MEAN INT	MEDIAN INT
101	4.8"	12.19	800	.040	16	148.3	2.10	1009	.456	.500
102	4.8"	12.19	800	.040	16	148.3	2.28	1012	.216	.342
103	4.8"	12.19	800	.040	16	148.3	2.18	1014	.342	.442
104	4.8"	12.19	800	.040	16	148.3	2.18	1019	.340	.439
105	4.8"	12.19	386	.019	16	148.3	2.18	1019	.502	.516
106	4.8"	12.19	1991	.100	16	148.3	2.18	1020	.162	.396
107	4.8"	12.19	556	.028	16	148.3	2.18	1016	.407	.457
108	4.8"	12.19	1152	.058	16	148.3	2.18	1021	.242	.393
109	4.8"	12.19	463	.023	16	148.3	2.18	1020	.451	.467
110	4.8"	12.19	1659	.083	16	148.3	2.18	1021	.182	.335
111	4.8"	12.19	667	.033	16	148.3	2.18	1021	.335	.396
112	4.8"	12.19	1382	.069	16	148.3	2.18	1021	.215	.338
113	4.8"	12.19	960	.048	16	148.3	2.18	1021	.275	.402
114	4.8"	12.19	800	.040	16	148.3	2.18	1020	.316	.427
115	4.8"	12.19	800	.040	8	87.3	1.38	1008	.346	.500
116	4.8"	12.19	800	.040	8	87.3	1.36	1014	.371	.500
117	4.8"	12.19	800	.040	8	87.3	1.36	1013	.368	.499
118	4.8"	12.19	386	.019	8	87.3	1.36	1013	.662	.614
119	4.8"	12.19	1991	.100	8	87.3	1.36	1013	.229	.500
120	4.8"	12.19	556	.028	8	87.3	1.36	1012	.452	.492
121	4.8"	12.19	1659	.083	8	87.3	1.36	1012	.241	.500
122	4.8"	12.19	463	.023	8	87.3	1.36	1012	.522	.517
123	4.8"	12.19	1152	.058	8	87.3	1.36	1012	.271	.499
124	4.8"	12.19	667	.033	8	87.3	1.36	1012	.366	.491
125	4.8"	12.19	1382	.069	8	87.3	1.36	1013	.257	.499
126	4.8"	12.19	960	.048	8	87.3	1.36	1013	.291	.499
127	4.8"	12.19	800	.040	8	87.3	1.36	1013	.339	.498
128	4.8"	12.19	800	.040	12	117.8	1.78	1015	.334	.482
129	4.8"	12.19	800	.040	12	117.8	1.76	1012	.355	.476
130	4.8"	12.19	800	.040	12	117.8	1.76	1012	.361	.469

TABLE IV

RUN NO	CAM	ZETA (CM)	N	TAU (S)	STA	X (CM)	Y (CM)	U (CM/S)	MEAN INT	MEDIAN INT
131	4.8"	12.19	1991	.100	12	117.8	1.76	1012	.228	.445
132	4.8"	12.19	386	.019	12	117.8	1.76	1012	.605	.596
133	4.8"	12.19	1152	.058	12	117.8	1.76	1012	.267	.473
134	4.8"	12.19	463	.023	12	117.8	1.76	1013	.522	.545
135	4.8"	12.19	960	.048	12	117.8	1.76	1013	.301	.476
136	4.8"	12.19	667	.033	12	117.8	1.76	1013	.368	.447
137	4.8"	12.19	1659	.083	12	117.8	1.76	1013	.223	.434
138	4.8"	12.19	556	.028	12	117.8	1.76	1013	.441	.482
139	4.8"	12.19	1382	.069	12	117.8	1.76	1013	.243	.437
140	4.8"	12.19	800	.040	12	117.8	1.76	1013	.349	.467
141	4.8"	12.19	2867	.143	12	117.8	1.76	1014	.220	.491
142	4.8"	12.19	322	.016	12	117.8	1.76	1012	.585	.569
143	4.8"	12.19	800	.040	20	178.8	2.52	1012	.344	.408
144	4.8"	12.19	800	.040	20	178.8	2.52	1012	.334	.413
145	4.8"	12.19	386	.019	20	178.8	2.52	1012	.470	.484
146	4.8"	12.19	1991	.100	20	178.8	2.52	1012	.176	.371
147	4.8"	12.19	667	.033	20	178.8	2.52	1012	.344	.376
148	4.8"	12.19	1659	.083	20	178.8	2.52	1012	.200	.330
149	4.8"	12.19	960	.048	20	178.8	2.52	1012	.288	.369
150	4.8"	12.19	1382	.069	20	178.8	2.52	1012	.234	.282
151	4.8"	12.19	556	.028	20	178.8	2.52	1012	.388	.405
152	4.8"	12.19	1152	.058	20	178.8	2.52	1013	.272	.347
153	4.8"	12.19	463	.023	20	178.8	2.52	1015	.430	.434
154	4.8"	12.19	800	.040	20	178.8	2.52	1015	.334	.393
155	4.8"	12.19	2867	.143	20	178.8	2.52	1015	.135	.442
156	4.8"	12.19	2389	.119	20	178.8	2.52	1015	.145	.414
157	4.8"	12.19	800	.040	24	209.3	2.89	1012	.359	.430
158	4.8"	12.19	800	.040	24	209.3	2.89	1012	.374	.396
159	4.8"	12.19	800	.040	24	209.3	2.89	1013	.380	.412
160	4.8"	12.19	800	.040	24	209.3	2.89	1012	.373	.468

TABLE IV

RUN NO	CAM	ZETA (CM)	N	TAU (S)	STA	X (CM)	Y (CM)	U (CM/S)	MEAN INT	MEDIAN INT
161	4,8"	12,19	800	,040	24	209,3	2,89	1012	,375	,404
162	4,8"	12,19	800	,040	24	209,3	2,89	1012	,353	,384
163	4,8"	12,19	800	,040	24	209,3	2,89	1014	,362	,390
164	4,8"	12,19	386	,019	24	209,3	2,89	1012	,462	,484
165	4,8"	12,19	1991	,100	24	209,3	2,89	1013	,205	,380
166	4,8"	12,19	463	,023	24	209,3	2,89	1013	,441	,460
167	4,8"	12,19	667	,033	24	209,3	2,89	1013	,371	,390
168	4,8"	12,19	960	,048	24	209,3	2,89	1013	,324	,358
169	4,8"	12,19	1659	,083	24	209,3	2,89	1014	,234	,336
170	4,8"	12,19	1152	,058	24	209,3	2,89	1013	,282	,337
171	4,8"	12,19	556	,028	24	209,3	2,89	1013	,395	,406
172	4,8"	12,19	1382	,069	24	209,3	2,89	1013	,261	,312
173	4,8"	12,19	386	,019	24	209,3	2,89	1012	,464	,470
174	4,8"	12,19	800	,040	24	209,3	2,89	1014	,341	,379
175	4,8"	12,19	2867	,143	24	209,3	2,89	1014	,141	,409
177	4,8"	12,19	4953	,248	24	209,3	2,89	1014	,148	,478
178	4,8"	12,19	800	,040	8	87,3	1,36	1011	,345	,498
179	4,8"	12,19	2867	,143	8	87,3	1,36	1013	,181	,500
180	4,8"	12,19	2389	,119	8	87,3	1,36	1012	,200	,500
181	4,8"	12,19	4953	,248	8	87,3	1,36	1013	,127	,500
182	4,8"	12,19	800	,040	16	148,3	2,18	1001	,311	,433
183	4,8"	12,19	2867	,143	16	148,3	2,18	1000	,151	,485
184	4,8"	12,19	2389	,119	16	148,3	2,18	1002	,140	,447
185	4,8"	12,19	800	,040	4	56,9	,83	1015	,275	,500
186	4,8"	12,19	800	,040	4	56,9	,71	1015	,344	,500
187	4,8"	12,19	800	,040	4	56,9	,63	1014	,380	,500
188	4,8"	12,19	800	,040	4	56,9	,63	1014	,361	,500
189	4,8"	12,19	386	,019	4	56,9	,63	1015	,869	,602
190	4,8"	12,19	1991	,100	4	56,9	,63	1015	,197	,500
191	4,8"	12,19	556	,028	4	56,9	,63	1014	,465	,500

TABLE IV

RUN NO	CAM	ZETA (CM)	N	TAU (S)	STA	X (CM)	Y (CM)	U (CM/S)	MEAN INT	MEDIAN INT
192	4.8"	12.19	960	.048	4	56.9	.63	1015	.302	.500
193	4.8"	12.19	667	.033	4	56.9	.63	1015	.353	.500
194	4.8"	12.19	1659	.083	4	56.9	.63	1015	.197	.500
195	4.8"	12.19	1152	.058	4	56.9	.63	1015	.229	.500
196	4.8"	12.19	463	.023	4	56.9	.63	1015	.585	.501
197	4.8"	12.19	1382	.069	4	56.9	.63	1015	.223	.500
198	4.8"	12.19	800	.040	4	56.9	.63	1015	.270	.499
199	4.8"	12.19	2867	.143	4	56.9	.63	1016	.149	.500
200	4.8"	12.19	2389	.119	4	56.9	.63	1017	.155	.500
201	4.8"	12.19	4953	.248	4	56.9	.63	1017	.119	.500
231	2.4"	6.10	800	.040	12	117.8	2.10	1008	.067	.150
232	2.4"	6.10	800	.040	12	117.8	1.78	1007	.522	.550
233	2.4"	6.10	800	.040	12	117.8	1.94	1004	.215	.286
234	2.4"	6.10	800	.040	12	117.8	1.86	1010	.350	.412
235	2.4"	6.10	386	.019	12	117.8	1.86	1010	.552	.516
237	2.4"	6.10	1991	.100	12	117.8	1.86	1011	.210	.468
238	2.4"	6.10	463	.023	12	117.8	1.86	1010	.479	.455
239	2.4"	6.10	960	.048	12	117.8	1.86	1011	.289	.384
240	2.4"	6.10	1659	.083	12	117.8	1.86	1011	.217	.451
241	2.4"	6.10	556	.028	12	117.8	1.86	1011	.418	.426
242	2.4"	6.10	1382	.069	12	117.8	1.86	1011	.228	.412
243	2.4"	6.10	667	.033	12	117.8	1.86	1011	.340	.371
244	2.4"	6.10	1152	.058	12	117.8	1.86	1012	.245	.371
245	2.4"	6.10	322	.016	12	117.8	1.86	1012	.577	.570
246	2.4"	6.10	800	.040	12	117.8	1.86	1011	.317	.384
247	2.4"	6.10	2867	.143	12	117.8	1.86	1012	.227	.499
248	2.4"	6.10	2389	.119	12	117.8	1.86	1012	.219	.495
249	2.4"	6.10	4953	.248	12	117.8	1.86	1012	.208	.461
250	2.4"	6.10	800	.040	8	87.3	1.46	1019	.304	.398
251	2.4"	6.10	800	.040	8	87.3	1.41	1014	.404	.464

TABLE IV

RUN NO	CAM	ZETA (CM)	N	TAU (S)	STA	X (CM)	Y (CM)	U (CM/S)	MEAN INT	MEDIAN INT
252	2.4"	6.10	800	.040	8	87.3	1.43	1010	.347	.441
253	2.4"	6.10	386	.019	8	87.3	1.43	1009	.668	.552
254	2.4"	6.10	1991	.100	8	87.3	1.43	1010	.277	.498
255	2.4"	6.10	667	.033	8	87.3	1.43	1010	.368	.448
256	2.4"	6.10	960	.048	8	87.3	1.43	1010	.294	.444
257	2.4"	6.10	463	.023	8	87.3	1.43	1010	.564	.515
258	2.4"	6.10	1659	.083	8	87.3	1.43	1010	.280	.494
259	2.4"	6.10	1152	.058	8	87.3	1.43	1010	.281	.444
260	2.4"	6.10	556	.028	8	87.3	1.43	1010	.478	.481
261	2.4"	6.10	1382	.069	8	87.3	1.43	1011	.279	.481
262	2.4"	6.10	322	.016	8	87.3	1.43	1011	.677	.594
263	2.4"	6.10	800	.040	8	87.3	1.43	1010	.331	.454
264	2.4"	6.10	2867	.143	8	87.3	1.43	1011	.243	.499
265	2.4"	6.10	2389	.119	8	87.3	1.43	1012	.274	.499
266	2.4"	6.10	4953	.248	8	87.3	1.43	1012	.188	.500
267	2.4"	6.10	800	.040	16	148.3	2.29	1013	.278	.330
268	2.4"	6.10	800	.040	16	148.3	2.25	1008	.336	.376
269	2.4"	6.10	386	.019	16	148.3	2.25	1009	.475	.484
270	2.4"	6.10	1991	.100	16	148.3	2.25	1009	.178	.359
271	2.4"	6.10	556	.028	16	148.3	2.25	1008	.393	.392
272	2.4"	6.10	960	.048	16	148.3	2.25	1009	.306	.352
273	2.4"	6.10	667	.033	16	148.3	2.25	1008	.338	.347
274	2.4"	6.10	1659	.083	16	148.3	2.25	1009	.195	.359
275	2.4"	6.10	1152	.058	16	148.3	2.25	1009	.253	.329
276	2.4"	6.10	463	.023	16	148.3	2.25	1009	.429	.429
277	2.4"	6.10	1382	.069	16	148.3	2.25	1009	.227	.319
278	2.4"	6.10	322	.016	16	148.3	2.25	1009	.481	.484
279	2.4"	6.10	800	.040	16	148.3	2.25	1009	.308	.364
280	2.4"	6.10	2867	.143	16	148.3	2.25	1009	.181	.432
281	2.4"	6.10	2389	.119	16	148.3	2.25	1009	.176	.414

TABLE IV

RUN NO	CAM	ZETA (CM)	N	TAU (S)	STA	X (CM)	Y (CM)	U (CM/S)	MEAN INT	MEDIAN INT
282	2.4"	6.10	4953	.248	16	148.3	2.25	1010	.207	.479
283	2.4"	6.10	800	.040	24	209.3	3.05	1010	.274	.284
284	2.4"	6.10	800	.040	24	209.3	3.01	1014	.307	.326
285	2.4"	6.10	800	.040	24	209.3	2.93	1010	.382	.381
286	2.4"	6.10	800	.040	24	209.3	2.95	1013	.362	.381
287	2.4"	6.10	386	.019	24	209.3	2.95	1013	.467	.467
288	2.4"	6.10	1991	.100	24	209.3	2.95	1013	.222	.285
289	2.4"	6.10	960	.048	24	209.3	2.95	1013	.345	.359
290	2.4"	6.10	556	.028	24	209.3	2.95	1013	.404	.407
291	2.4"	6.10	556	.028	24	209.3	2.95	1013	.398	.407
292	2.4"	6.10	1382	.069	24	209.3	2.95	1013	.292	.330
293	2.4"	6.10	463	.023	24	209.3	2.95	1014	.435	.443
294	2.4"	6.10	463	.023	24	209.3	2.95	1014	.436	.438
295	2.4"	6.10	1152	.058	24	209.3	2.95	1013	.318	.326
296	2.4"	6.10	667	.033	24	209.3	2.95	1014	.363	.363
297	2.4"	6.10	1659	.083	24	209.3	2.95	1014	.257	.330
298	2.4"	6.10	322	.016	24	209.3	2.95	1014	.476	.477
299	2.4"	6.10	800	.040	24	209.3	2.95	1014	.349	.352
300	2.4"	6.10	2867	.143	24	209.3	2.95	1014	.162	.294
301	2.4"	6.10	2867	.143	24	209.3	2.95	1014	.160	.290
302	2.4"	6.10	4953	.248	24	209.3	2.95	1015	.179	.288
303	2.4"	6.10	800	.040	20	178.8	2.61	1013	.316	.324
304	2.4"	6.10	800	.040	20	178.8	2.57	1014	.364	.396
305	2.4"	6.10	800	.040	20	178.8	2.57	1014	.378	.400
306	2.4"	6.10	1991	.100	20	178.8	2.57	1014	.216	.337
307	2.4"	6.10	322	.016	20	178.8	2.57	1014	.502	.496
308	2.4"	6.10	386	.019	20	178.8	2.57	1014	.493	.500
309	2.4"	6.10	960	.048	20	178.8	2.57	1014	.348	.393
310	2.4"	6.10	556	.028	20	178.8	2.57	1014	.415	.419
311	2.4"	6.10	1382	.069	20	178.8	2.57	1014	.281	.311

TABLE IV

RUN NO	CAM	ZETA (CM)	N	TAU (S)	STA	X (CM)	Y (CM)	U (CM/S)	MEAN INT	MEDIAN INT
312	2.4"	6.10	667	.033	20	178.8	2.57	1014	.371	.386
313	2.4"	6.10	1152	.058	20	178.8	2.57	1014	.309	.323
314	2.4"	6.10	1659	.083	20	178.8	2.57	1014	.246	.339
315	2.4"	6.10	463	.023	20	178.8	2.57	1014	.452	.450
316	2.4"	6.10	800	.040	20	178.8	2.57	1014	.349	.392
317	2.4"	6.10	2867	.143	20	178.8	2.57	1014	.179	.398
318	2.4"	6.10	4953	.248	20	178.8	2.57	1015	.206	.373
319	2.4"	6.10	268	.013	20	178.8	2.57	1015	.500	.500
320	2.4"	6.10	800	.040	4	56.9	.67	1007	.677	.500
321	2.4"	6.10	800	.040	4	56.9	.75	1009	.604	.500
322	2.4"	6.10	800	.040	4	56.9	.91	1010	.373	.500
323	2.4"	6.10	800	.040	4	56.9	.91	1010	.357	.500
324	2.4"	6.10	800	.040	4	56.9	.89	1014	.385	.500
325	2.4"	6.10	322	.016	4	56.9	.89	1015	.915	.718
326	2.4"	6.10	463	.023	4	56.9	.89	1015	.716	.504
327	2.4"	6.10	1991	.100	4	56.9	.89	1014	.235	.499
328	2.4"	6.10	960	.048	4	56.9	.89	1015	.330	.500
329	2.4"	6.10	667	.033	4	56.9	.89	1015	.403	.498
330	2.4"	6.10	1382	.069	4	56.9	.89	1015	.271	.498
331	2.4"	6.10	1152	.058	4	56.9	.89	1015	.278	.499
332	2.4"	6.10	556	.028	4	56.9	.89	1015	.513	.500
333	2.4"	6.10	1659	.083	4	56.9	.89	1015	.238	.500
334	2.4"	6.10	386	.019	4	56.9	.89	1016	.841	.538
335	2.4"	6.10	268	.013	4	56.9	.89	1016	.893	.847
336	2.4"	6.10	268	.013	4	56.9	.89	1017	.883	.837
337	2.4"	6.10	800	.040	4	56.9	.89	1016	.290	.493
338	2.4"	6.10	2867	.143	4	56.9	.89	1017	.170	.497
339	2.4"	6.10	4953	.248	4	56.9	.89	1017	.144	.438
340	2.4"	6.10	2389	.119	4	56.9	.89	1017	.198	.497
341	2.4"	6.10	800	.040	4	56.9	.89	1007	.423	.500

TABLE IV

RUN NO	CAM	ZETA (CM)	N	TAU (S)	STA	X (CM)	Y (CM)	U (CM/S)	MEAN INT	MEDIAN INT
383	3.6"	9.14	800	.040	12	117.8	1.82	1007	.306	.424
384	3.6"	9.14	800	.040	12	117.8	1.78	1011	.377	.464
385	3.6"	9.14	800	.040	12	117.8	1.78	1011	.374	.450
386	3.6"	9.14	386	.019	12	117.8	1.78	1011	.543	.535
387	3.6"	9.14	322	.016	12	117.8	1.78	1011	.586	.564
388	3.6"	9.14	960	.048	12	117.8	1.78	1011	.306	.439
389	3.6"	9.14	1152	.058	12	117.8	1.78	1011	.261	.355
390	3.6"	9.14	1991	.100	12	117.8	1.78	1012	.233	.474
391	3.6"	9.14	1659	.083	12	117.8	1.78	1012	.229	.440
392	3.6"	9.14	556	.028	12	117.8	1.78	1012	.386	.454
393	3.6"	9.14	463	.023	12	117.8	1.78	1012	.482	.498
394	3.6"	9.14	1382	.069	12	117.8	1.78	1012	.252	.418
395	3.6"	9.14	667	.033	12	117.8	1.78	1011	.350	.437
396	3.6"	9.14	800	.040	12	117.8	1.78	1012	.348	.446
397	3.6"	9.14	2867	.143	12	117.8	1.78	1012	.238	.500
398	3.6"	9.14	2389	.119	12	117.8	1.78	1013	.237	.496
399	3.6"	9.14	4953	.248	12	117.8	1.78	1013	.207	.498
400	3.6"	9.14	268	.013	12	117.8	1.78	1012	.572	.547
401	3.6"	9.14	800	.040	20	178.8	2.55	1011	.334	.356
402	3.6"	9.14	800	.040	20	178.8	2.53	1013	.349	.358
403	3.6"	9.14	800	.040	20	178.8	2.53	1013	.346	.370
404	3.6"	9.14	800	.040	20	178.8	2.52	1017	.367	.397
405	3.6"	9.14	386	.019	20	178.8	2.52	1017	.473	.474
406	3.6"	9.14	322	.016	20	178.8	2.52	1017	.477	.486
407	3.6"	9.14	1991	.100	20	178.8	2.52	1017	.203	.359
408	3.6"	9.14	1659	.083	20	178.8	2.52	1018	.235	.360
409	3.6"	9.14	463	.023	20	178.8	2.52	1018	.443	.447
410	3.6"	9.14	556	.028	20	178.8	2.52	1017	.401	.422
411	3.6"	9.14	960	.048	20	178.8	2.52	1017	.324	.354
412	3.6"	9.14	1152	.058	20	178.8	2.52	1018	.283	.344

TABLE IV

RUN NO	CAM	ZETA (CM)	N	TAU (S)	STA	X (CM)	Y (CM)	U (CM/S)	MEAN INT	MEDIAN INT
413	3.6"	9.14	667	.033	20	178.8	2.52	1018	.372	.379
414	3.6"	9.14	1382	.069	20	178.8	2.52	1018	.272	.383
415	3.6"	9.14	800	.040	20	178.8	2.52	1017	.367	.389
416	3.6"	9.14	2867	.143	20	178.8	2.52	1018	.172	.437
417	3.6"	9.14	4953	.248	20	178.8	2.52	1019	.196	.451
418	3.6"	9.14	268	.013	20	178.8	2.52	1019	.498	.512
419	3.6"	9.14	2389	.119	20	178.8	2.52	1019	.186	.398
420	3.6"	9.14	800	.040	8	87.3	1.40	1011	.343	.494
421	3.6"	9.14	800	.040	8	87.3	1.36	1013	.360	.496
422	3.6"	9.14	800	.040	8	87.3	1.36	1012	.368	.492
423	3.6"	9.14	386	.019	8	87.3	1.36	1012	.628	.599
424	3.6"	9.14	322	.016	8	87.3	1.36	1011	.660	.591
426	3.6"	9.14	1991	.100	8	87.3	1.36	1012	.271	.499
427	3.6"	9.14	1659	.083	8	87.3	1.36	1012	.282	.493
428	3.6"	9.14	667	.033	8	87.3	1.36	1012	.344	.486
429	3.6"	9.14	556	.028	8	87.3	1.36	1012	.397	.484
431	3.6"	9.14	960	.048	8	87.3	1.36	1013	.300	.481
432	3.6"	9.14	1152	.058	8	87.3	1.36	1012	.266	.482
433	3.6"	9.14	463	.023	8	87.3	1.36	1012	.501	.488
434	3.6"	9.14	1382	.069	8	87.3	1.36	1012	.286	.492
435	3.6"	9.14	800	.040	8	87.3	1.36	1013	.340	.489
436	3.6"	9.14	2867	.143	8	87.3	1.36	1013	.229	.500
437	3.6"	9.14	4953	.248	8	87.3	1.36	1014	.165	.500
438	3.6"	9.14	2389	.119	8	87.3	1.36	1014	.251	.499
439	3.6"	9.14	268	.013	8	87.3	1.36	1013	.640	.594
440	3.6"	9.14	800	.040	16	148.3	2.18	1009	.356	.394
441	3.6"	9.14	800	.040	16	148.3	2.18	1009	.353	.405
442	3.6"	9.14	386	.019	16	148.3	2.18	1009	.486	.514
443	3.6"	9.14	322	.016	16	148.3	2.18	1009	.506	.529
444	3.6"	9.14	1991	.100	16	148.3	2.18	1009	.195	.446

TABLE IV

RUN NO	CAM	ZETA (CM)	N	TAU (S)	STA	X (CM)	Y (CM)	U (CM/S)	MEAN INT	MEDIAN INT
445	3.6"	9.14	1659	.083	16	148.3	2.18	1009	.216	.420
446	3.6"	9.14	556	.028	16	148.3	2.18	1009	.409	.438
447	3.6"	9.14	463	.023	16	148.3	2.18	1008	.463	.475
448	3.6"	9.14	1152	.058	16	148.3	2.18	1009	.262	.347
449	3.6"	9.14	960	.048	16	148.3	2.18	1009	.312	.371
450	3.6"	9.14	1382	.069	16	148.3	2.18	1009	.246	.391
451	3.6"	9.14	667	.033	16	148.3	2.18	1009	.345	.399
452	3.6"	9.14	800	.040	16	148.3	2.18	1010	.345	.404
453	3.6"	9.14	2867	.143	16	148.3	2.18	1010	.177	.479
454	3.6"	9.14	4953	.248	16	148.3	2.18	1011	.204	.495
455	3.6"	9.14	2389	.119	16	148.3	2.18	1010	.184	.441
456	3.6"	9.14	268	.013	16	148.3	2.18	1010	.505	.512
457	3.6"	9.14	800	.040	24	209.3	2.89	1010	.373	.380
458	3.6"	9.14	800	.040	24	209.3	2.89	1008	.373	.375
459	3.6"	9.14	322	.016	24	209.3	2.89	1008	.475	.474
460	3.6"	9.14	386	.019	24	209.3	2.89	1008	.461	.462
461	3.6"	9.14	1659	.083	24	209.3	2.89	1009	.272	.351
462	3.6"	9.14	1991	.100	24	209.3	2.89	1009	.235	.347
463	3.6"	9.14	960	.048	24	209.3	2.89	1009	.347	.363
464	3.6"	9.14	1152	.058	24	209.3	2.89	1009	.312	.367
465	3.6"	9.14	667	.033	24	209.3	2.89	1009	.358	.367
467	3.6"	9.14	556	.028	24	209.3	2.89	1009	.399	.436
469	3.6"	9.14	1382	.069	24	209.3	2.89	1009	.297	.342
470	3.6"	9.14	463	.023	24	209.3	2.89	1009	.428	.430
471	3.6"	9.14	800	.040	24	209.3	2.89	1009	.359	.382
472	3.6"	9.14	2867	.143	24	209.3	2.89	1010	.180	.373
473	3.6"	9.14	2389	.119	24	209.3	2.89	1010	.200	.357
474	3.6"	9.14	4953	.248	24	209.3	2.89	1011	.186	.447
475	3.6"	9.14	268	.013	24	209.3	2.89	1010	.482	.492
476	3.6"	9.14	800	.040	4	56.9	.76	1011	.343	.500

TABLE IV

RUN NO	CAM	ZETA (CM)	N	TAU (S)	STA	X (CM)	Y (CM)	U (CM/S)	MEAN INT	MEDIAN INT
477	3.6"	9.14	800	.040	4	56.9	.72	1011	.388	.500
478	3.6"	9.14	800	.040	4	56.9	.73	1013	.356	.500
479	3.6"	9.14	386	.019	4	56.9	.73	1013	.746	.579
480	3.6"	9.14	322	.016	4	56.9	.73	1013	.918	.776
481	3.6"	9.14	1659	.083	4	56.9	.73	1013	.257	.500
482	3.6"	9.14	1991	.100	4	56.9	.73	1013	.225	.500
483	3.6"	9.14	667	.033	4	56.9	.73	1013	.370	.500
484	3.6"	9.14	463	.023	4	56.9	.73	1013	.586	.505
485	3.6"	9.14	960	.048	4	56.9	.73	1013	.360	.500
486	3.6"	9.14	1382	.069	4	56.9	.73	1013	.275	.500
487	3.6"	9.14	556	.028	4	56.9	.73	1013	.420	.496
488	3.6"	9.14	1152	.058	4	56.9	.73	1013	.279	.500
489	3.6"	9.14	800	.040	4	56.9	.73	1013	.412	.500
490	3.6"	9.14	2867	.143	4	56.9	.73	1014	.162	.500
491	3.6"	9.14	2389	.119	4	56.9	.73	1013	.185	.500
492	3.6"	9.14	4953	.248	4	56.9	.73	1014	.140	.500
493	3.6"	9.14	268	.013	4	56.9	.73	1014	.877	.778
494	3.6"	9.14	800	.040	16	148.3	2.18	1010	.353	.422
495	3.6"	9.14	1382	.069	16	148.3	2.18	1013	.258	.418
496	3.6"	9.14	1382	.069	16	148.3	2.18	1217	.339	.474
497	3.6"	9.14	1382	.069	16	148.3	2.18	817	.038	.111
498	3.6"	9.14	1382	.069	16	148.3	2.18	1422	.371	.488
499	3.6"	9.14	1382	.069	16	148.3	2.18	920	.143	.362
500	3.6"	9.14	1382	.069	16	148.3	2.18	1521	.378	.494
501	3.6"	9.14	800	.040	16	148.3	2.18	1521	.514	.548
502	3.6"	9.14	1382	.069	16	148.3	2.18	1020	.248	.416
503	3.6"	9.14	800	.040	16	148.3	2.18	1020	.329	.379
504	SPOT		800	.040	16	148.3	2.18	1011		.206
505	SPOT		800	.040	16	148.3	1.94	1011		.381
506	SPOT		386	.019	16	148.3	1.94	1011		.382

TABLE IV

RUN NO	CAM	ZETA (CM)	N	TAU (S)	STA	X (CM)	Y (CM)	U (CM/S)	MEAN INT	MEDIAN INT
507	SPOT		1991	.100	16	148.3	1.94	1011		.488
508	SPOT		800	.040	24	209.3	2.89	1012		.169
509	SPOT		800	.040	24	209.3	2.67	1016		.320
510	SPOT		386	.019	24	209.3	2.67	1017		.346
511	SPOT		1991	.100	24	209.3	2.67	1017		.327
512	SPOT		800	.040	12	117.8	1.76	1013		.276
513	SPOT		800	.040	12	117.8	1.59	1012		.431
514	SPOT		386	.019	12	117.8	1.59	1012		.405
515	SPOT		1991	.100	12	117.8	1.59	1014		.499
516	SPOT		800	.040	20	178.8	2.52	1007		.179
517	SPOT		800	.040	20	178.8	2.29	1009		.339
518	SPOT		386	.019	20	178.8	2.29	1009		.358
519	SPOT		1991	.100	20	178.8	2.29	1008		.425
520	SPOT		800	.040	8	87.3	1.36	1010		.449
521	SPOT		386	.019	8	87.3	1.36	1010		.309
522	SPOT		1991	.100	8	87.3	1.36	1010		.498
523	SPOT		800	.040	8	87.3	1.14	1014		.499
524	SPOT		386	.019	8	87.3	1.14	1015		.485
525	SPOT		1991	.100	8	87.3	1.14	1015		.500
526	SPOT		800	.040	4	56.9	.63	1011		.499
527	SPOT		800	.040	4	56.9	.51	1018		.500
528	SPOT		386	.019	4	56.9	.51	1019		.499
529	SPOT		1991	.100	4	56.9	.51	1018		.499
530	SPOT		268	.013	4	56.9	.51	1018		.500
531	SPOT		1991	.100	4	56.9	1.34	1011		.004
532	SPOT		1991	.100	4	56.9	.67	1014		.500
533	SPOT		386	.019	4	56.9	.67	1014		.498
534	SPOT		800	.040	4	56.9	.67	1014		.499
535	SPOT		1991	.100	8	87.3	2.03	1016		.006
536	SPOT		1991	.100	8	87.3	1.02	1016		.500

TABLE IV

RUN NO	CAM	ZETA (CM)	N	TAU (S)	STA	X (CM)	Y (CM)	U (CM/S)	MEAN INT	MEDIAN INT
537	SPOT		386	,019	8	87,3	1,02	1016		,500
538	SPOT		800	,040	8	87,3	1,02	1016		,500
539	SPOT		1991	,100	24	209,3	4,10	1017		,018
540	SPOT		1991	,100	24	209,3	2,06	1016		,500
541	SPOT		386	,019	24	209,3	2,06	1015		,896
542	SPOT		800	,040	24	209,3	2,06	1016		,526
543	SPOT		1991	,100	20	178,8	3,68	1016		,010
544	SPOT		1991	,100	20	178,8	1,84	1016		,500
545	SPOT		386	,019	20	178,8	1,84	1016		,806
546	SPOT		800	,040	20	178,8	1,84	1016		,497
547	SPOT		1991	,100	12	117,8	2,57	1013		,017
548	SPOT		1991	,100	12	117,8	1,29	1013		,500
549	SPOT		386	,019	12	117,8	1,29	1012		,501
550	SPOT		800	,040	12	117,8	1,29	1012		,500
551	SPOT		1991	,100	16	148,3	3,13	1016		,015
552	SPOT		386	,019	16	148,3	1,57	1017		,658
553	SPOT		800	,040	16	148,3	1,57	1017		,500
554	SPOT		1991	,100	16	148,3	1,57	1018		,500
555	SPOT		800	,040	16	148,3	1,57	1017		,500
556	SPOT		800	,040	16	148,3	1,57	1017		,500
557	SPOT		800	,040	16	148,3	1,57	1245		,500
558	SPOT		800	,040	16	148,3	1,57	849		,046
559	SPOT		800	,040	16	148,3	1,57	1403		,500
560	SPOT		800	,040	16	148,3	1,57	923		,500
561	SPOT		800	,040	16	148,3	1,57	807		,002
562	SPOT		800	,040	16	148,3	1,57	1010		,500
563	SPOT		800	,040	16	148,3	1,57	979		,499
564	SPOT		800	,040	16	148,3	1,57	911		,358
565	SPOT		800	,040	16	148,3	1,57	862		,034
566	SPOT		800	,040	16	148,3	1,57	961		,487

TABLE IV

RUN NO	CAM	ZETA (CM)	N	TAU (S)	STA	X (CM)	Y (CM)	U (CM/S)	MEAN INT	MEDIAN INT
567	SPOT		800	.040	16	148.3	1.57	807		.004
568	SPOT		800	.040	16	148.3	1.57	912		.228
569	SPOT		800	.040	16	148.3	1.57	887		.050
570	SPOT		800	.040	16	148.3	1.57	951		.484
571	SPOT		800	.040	16	148.3	1.57	922		.272
572	SPOT		800	.040	16	148.3	1.57	895		.039
573	SPOT		800	.040	16	148.3	1.57	942		.464
574	SPOT		800	.040	16	148.3	1.57	922		.479
575	SPOT		800	.040	16	148.3	1.57	1000		.500
576	SPOT		800	.040	16	148.3	1.57	836		.029
577	SPOT		800	.040	16	148.3	1.57	1110		.500
578	SPOT		800	.040	16	148.3	1.57	1286		.500
579	SPOT		800	.040	16	148.3	1.57	956		.499
580	SPOT		800	.040	16	148.3	1.57	900		.415
581	SPOT		800	.040	16	148.3	1.57	1027		.500

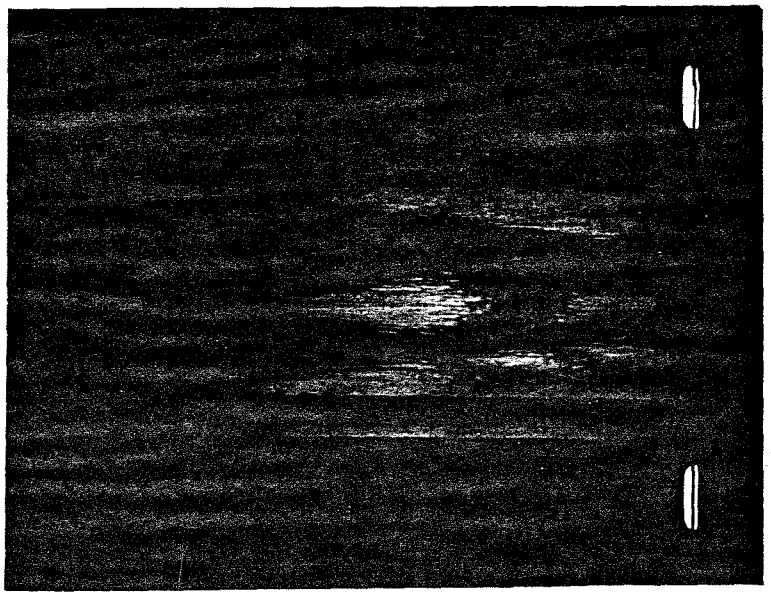

(a)

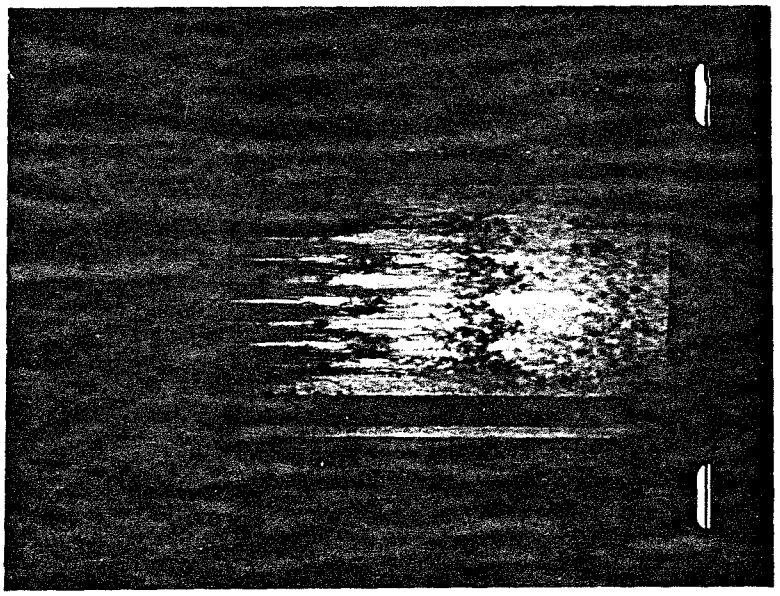

(b)

Figure 1. Dye visualization in water channel, from flow studies by Coles and Barker (Coles, private communication).
(a) turbulent spot;
(b) synthetic turbulent boundary layer.

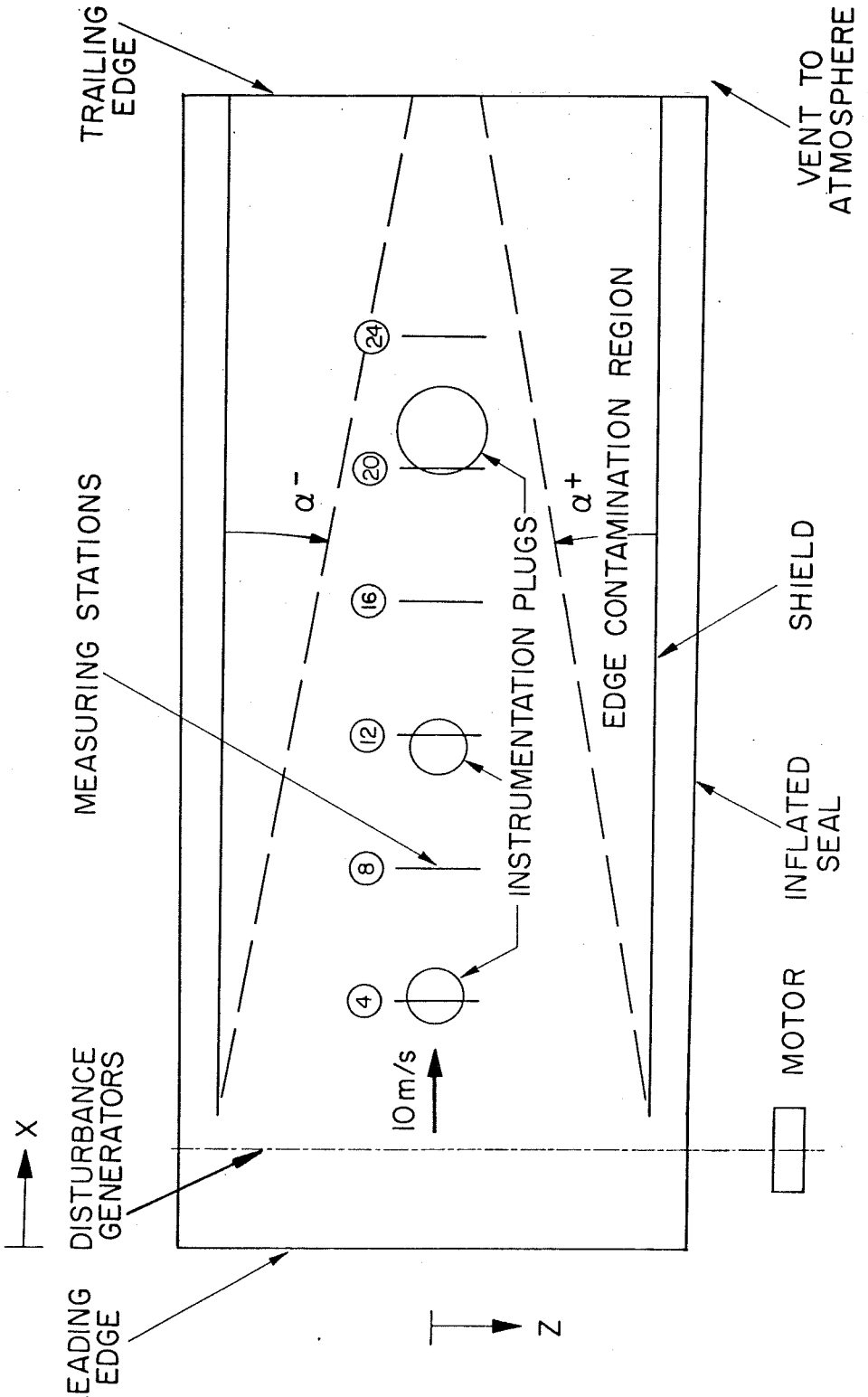

Figure 2. Plan view of flat-plate model. Experimentally determined boundaries of transverse-contamination regions are shown as dashed lines. For coordinates of measuring stations 4 - 24, see Table I.

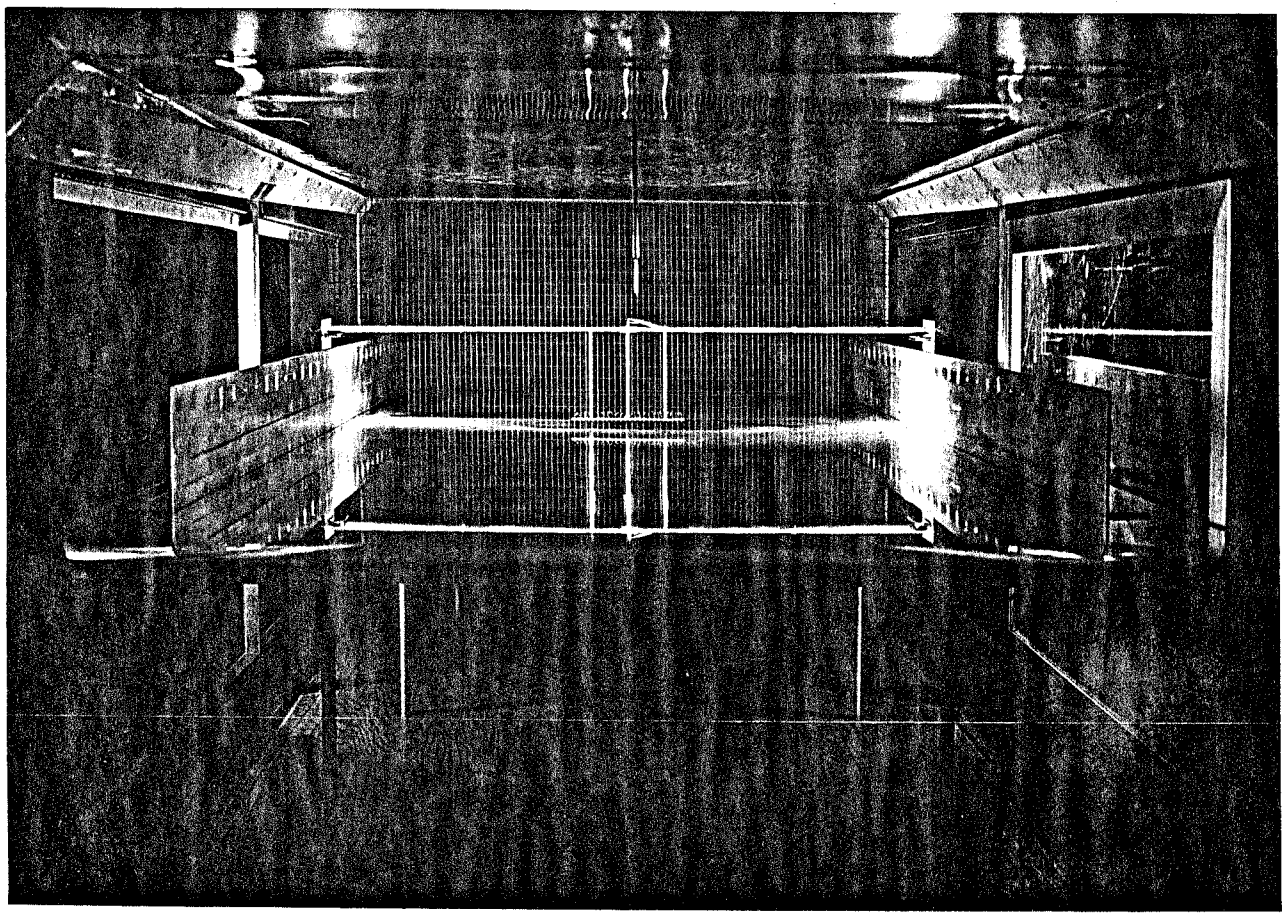

Figure 3. Photograph of model in tunnel, looking downstream. Note pitot-static probe in foreground, screen in background, and hot-wire rake supported from bridge structure attached to flow shields.

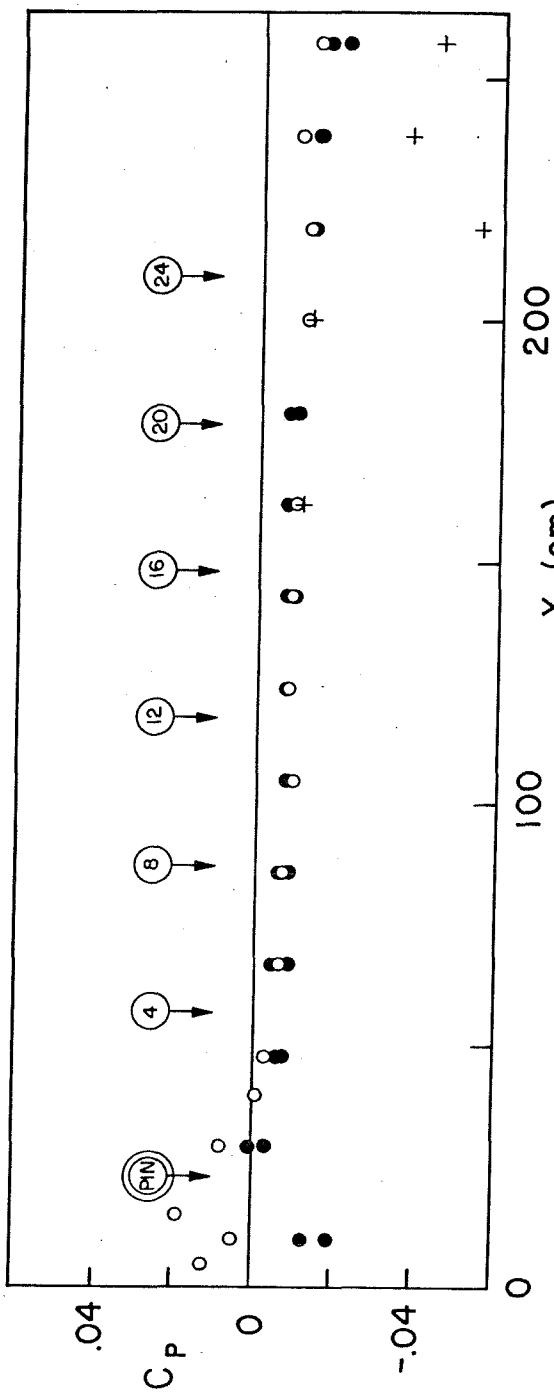

Figure 4. Static pressure distribution on plate. Open symbols and crosses: data on centerline. Solid symbols: data off centerline ($z = \pm 30.5$ cm). Arrows indicate locations of disturbance generator and measuring stations. Crosses show effect of mounting hot wire rake at station 24.

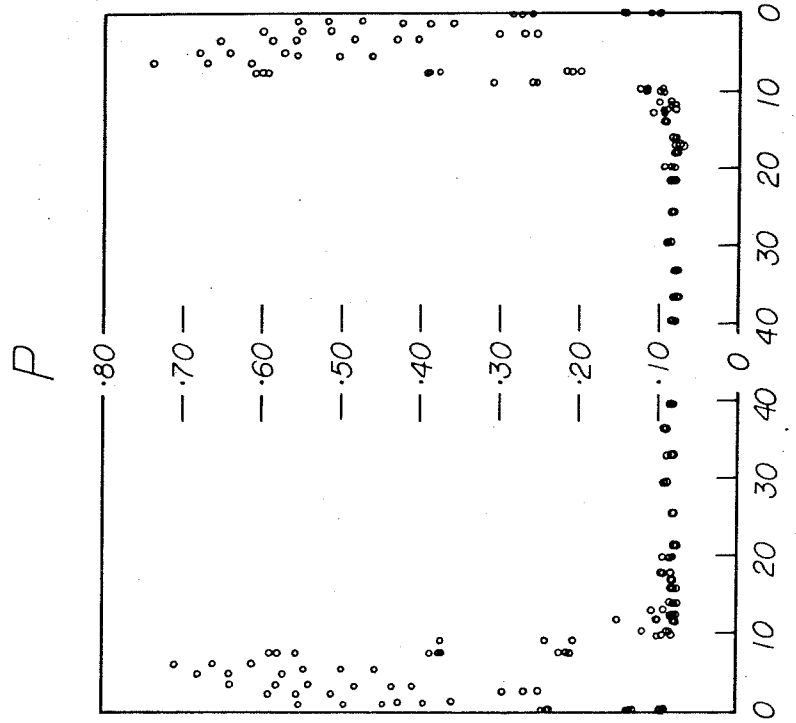

Figure 5. Surface-tube measurements mapping edge-contamination regions in undisturbed flow. P is non-dimensional surface-tube pressure and α^- and α^+ are angles (in degrees) measured as shown in Figure 2. Measurements include data at x = 89 cm, 165 cm, and 241 cm and at U = 9.6 m/s, 10.7 m/s, and 11.7 m/s. Constant low value of P indicates laminar flow.

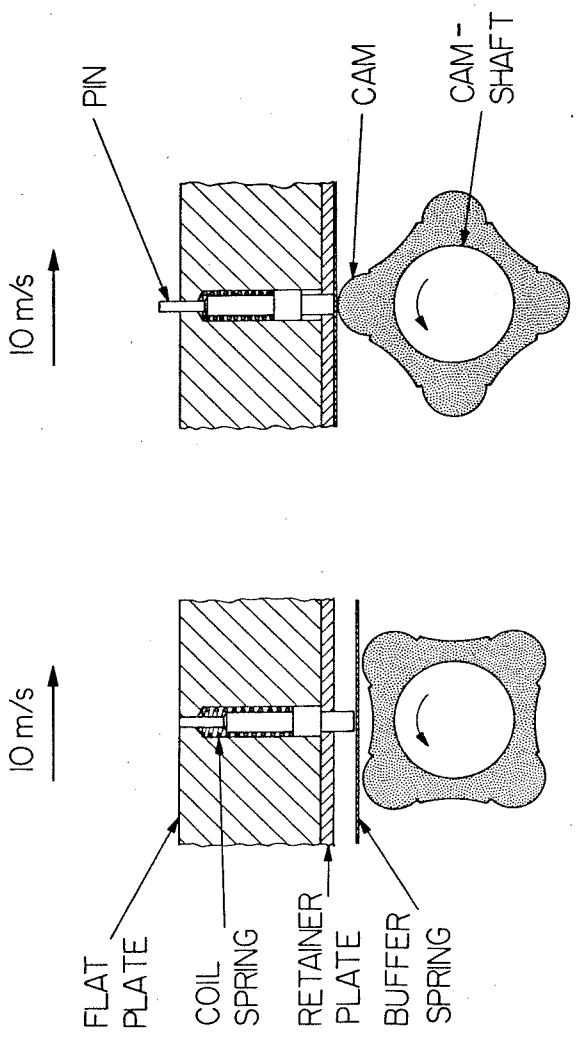

Figure 6. Detail of disturbance-generating mechanism. Left: pin retracted. Right: pin displaced into boundary layer.

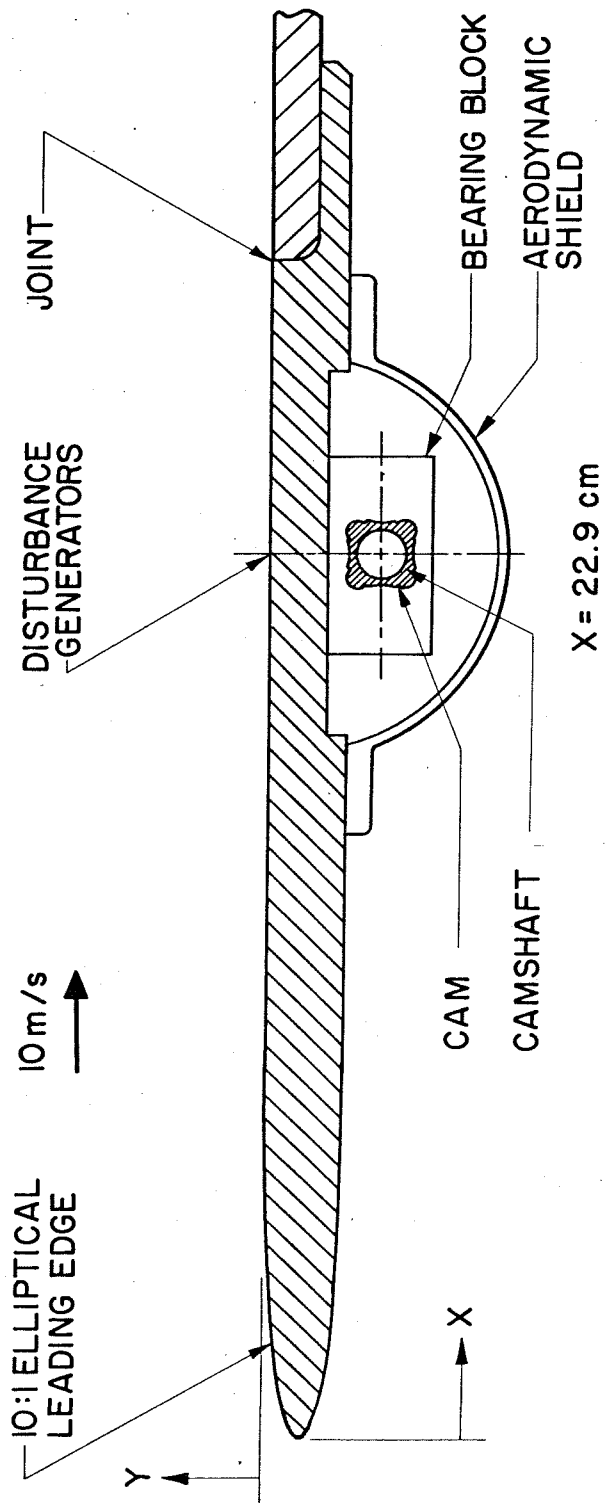

Figure 7. Detail of front section of plate, showing location of camshaft and windshield.

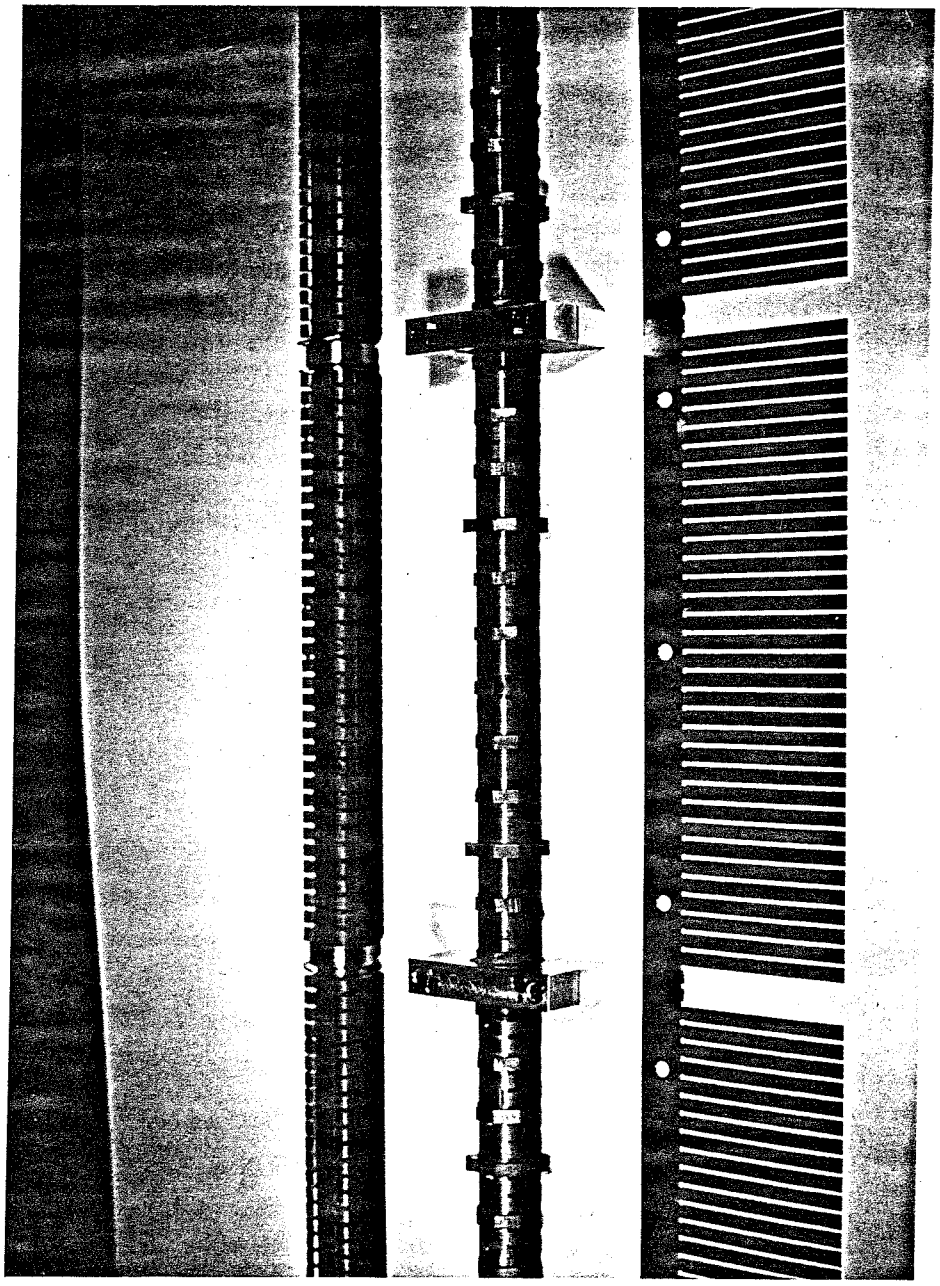

Figure 8. Photograph of camshaft. Top: before final machining (all cam lobes present). Note needle bearing between adjacent sleeves. Center: 9.1-cm cam after final machining, with bearing block installed. Bottom: leaf or buffer spring used between cam and pins as shown in Figure 6.

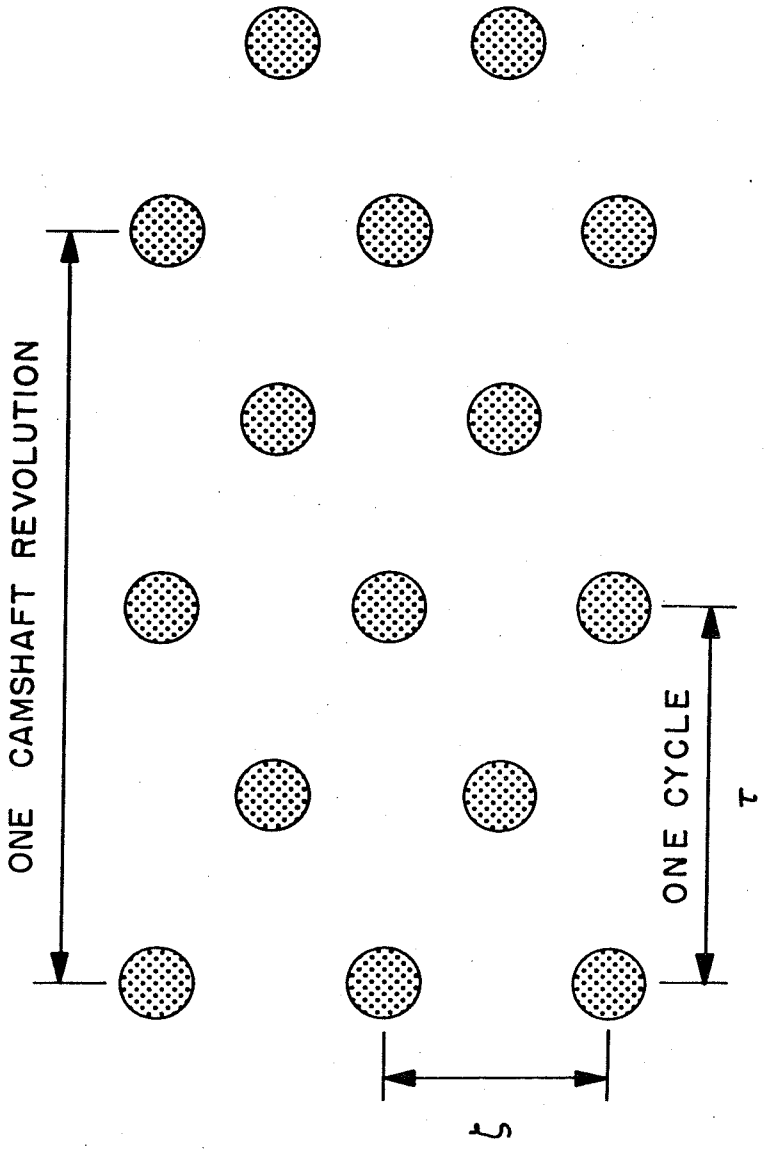

Figure 9. Close-packed hexagonal disturbance pattern in (z,t) plane. Periods ζ and τ in z and t directions are defined as shown.

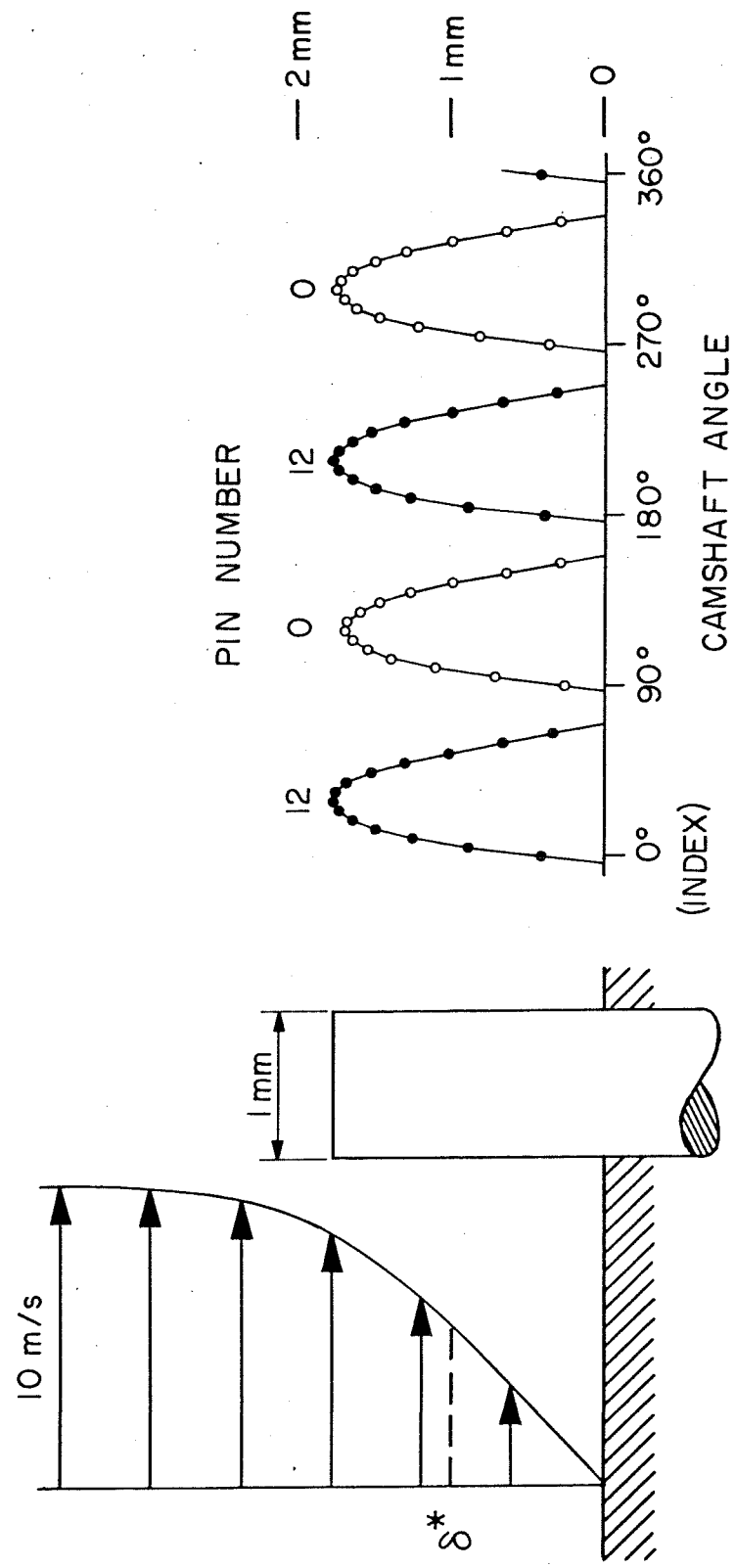

Figure 10. Pin displacement against camshaft angle for 12.2-cm cam. Open symbols: center pin. Solid symbols: pin at $z = 6.1$ cm. At left, maximum pin displacement is compared with estimated profile in Blasius boundary layer at pin location.

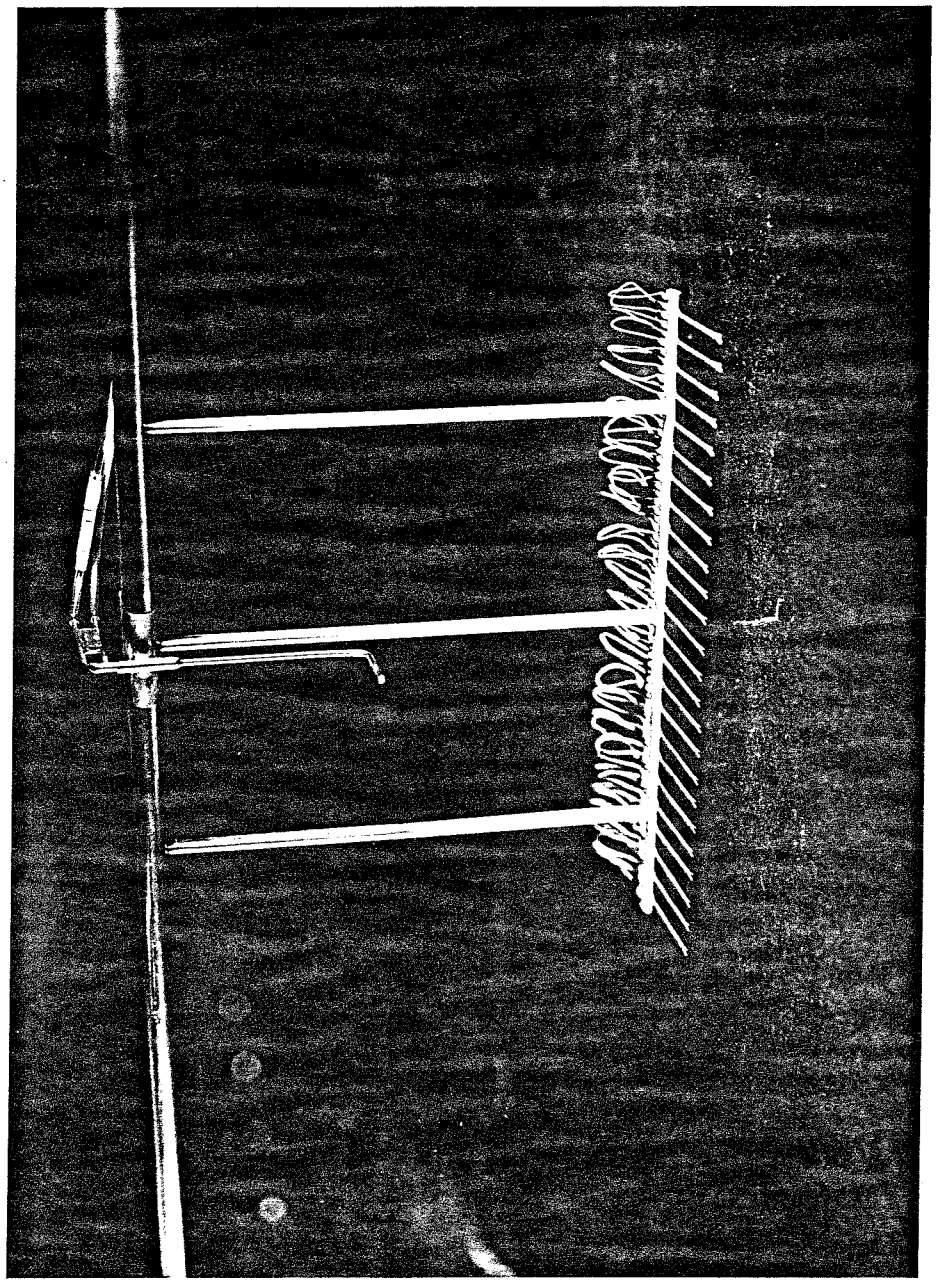

Figure 11. Close view of hot-wire rake.

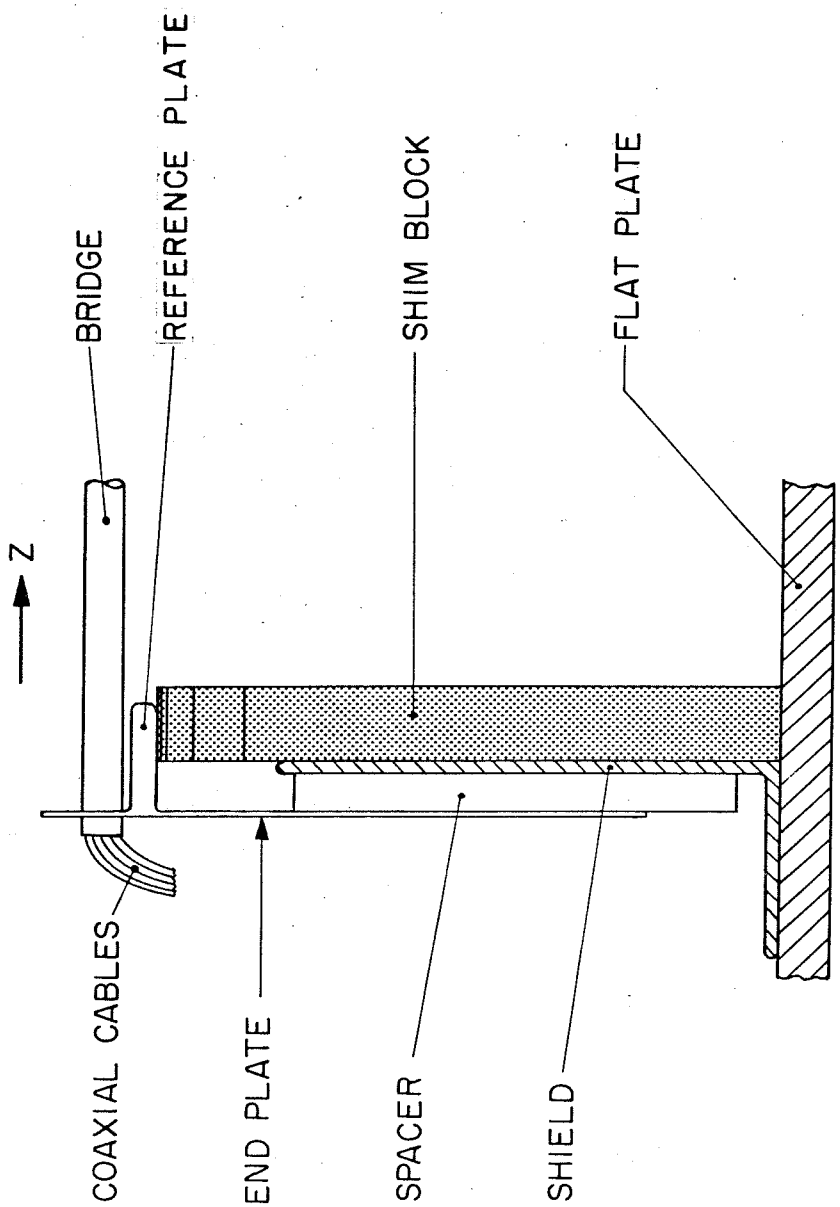

Figure 12. Bridge end connection, showing use of shims to position rake above plate.

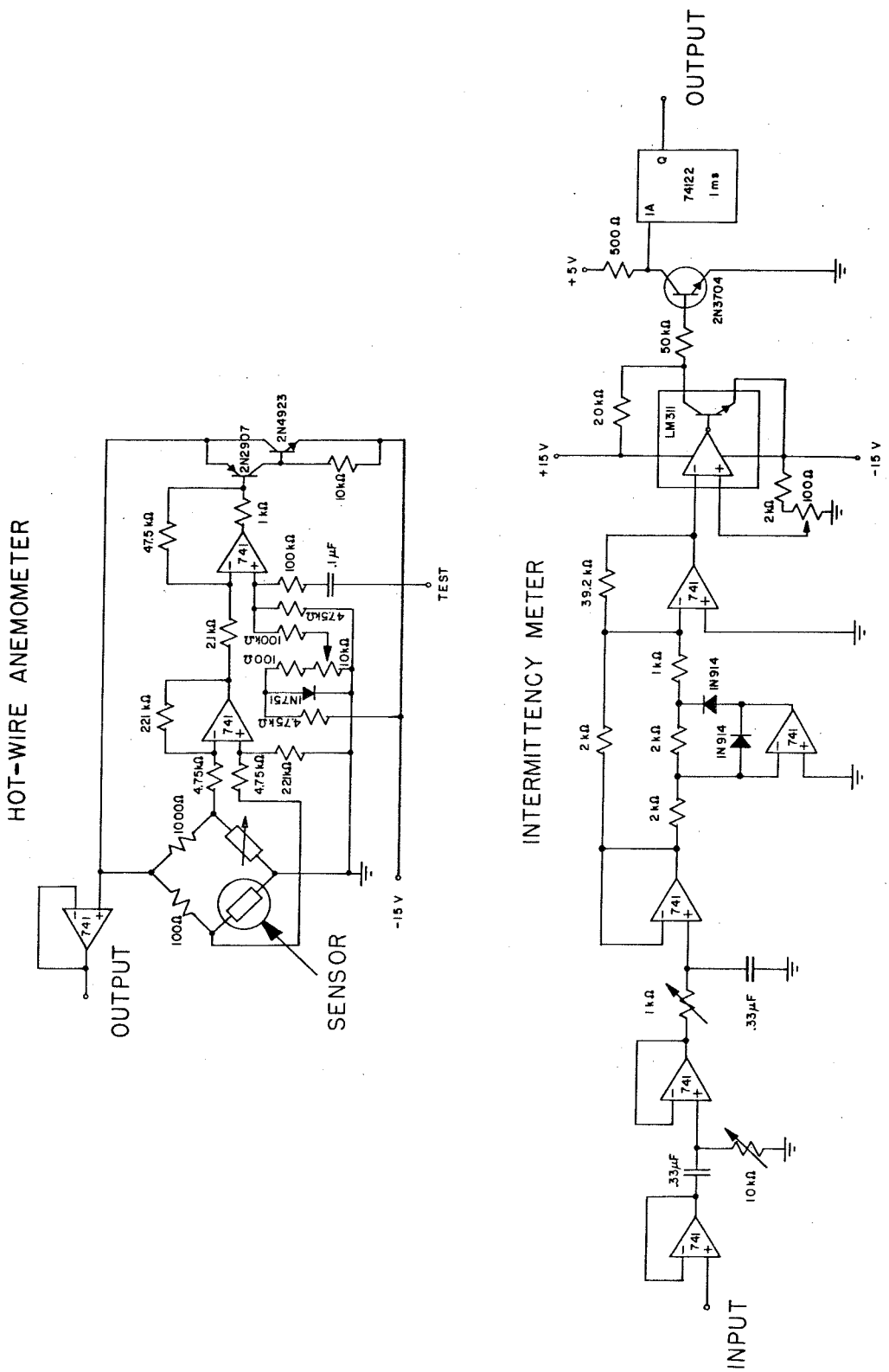

Figure 13. Circuit diagram for hot-wire anemometers. Top: constant-temperature bridge circuit. Bottom: intermittency circuit.

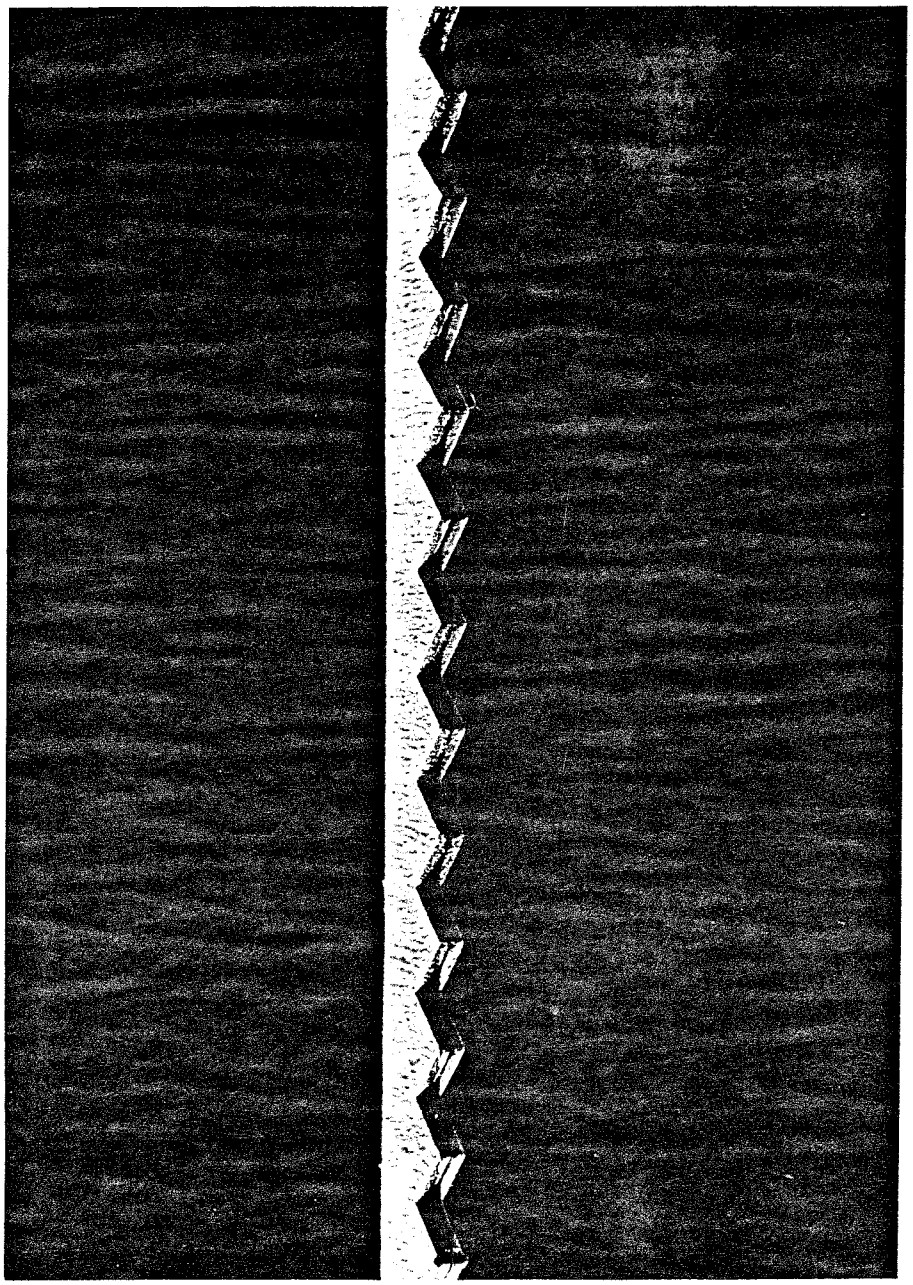

Figure 14. Serrated-tape tripping device attached to plate, looking downstream. Pitch is 0.64 cm. Tape thickness of 0.085 cm appears doubled by reflection from plate surface.

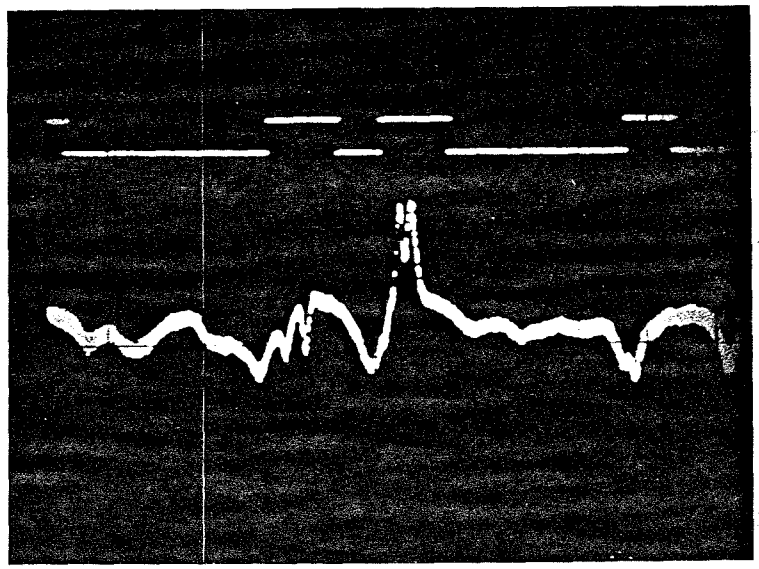

(a)

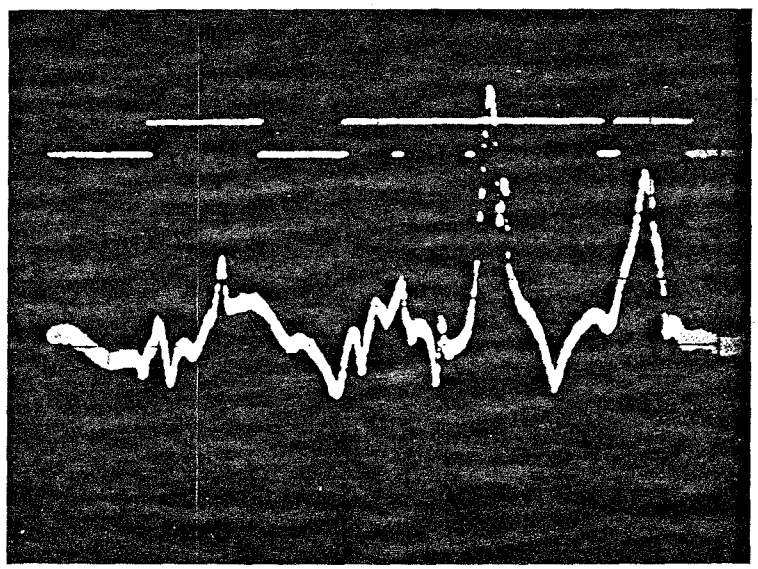

(b)

Figure 15. Two samples of hot-wire anemometer analog outputs and associated intermittency signals for boundary layer tripped by device shown in Figure 14. Sweep time = 2 ms/division, U = 10 m/s, x = 117.8 cm, y = 2.02 cm.

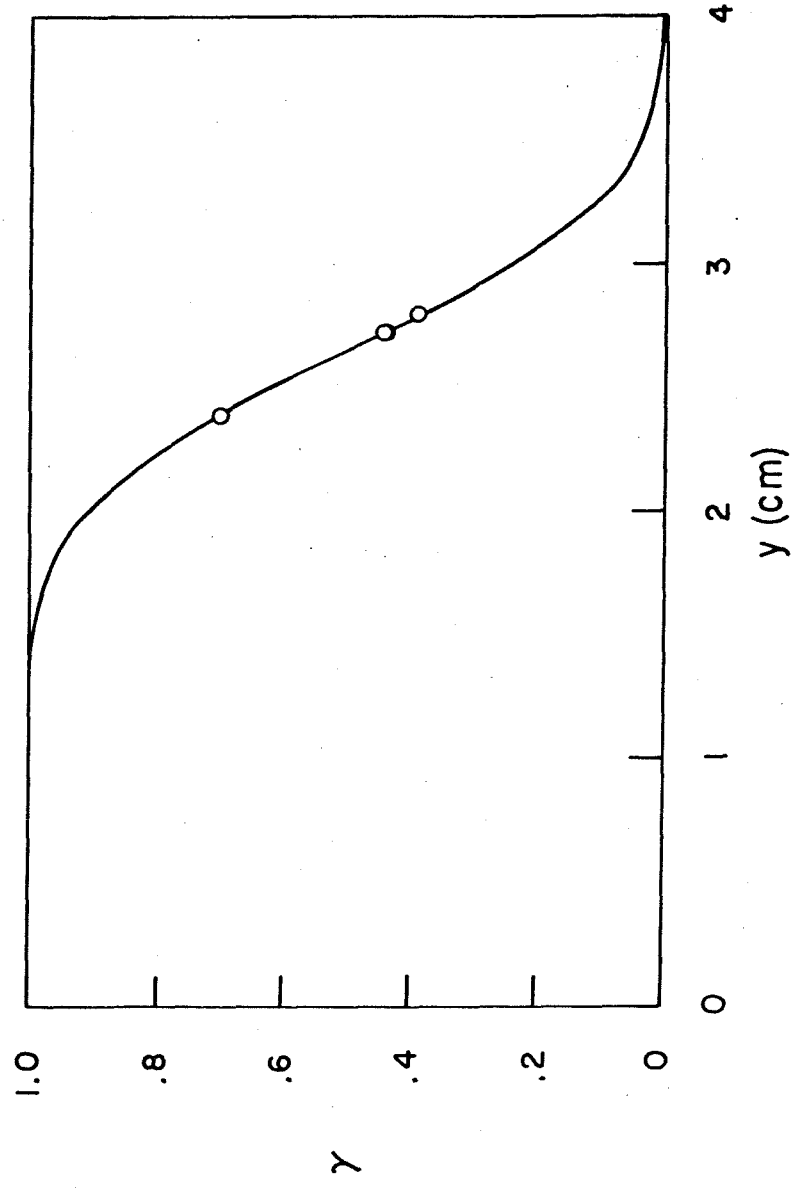

Figure 16. Distribution of intermittency in turbulent boundary layer generated by trip shown in Figure 14, with $U = 10$ m/s, $x = 178.8$ cm. Fitted curve is Gaussian, after Klebanoff (1954), with $\delta = 3.4$ cm.

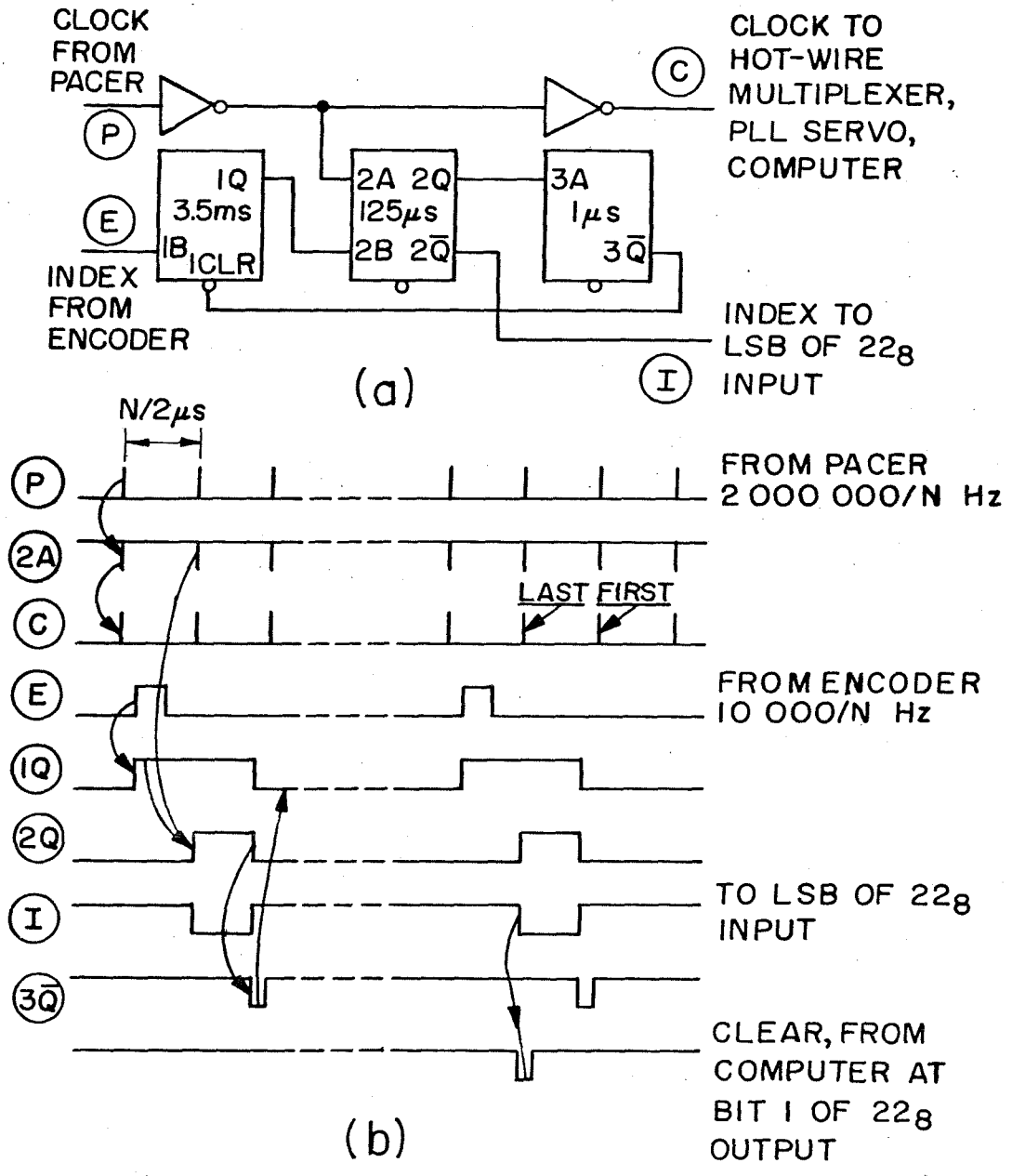

Figure 17. Timing of data acquisition. Circled labels for signal traces in timing diagram correspond to wire or pin labels in circuit diagram.

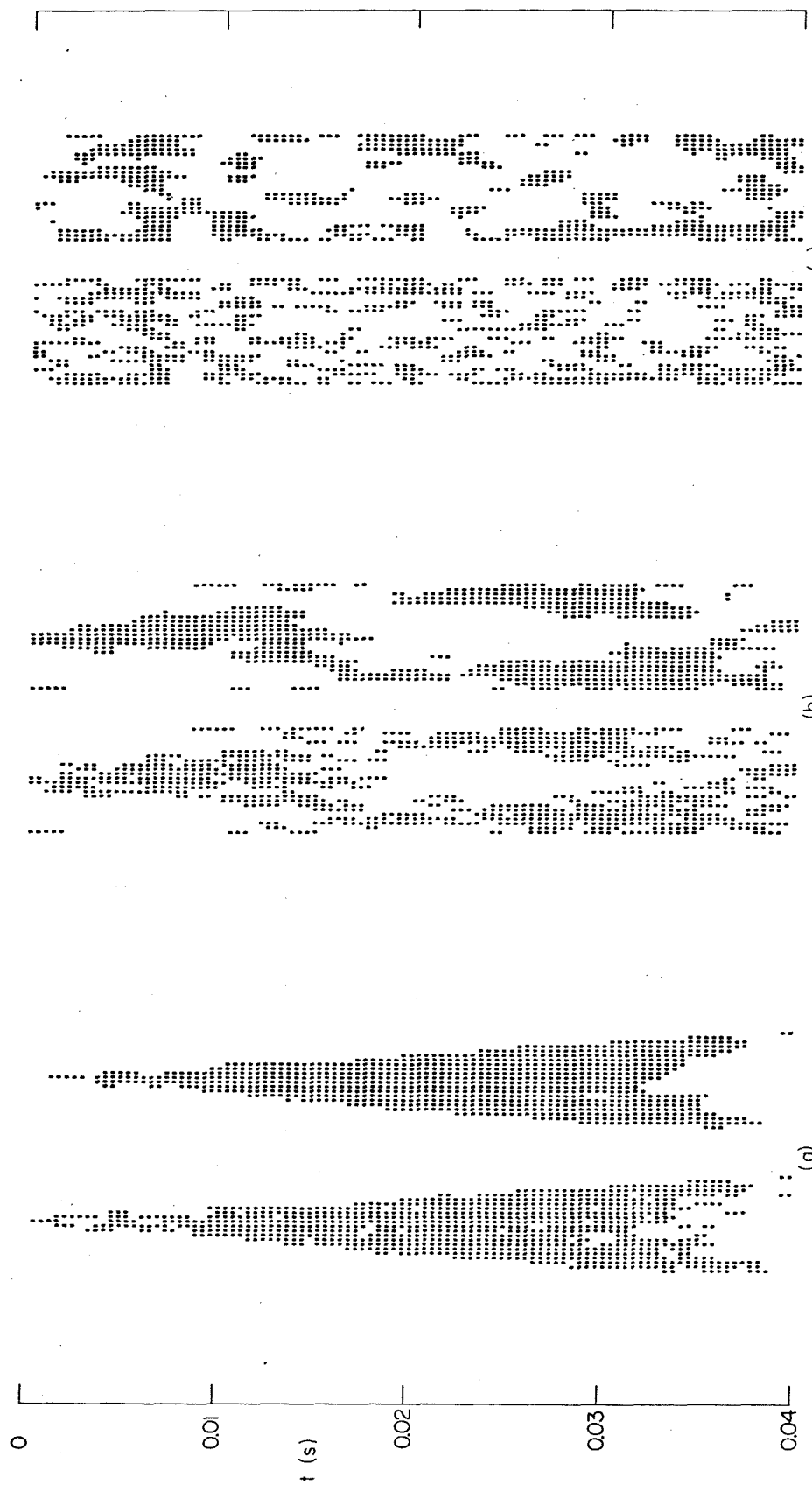

Figure 18. Typical unfiltered and filtered raw intermittency data for U = 10 m/s, x = 87.3 cm.
(a) spot; y = 1.02 cm, N = 800 (Run 538)
(b) synthetic boundary layer; y = 1.36 cm, 12.2-cm cam, N = 800, (Run 117)
(c) tripped boundary layer; y = 1.70 cm.

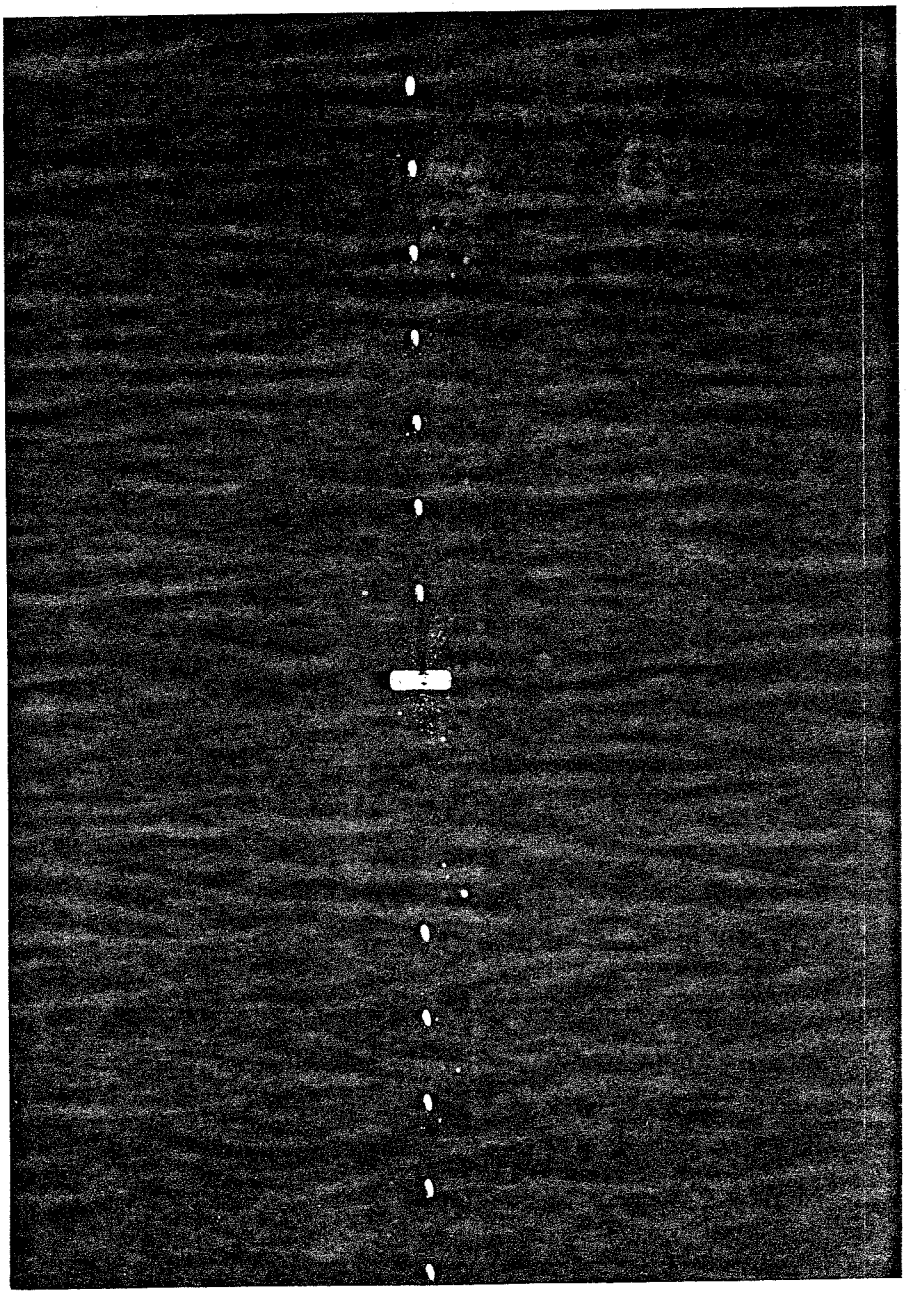

Figure 19. View of center pin displaced into flow with other pins retracted. Note missing pins above bearing block.

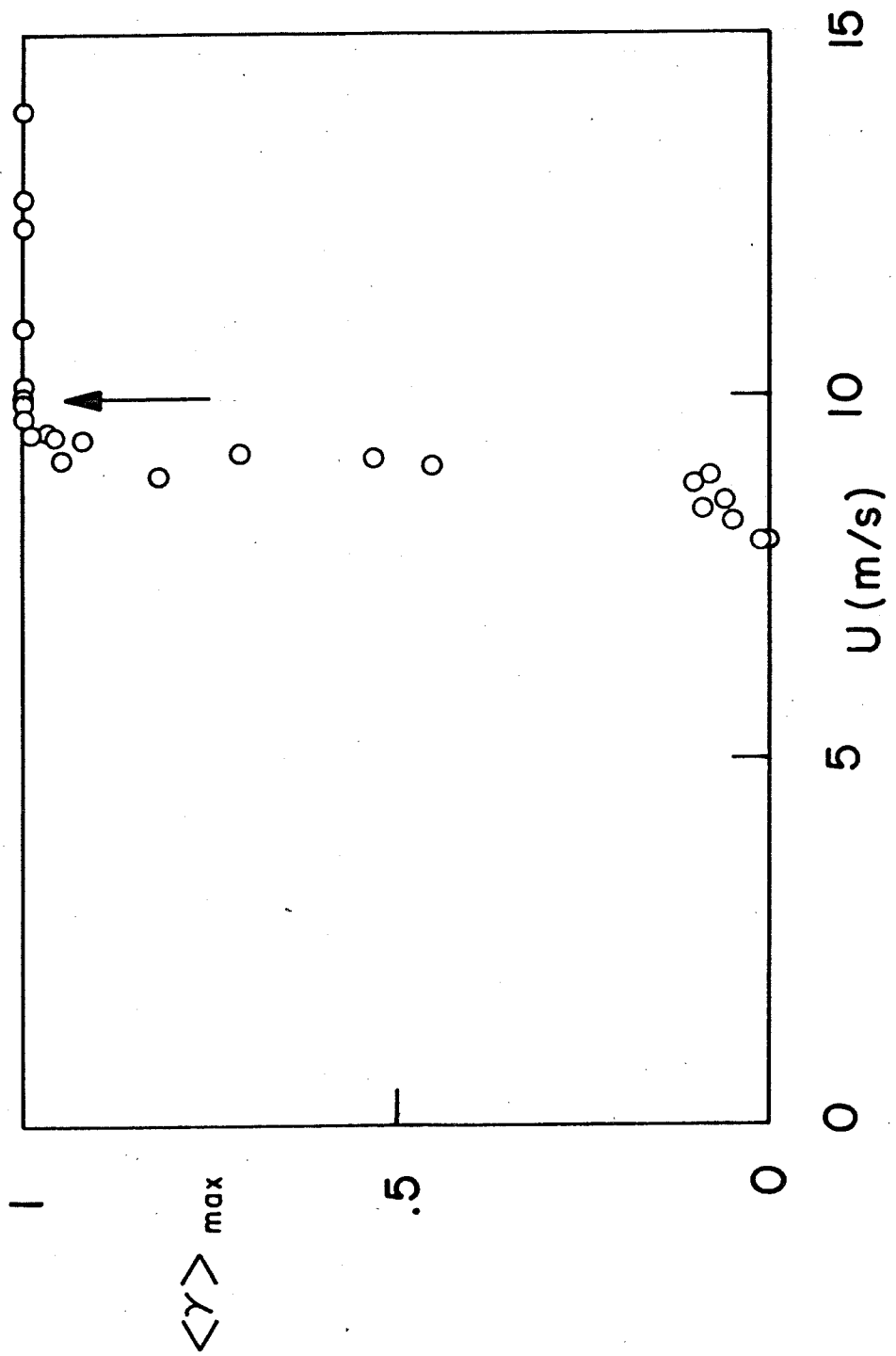

Figure 20. Probability of generating a spot with 0.165-cm pin displacement as a function of free-stream speed U. Arrow indicates standard operating point at U = 10 m/s.

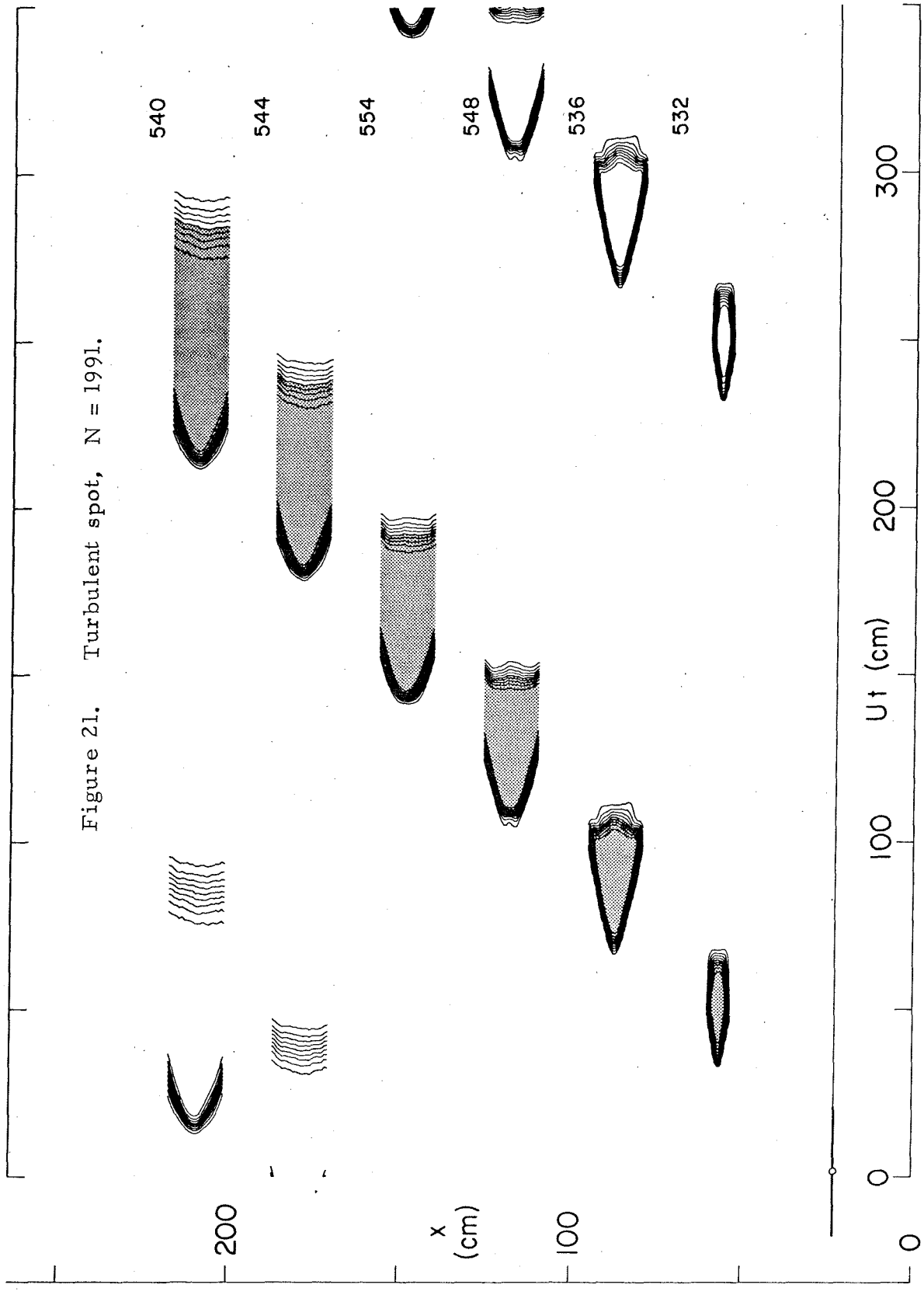

Figure 21. Turbulent spot, N = 1991.

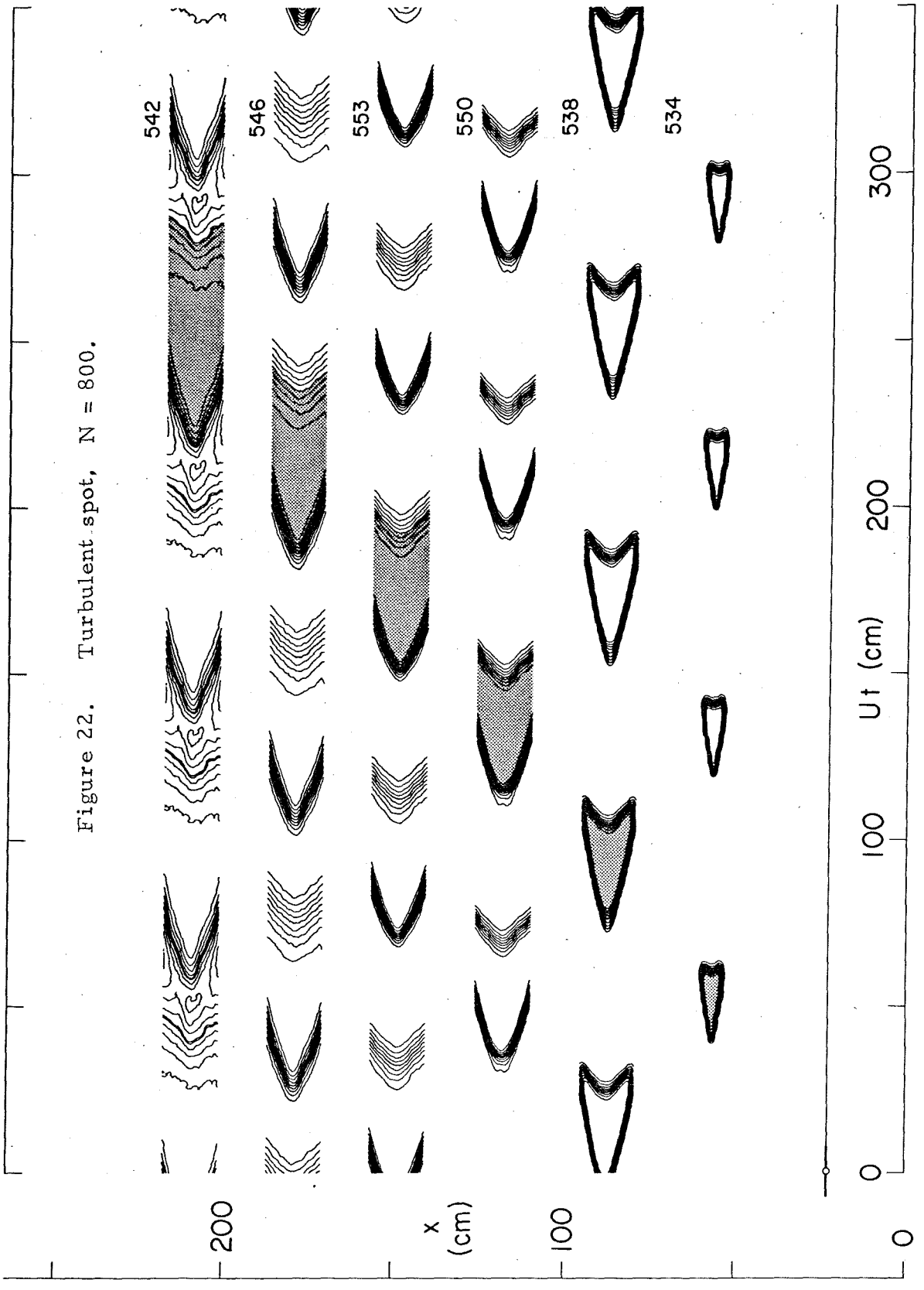

Figure 22. Turbulent spot, N = 800.

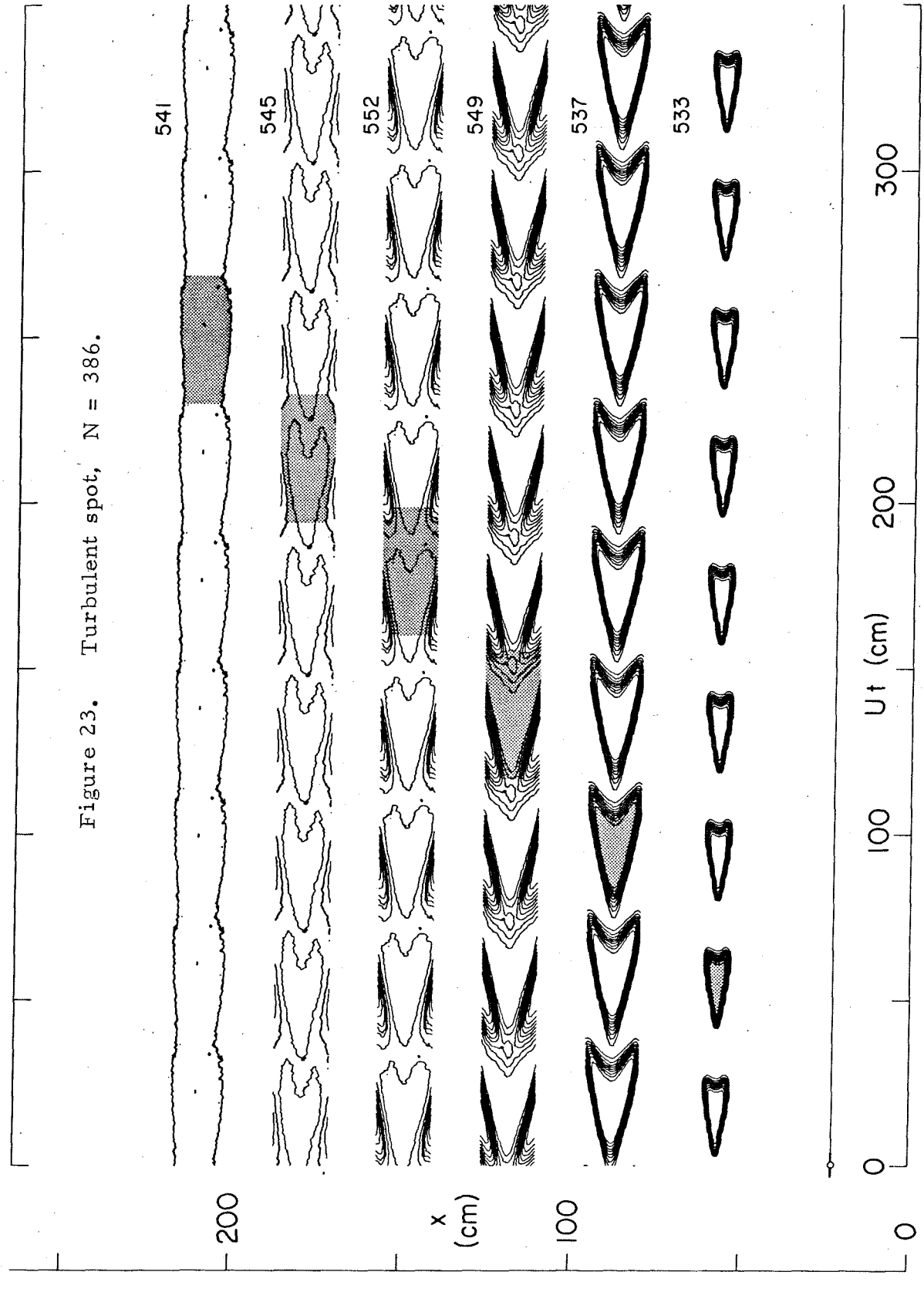

Figure 23. Turbulent spot, N = 386.

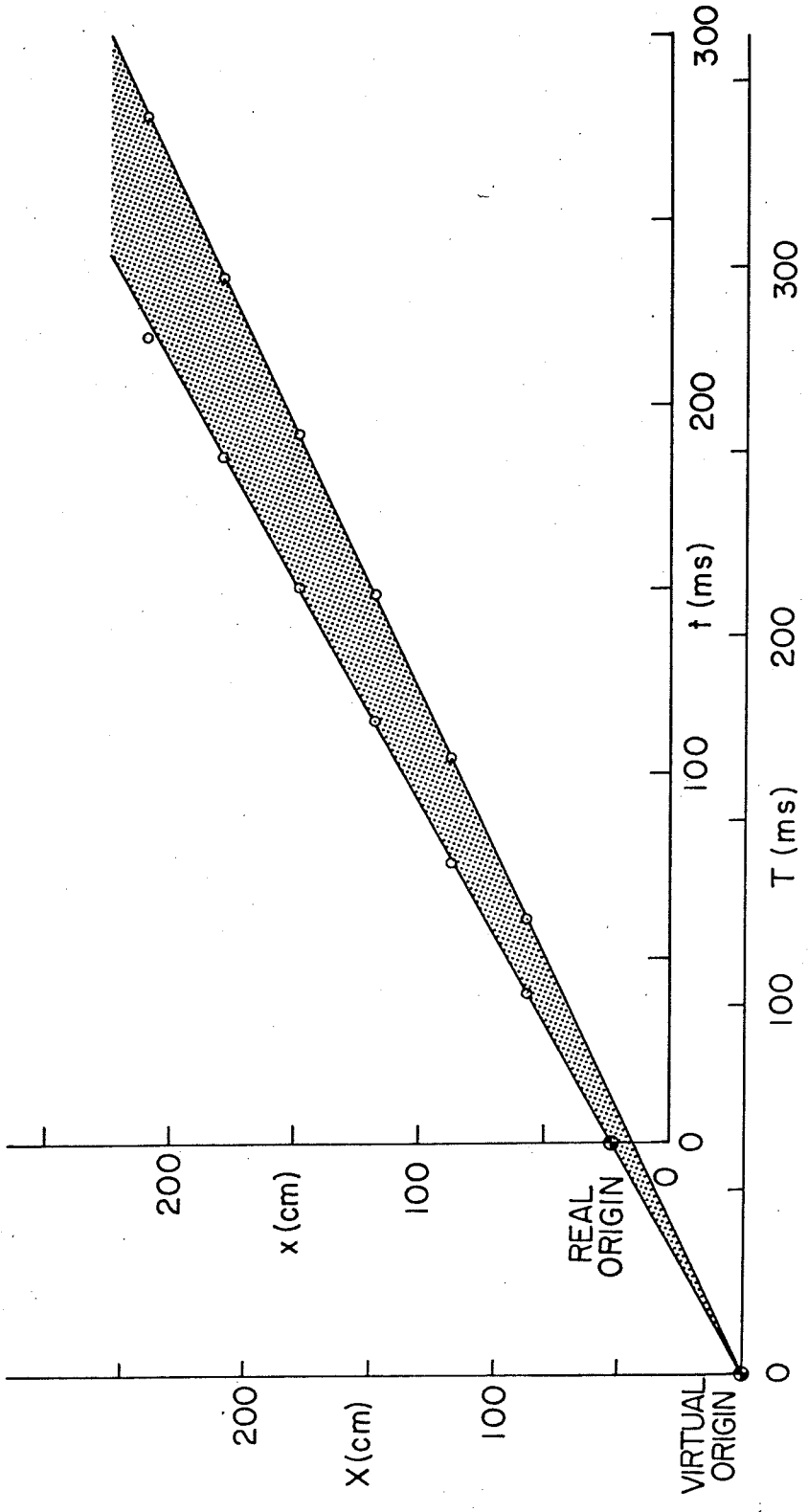

Figure 24. Determination of phase velocities (celerities) for leading and trailing edge of spot. Virtual origin is at(-30 cm, -63 ms).

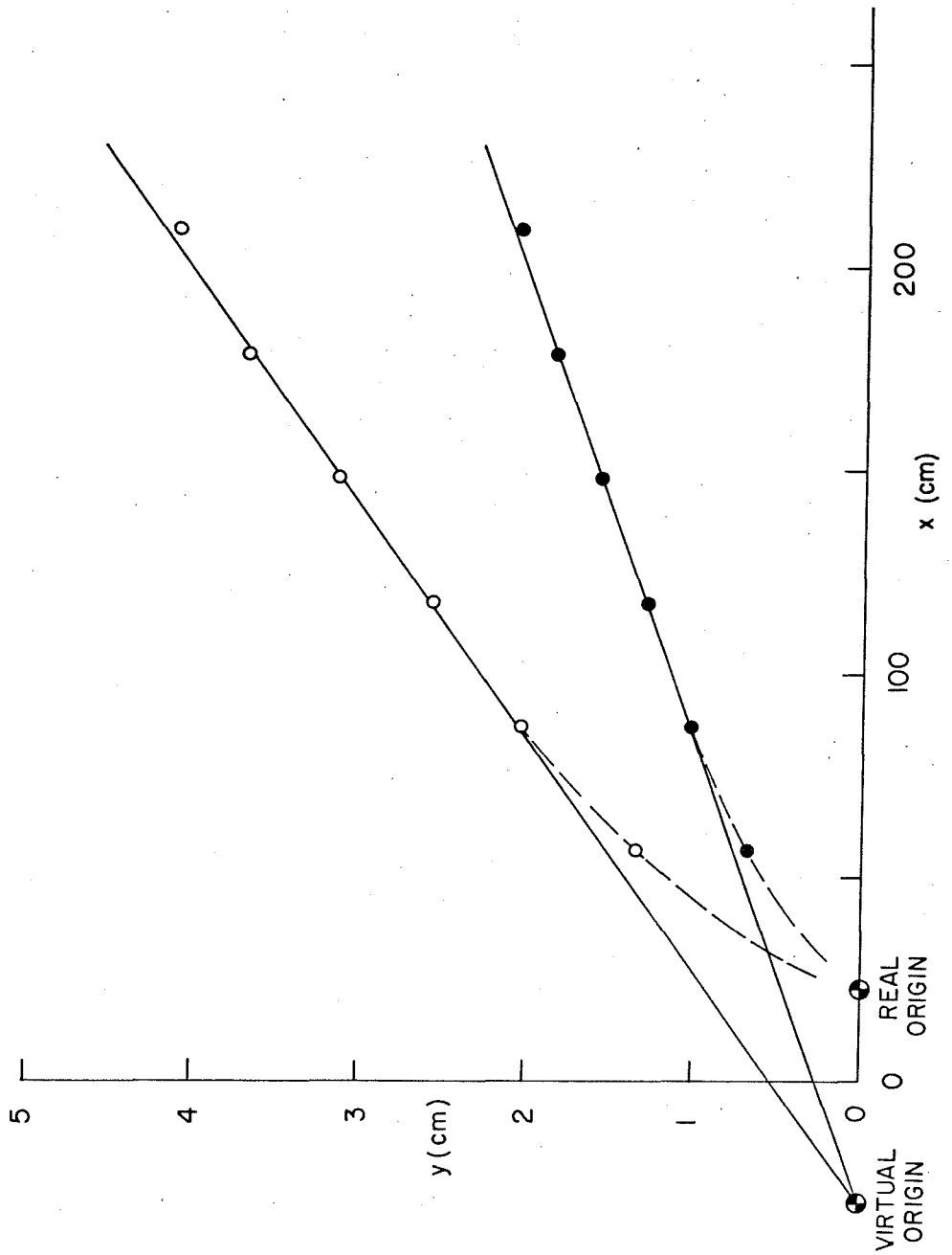

Figure 25. Virtual origin for growth of spot thickness. Open symbols: crest of spot. Solid symbols: half-height in spot. Virtual origin is at x_o = -30 cm.

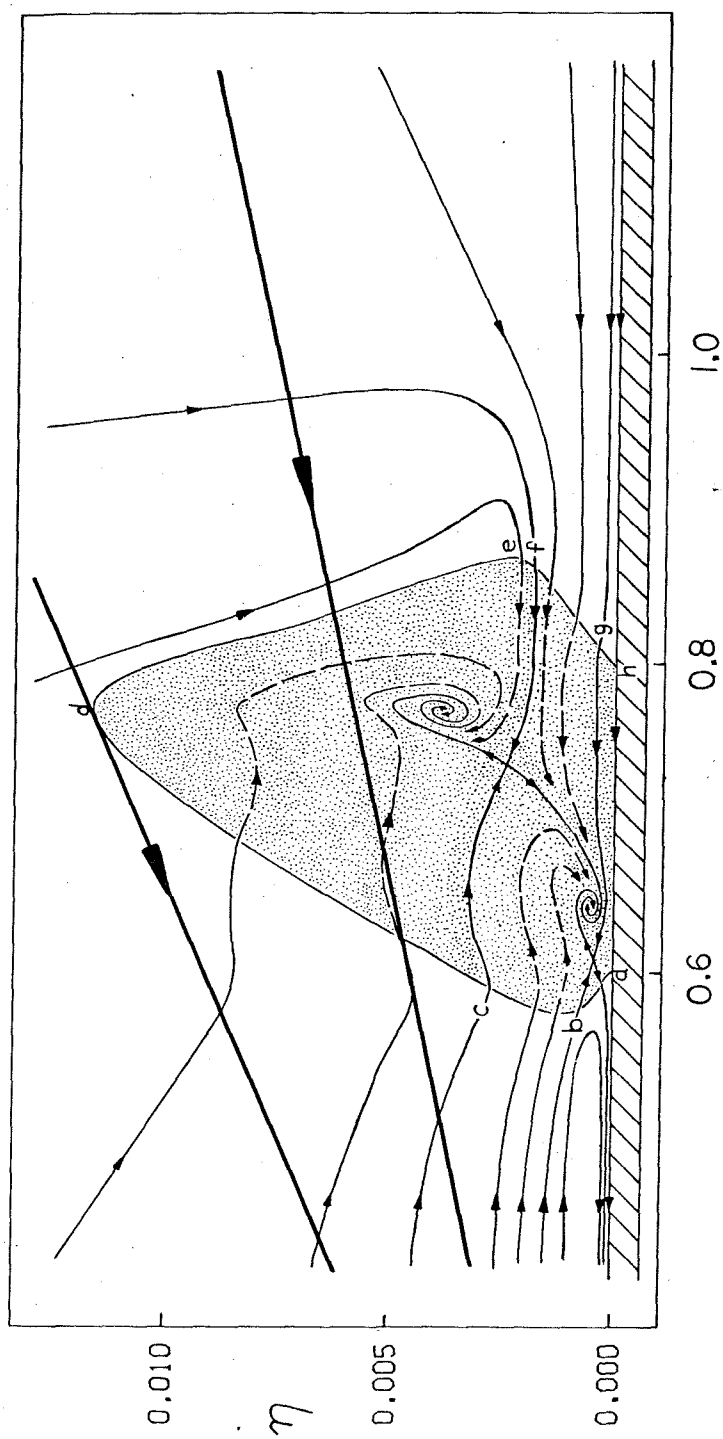

Figure 26. Rake trajectories in (ξ, η) plane with respect to cross-section of turbulent spot as defined by Cantwell et al. (1978). Upper ray at crest, lower ray at half-height.

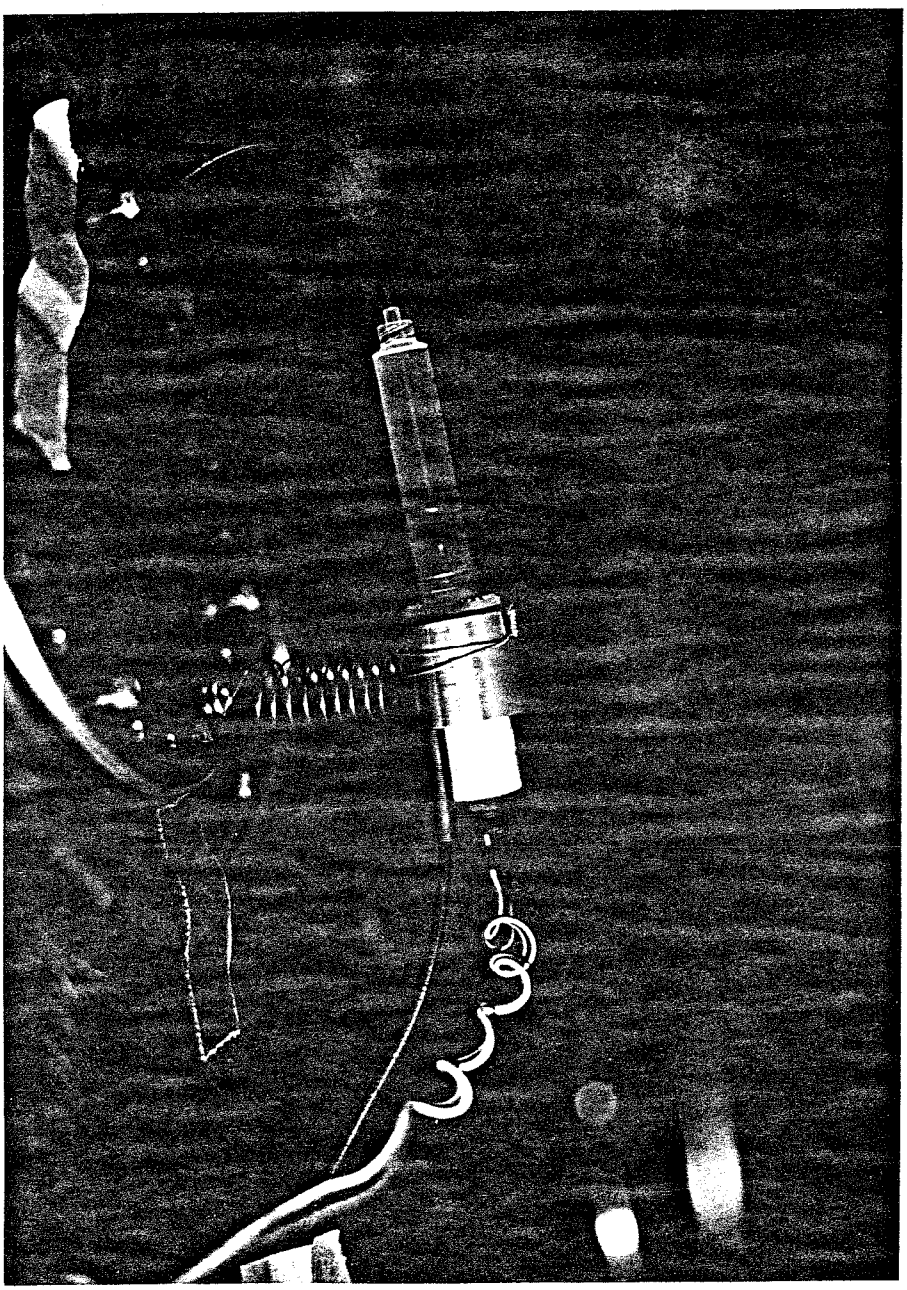

Figure 27. Pitran pressure transducer suspended under plate. Note syringe cavity and piston on signal side of transducer.

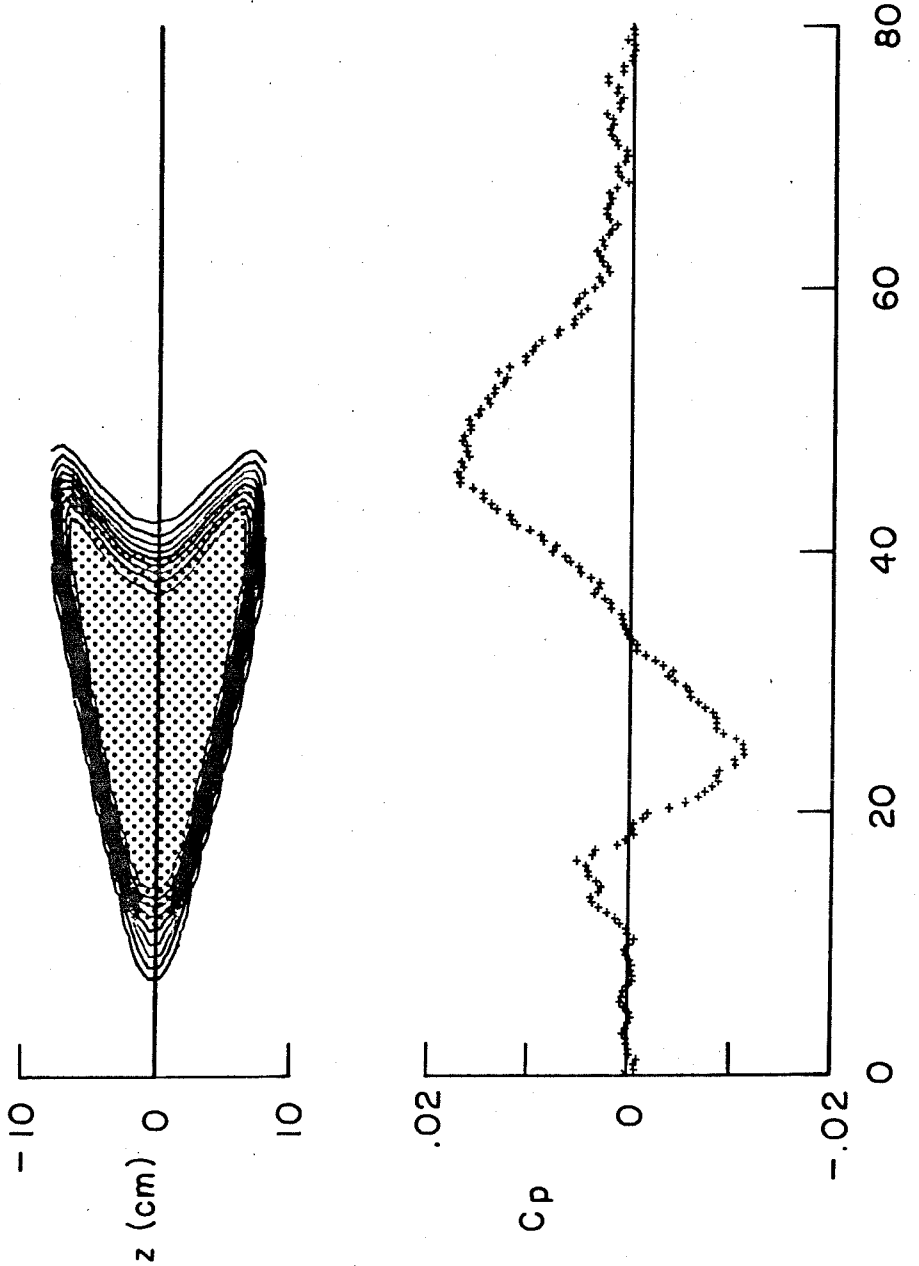

Figure 28. Bottom: ensemble-averaged surface-pressure signature in plane of symmetry of turbulent spot. Top: associated ensemble-averaged intermittency contours at half-height (cf. Run 538 in Figure 22).

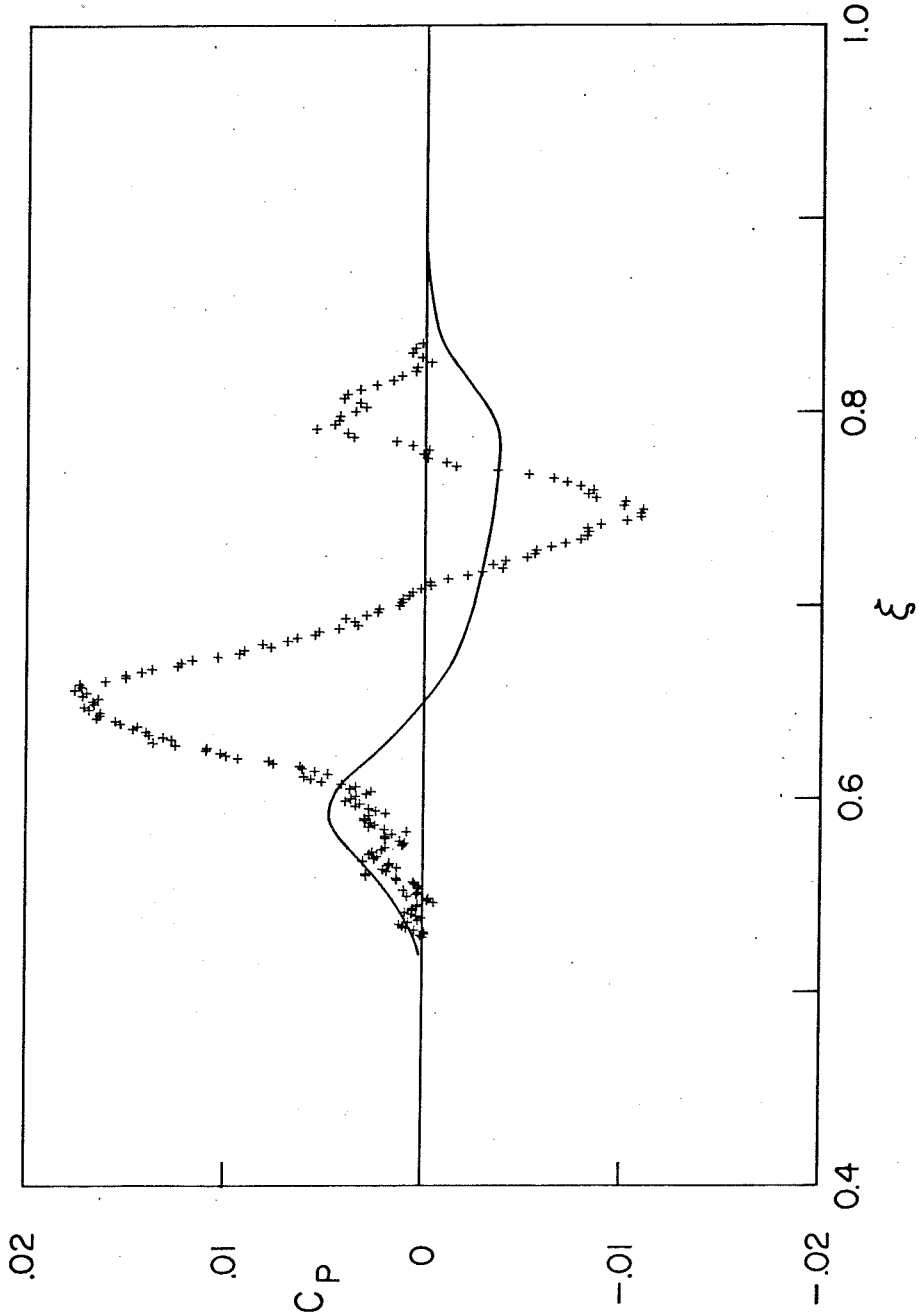

Figure 29. Comparison of present pressure measurement on surface (crosses) with indirect pressure measurement in free stream by Cantwell et al. (solid line). Data are the same as in Figure 28 but transformed to conical similarity coordinates for turbulent spot.

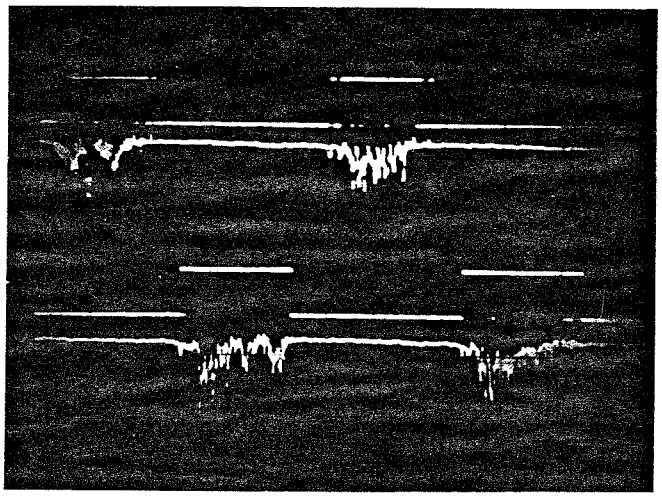

Figure 30. Examples of hot-wire analog outputs and associated intermittency signals in synthetic turbulent boundary layer. Flow is for 12.2-cm cam, N=1991, x = 56.9 cm, y = 0.63 cm (Run 190, Figure 34). Oscilloscope triggered at index pulse. Upper traces: hot-wire 13 (z = 0.38 cm). Lower traces: hot-wire 21 (z = 6.48 cm). One camshaft revolution is shown, at sweep rate of 20 ms/div.

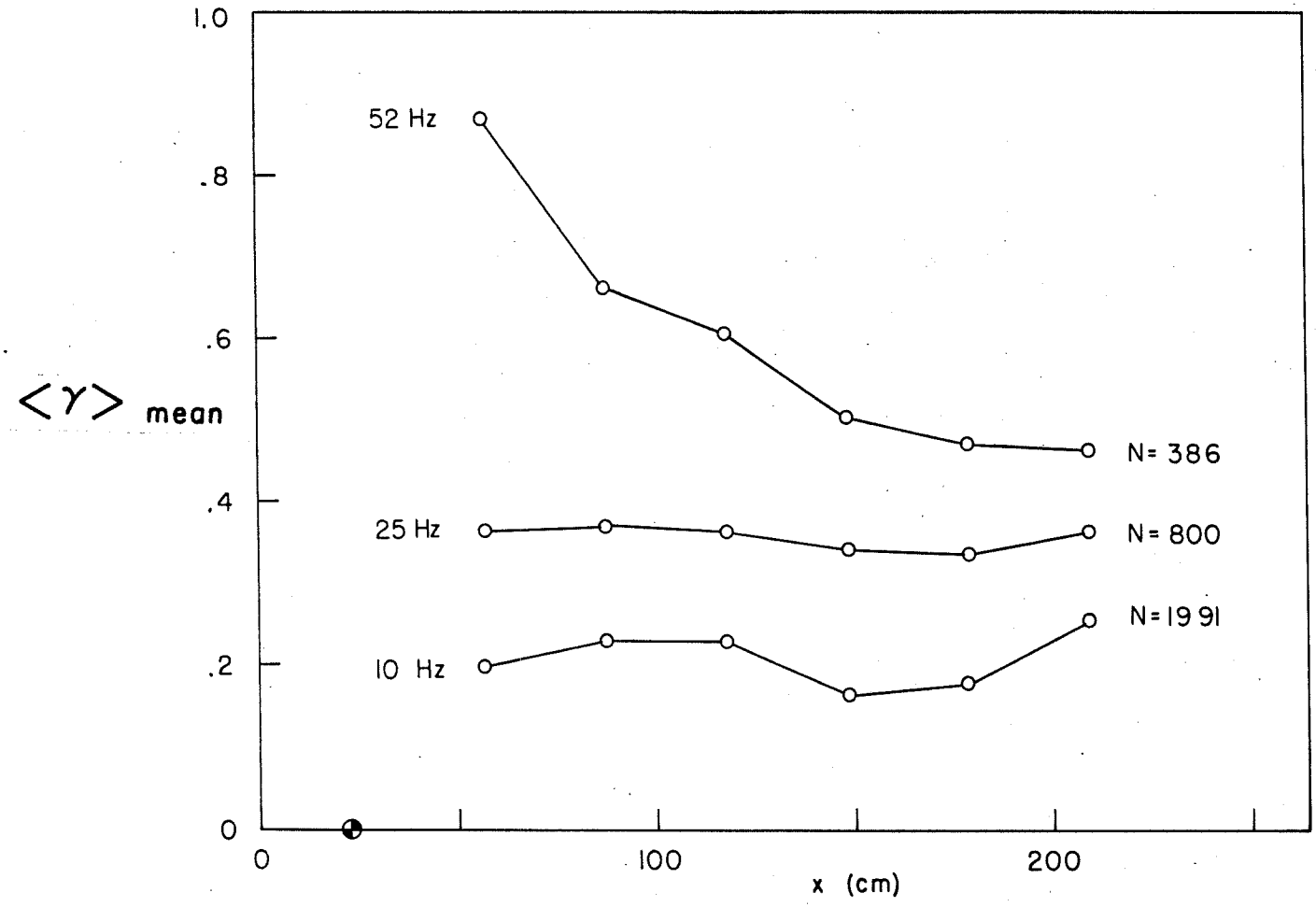

Figure 31. Variation of global intermittency as seen by rake for a constant disturbance frequency but different rake stations. Data are for 12.2-cm cam.

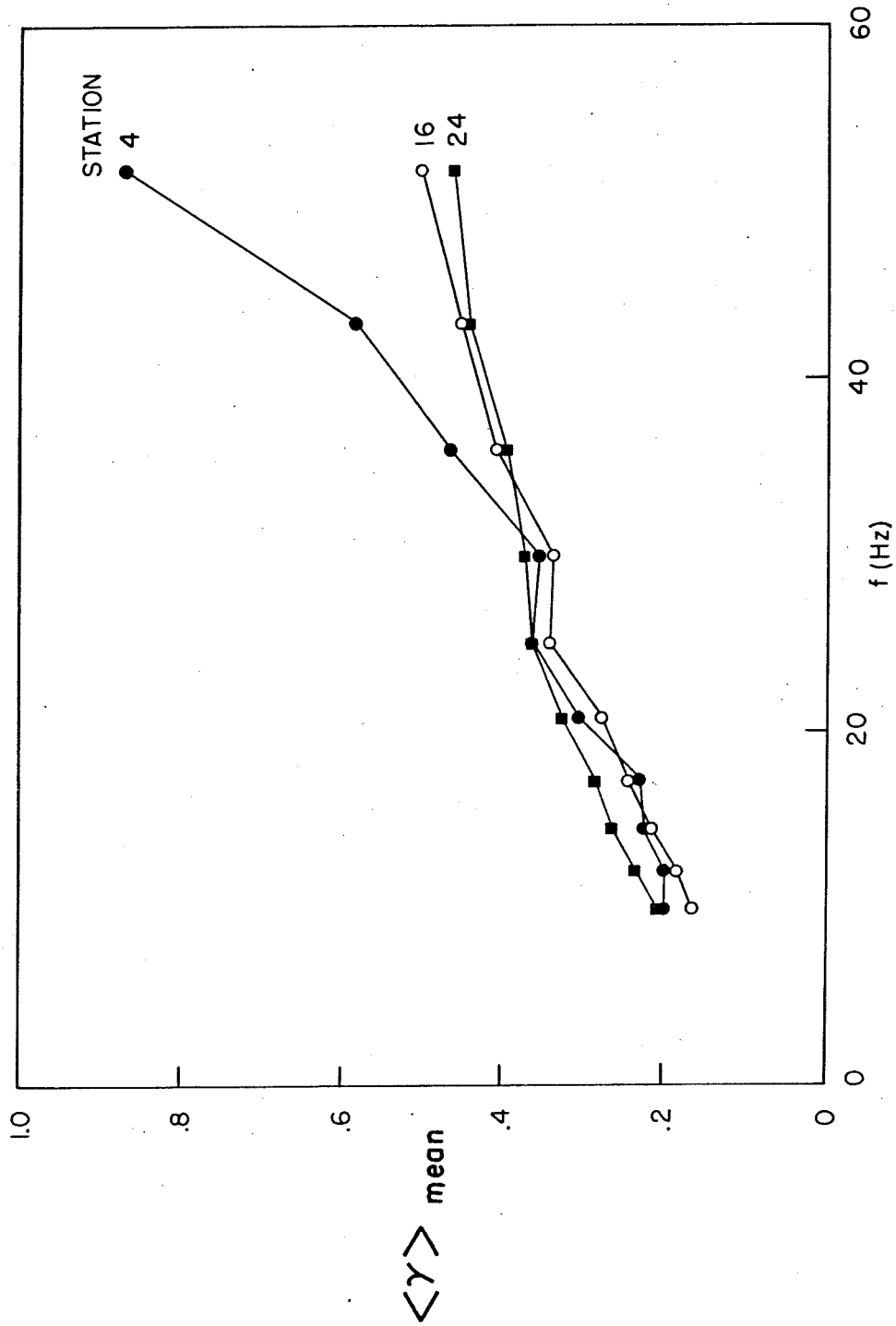

Figure 32. Variation of global intermittency as seen by rake for a fixed position in the flow but different disturbance frequencies. Data are for 12.2-cm cam (for stations, see Table II).

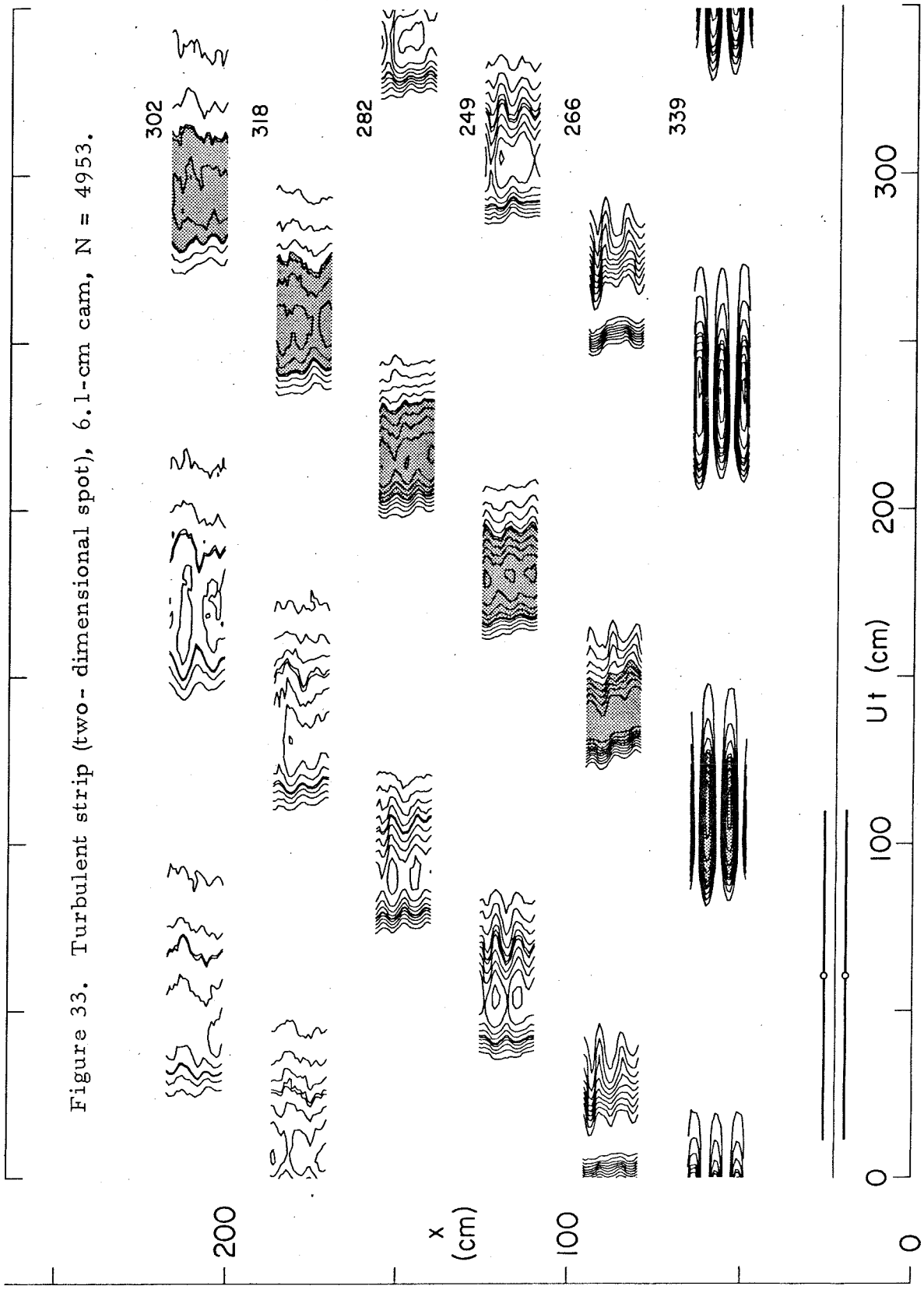

Figure 33. Turbulent strip (two- dimensional spot), 6.1-cm cam, N = 4953.

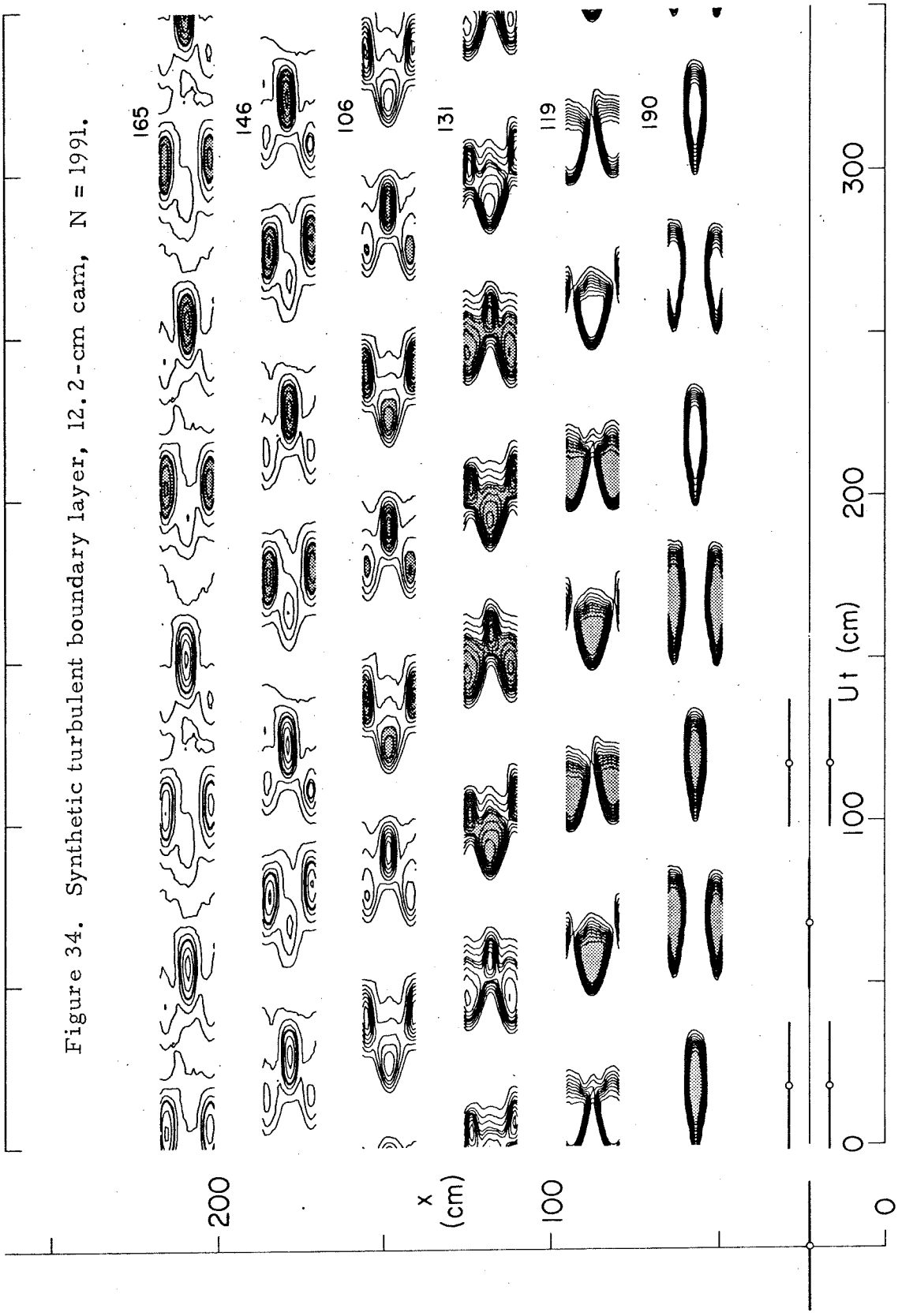

Figure 34. Synthetic turbulent boundary layer, 12.2-cm cam, N = 1991.

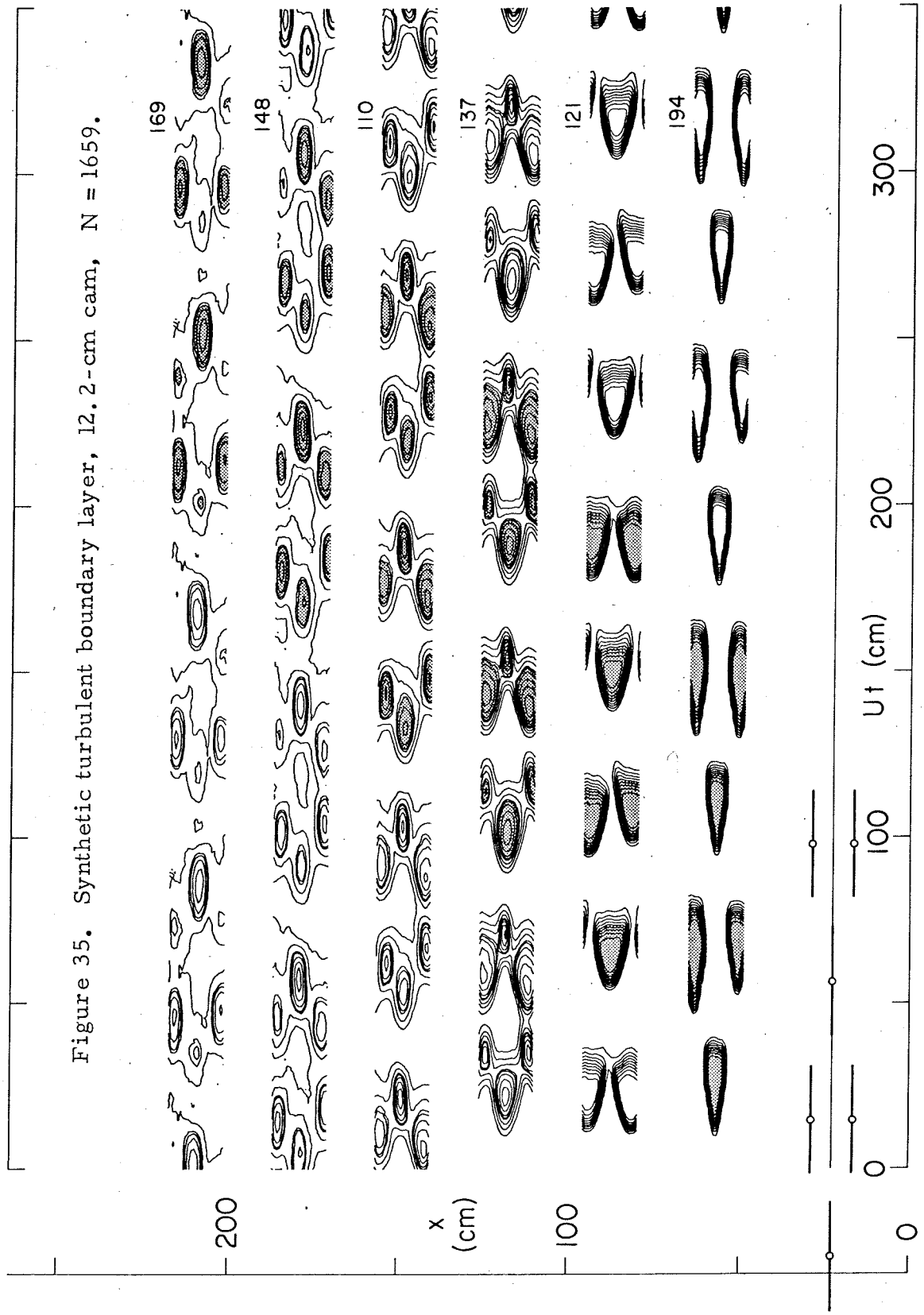

Figure 35. Synthetic turbulent boundary layer, 12.2-cm cam, N = 1659.

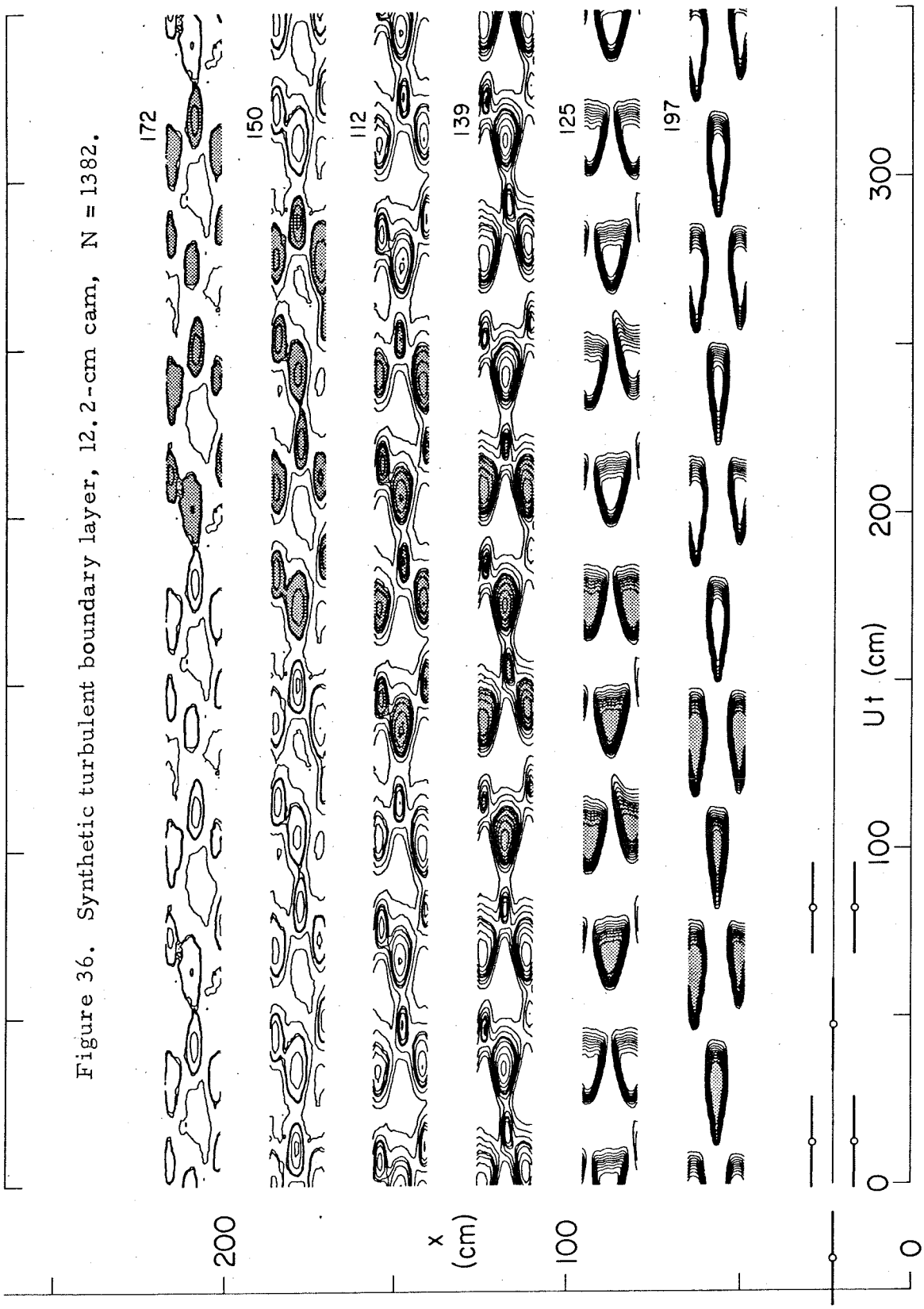

Figure 36. Synthetic turbulent boundary layer, 12.2-cm cam, N = 1382.

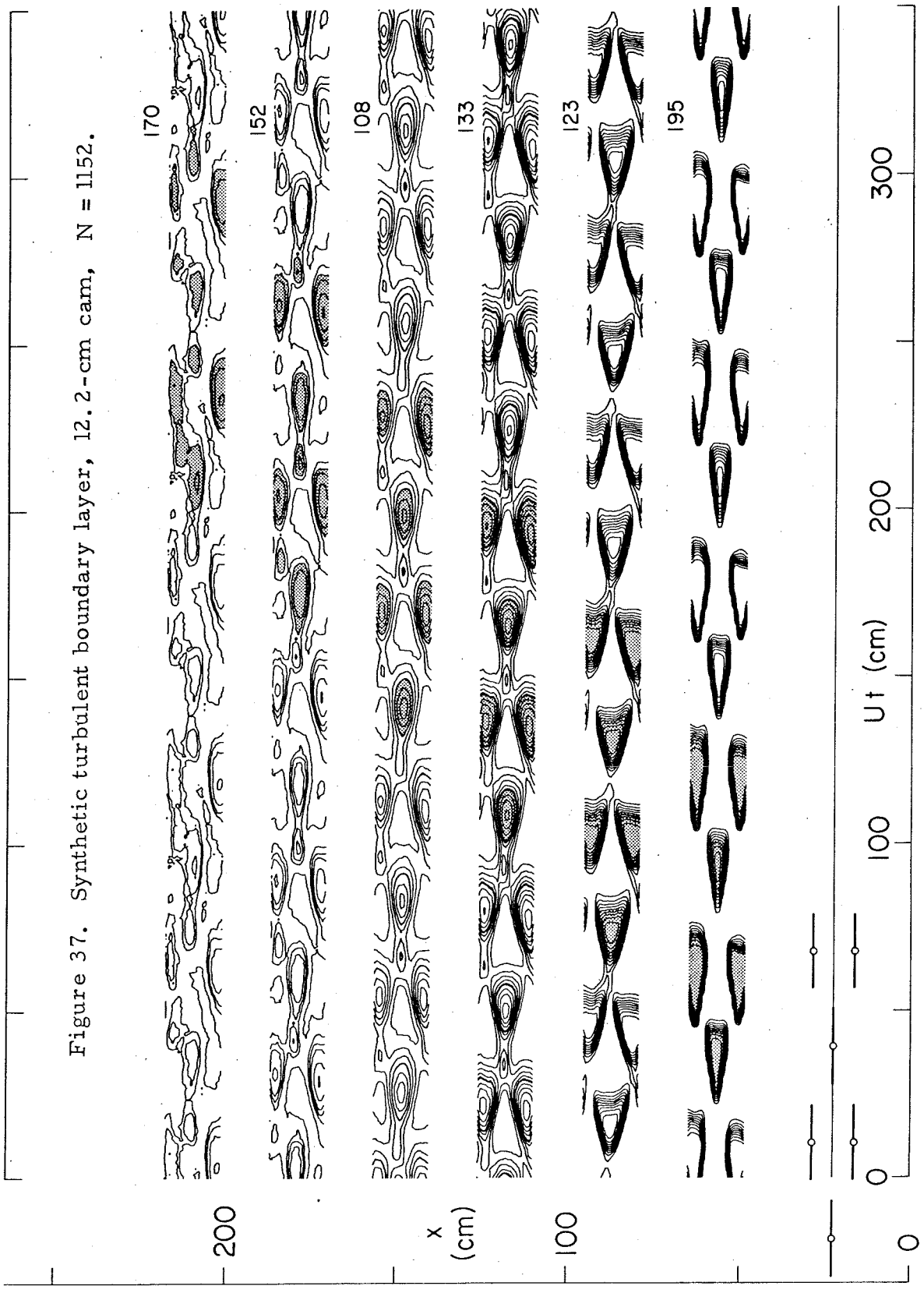

Figure 37. Synthetic turbulent boundary layer, 12.2-cm cam, N = 1152.

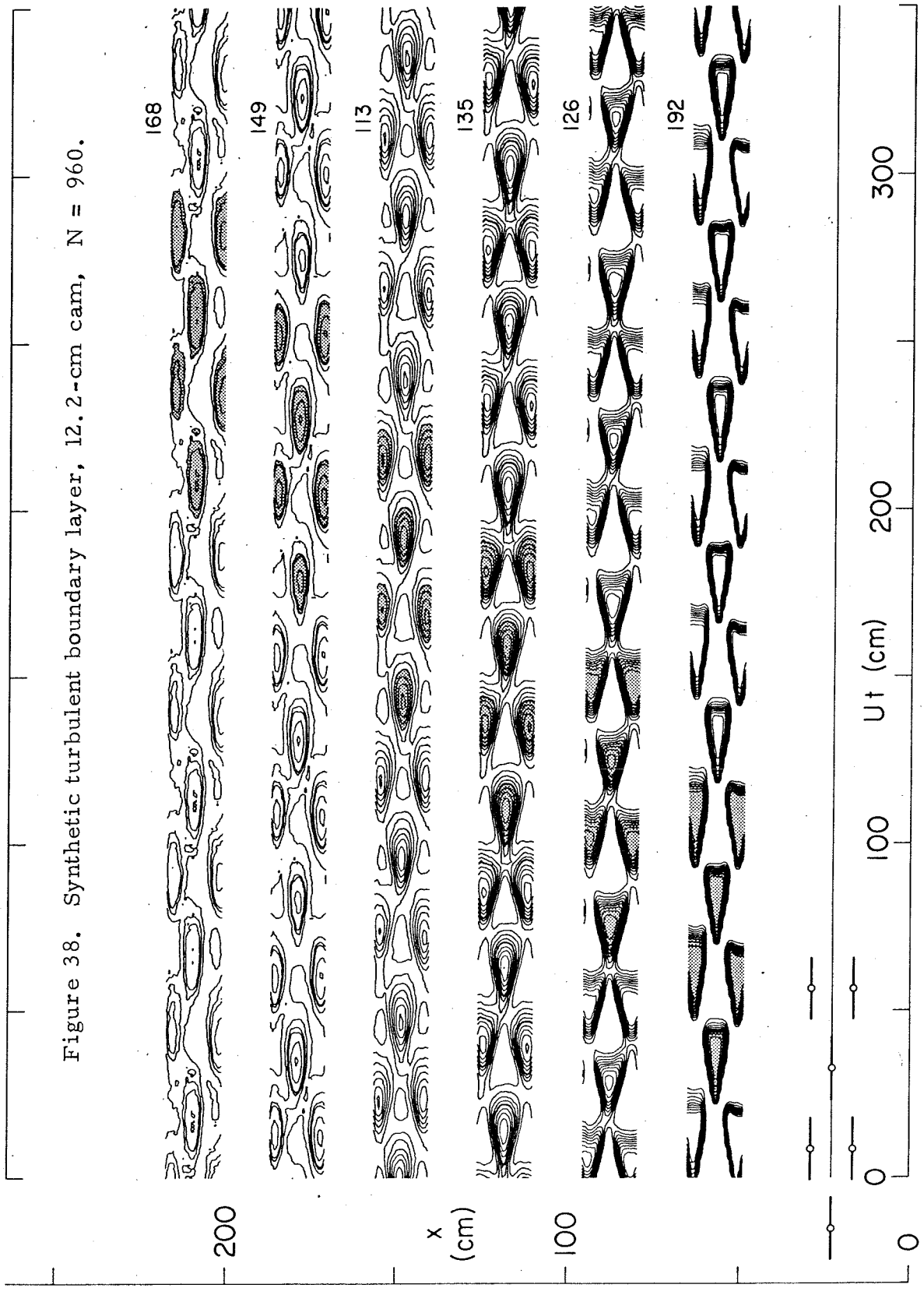

Figure 38. Synthetic turbulent boundary layer, 12.2-cm cam, N = 960.

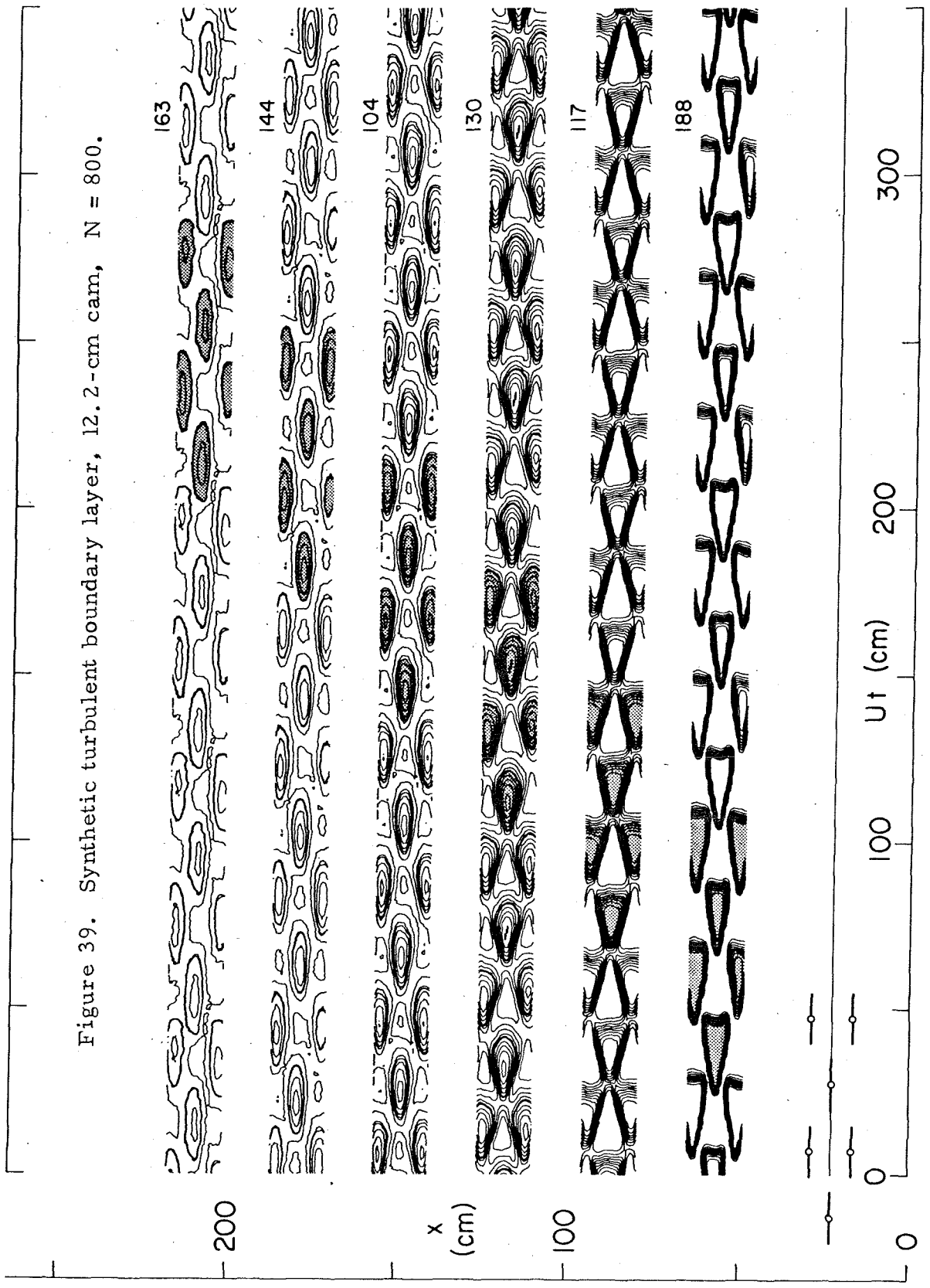

Figure 39. Synthetic turbulent boundary layer, 12.2-cm cam, N = 800.

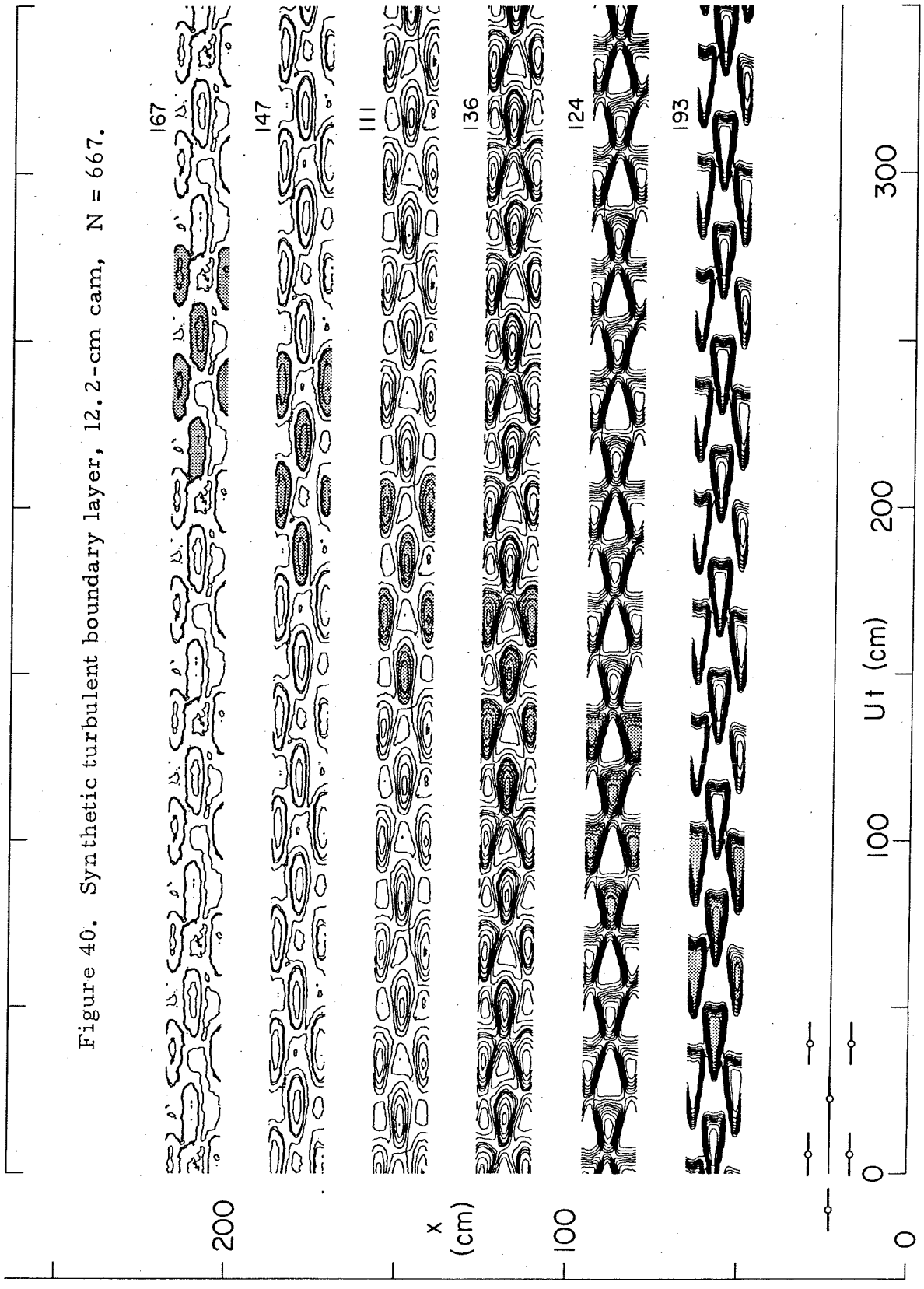

Figure 40. Synthetic turbulent boundary layer, 12.2-cm cam, N = 667.

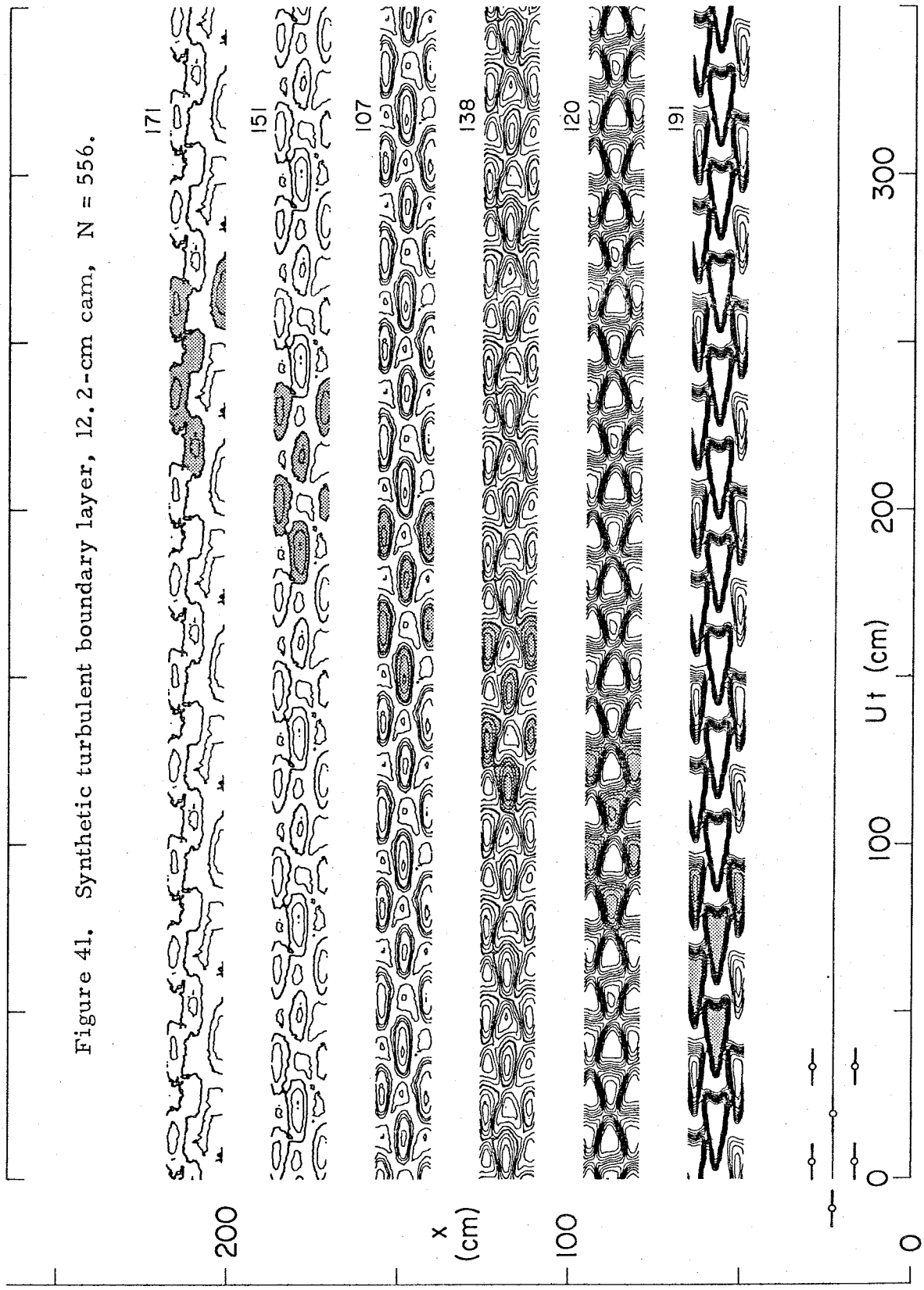

Figure 41. Synthetic turbulent boundary layer, 12.2-cm cam, N = 556.

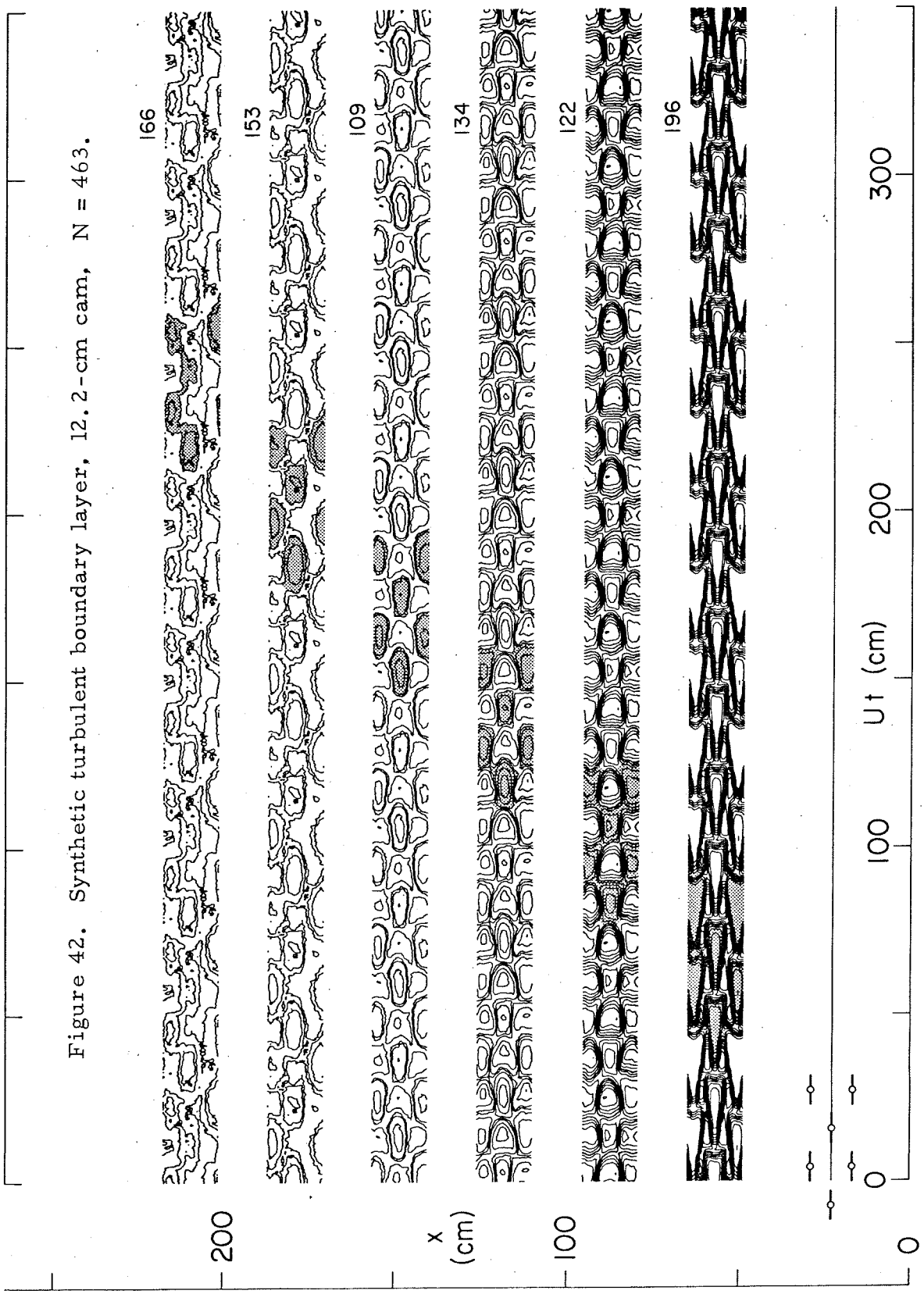

Figure 42. Synthetic turbulent boundary layer, 12.2-cm cam, N = 463.

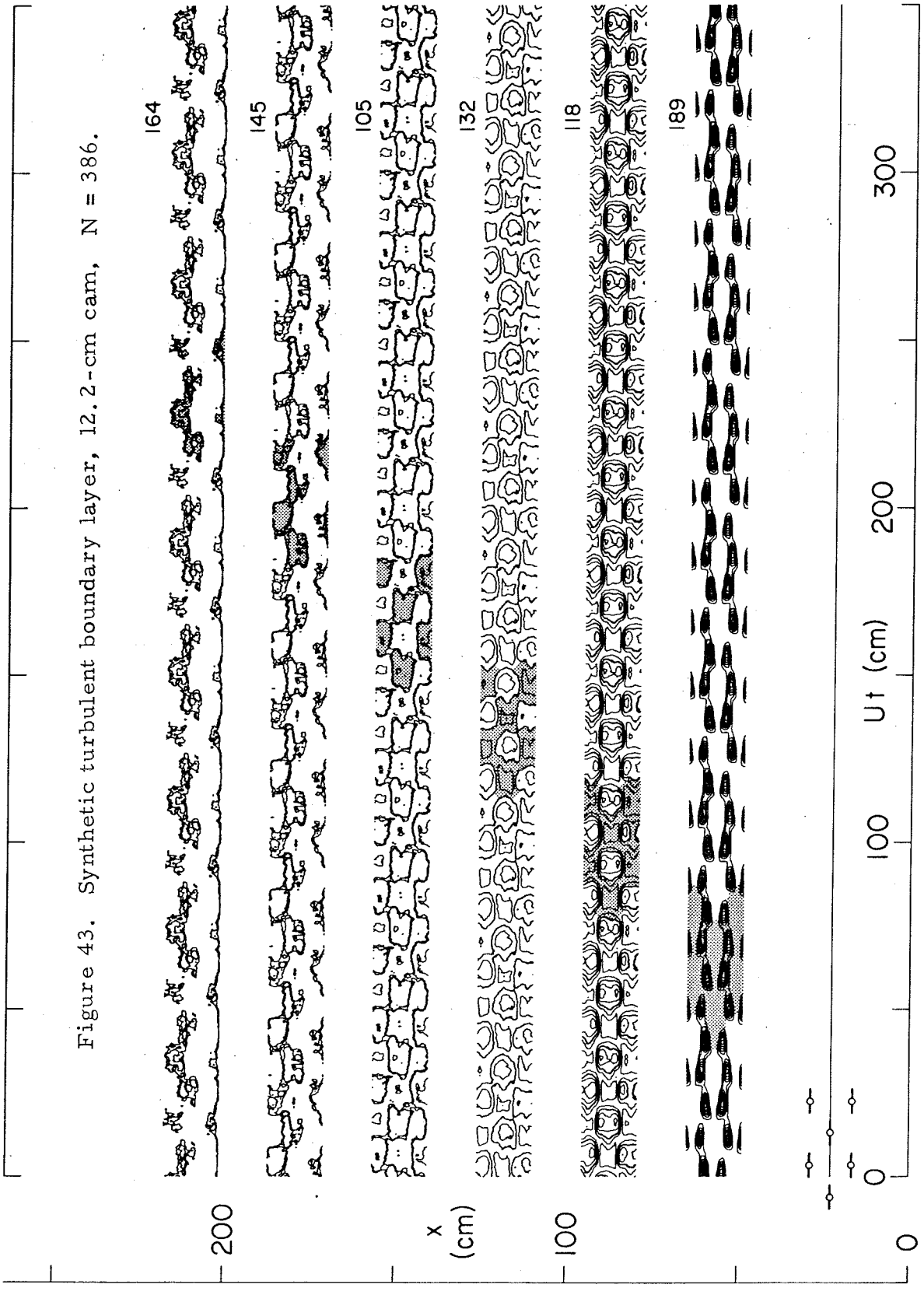

Figure 43. Synthetic turbulent boundary layer, 12.2-cm cam, N = 386.

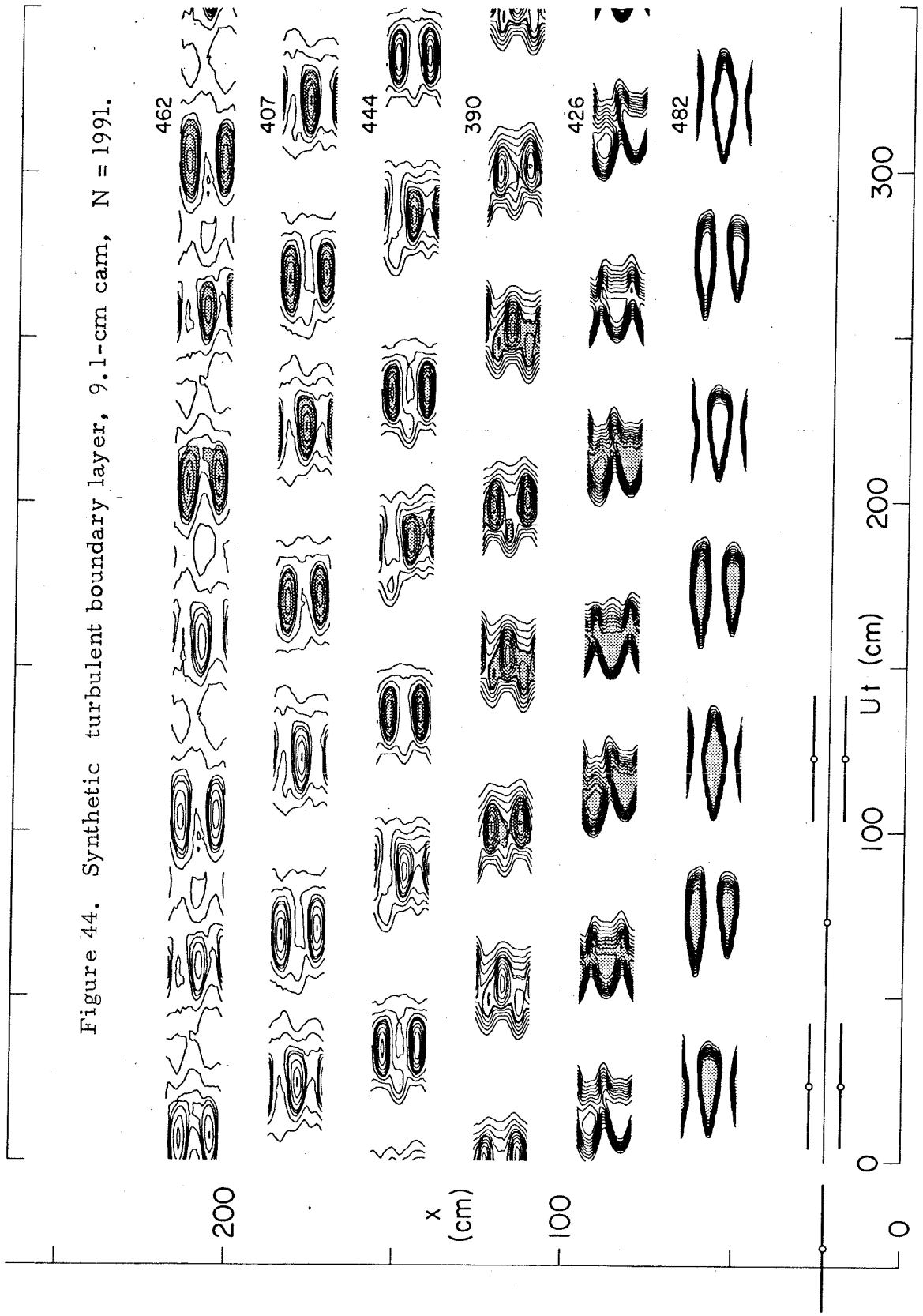

Figure 44. Synthetic turbulent boundary layer, 9.1-cm cam, N = 1991.

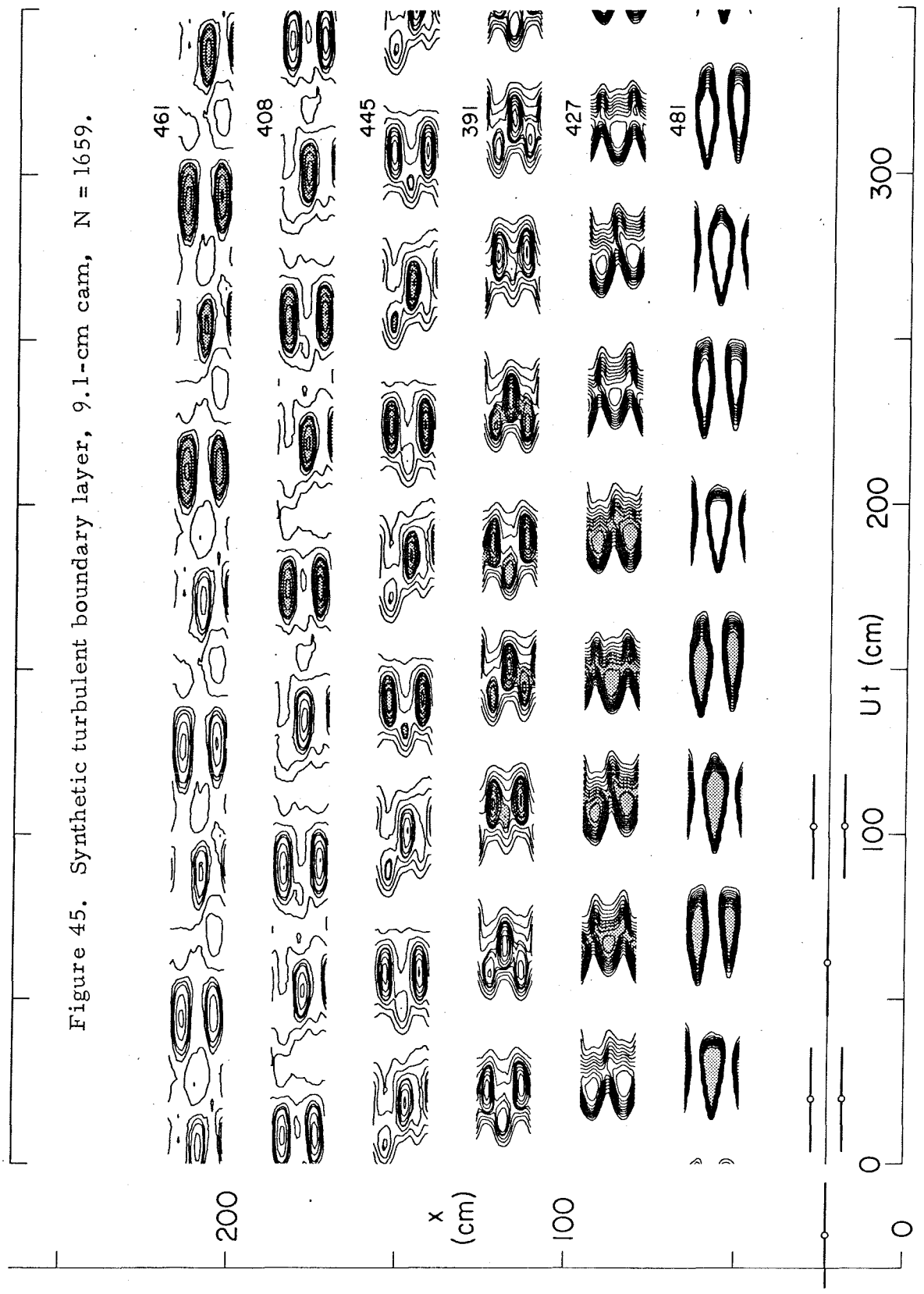

Figure 45. Synthetic turbulent boundary layer, 9.1-cm cam, N = 1659.

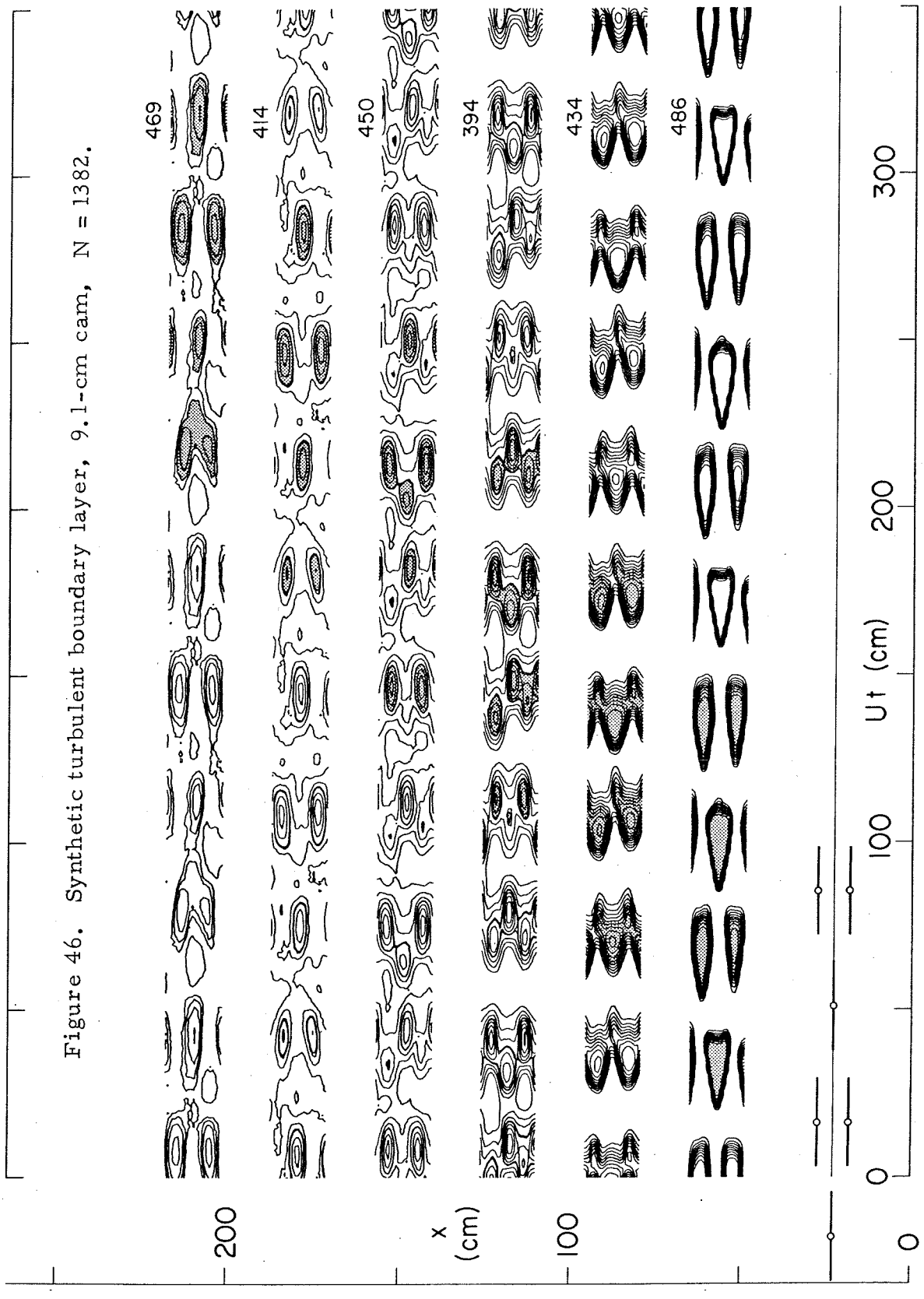

Figure 46. Synthetic turbulent boundary layer, 9.1-cm cam, N = 1382.

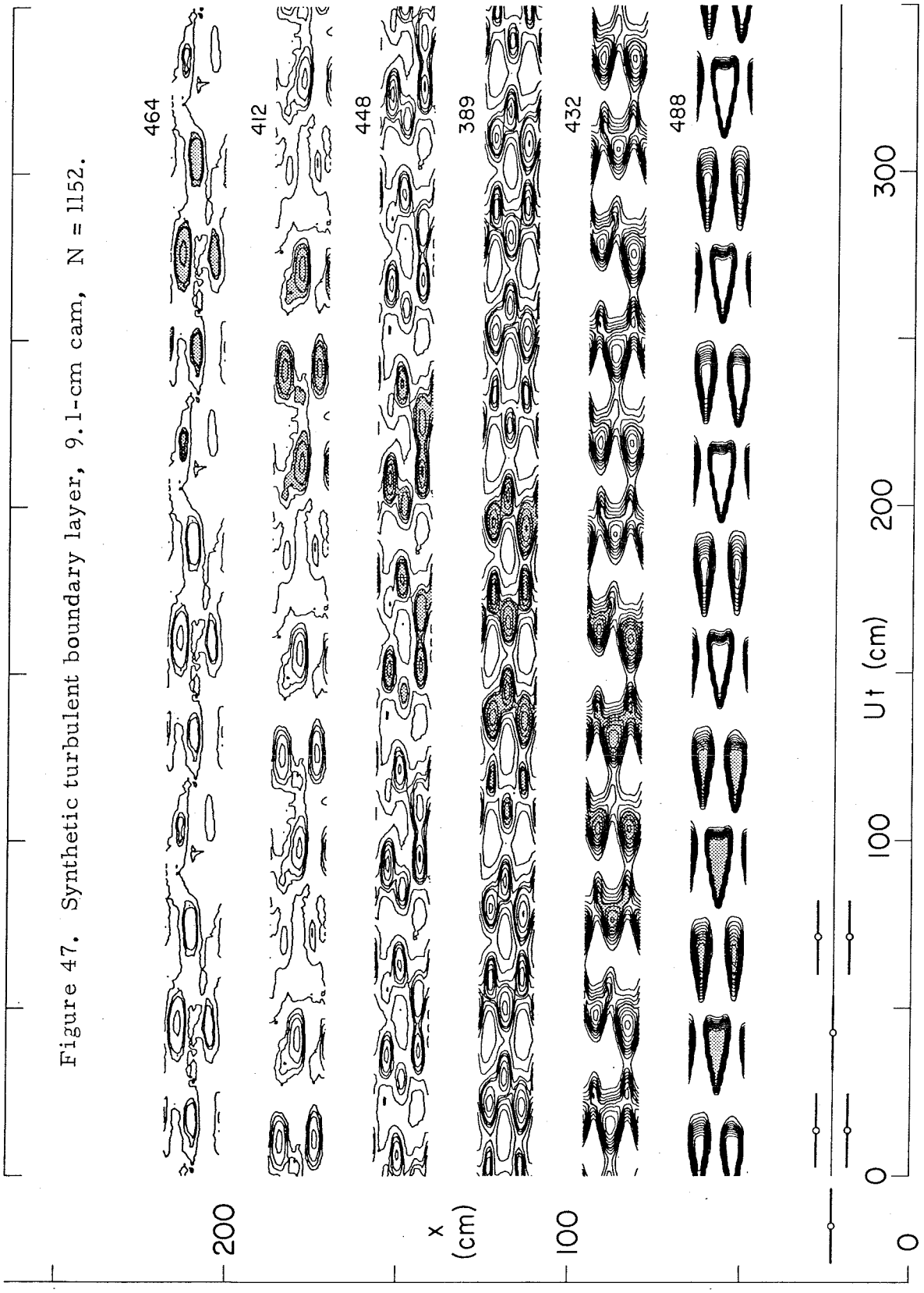

Figure 47. Synthetic turbulent boundary layer, 9.1-cm cam, N = 1152.

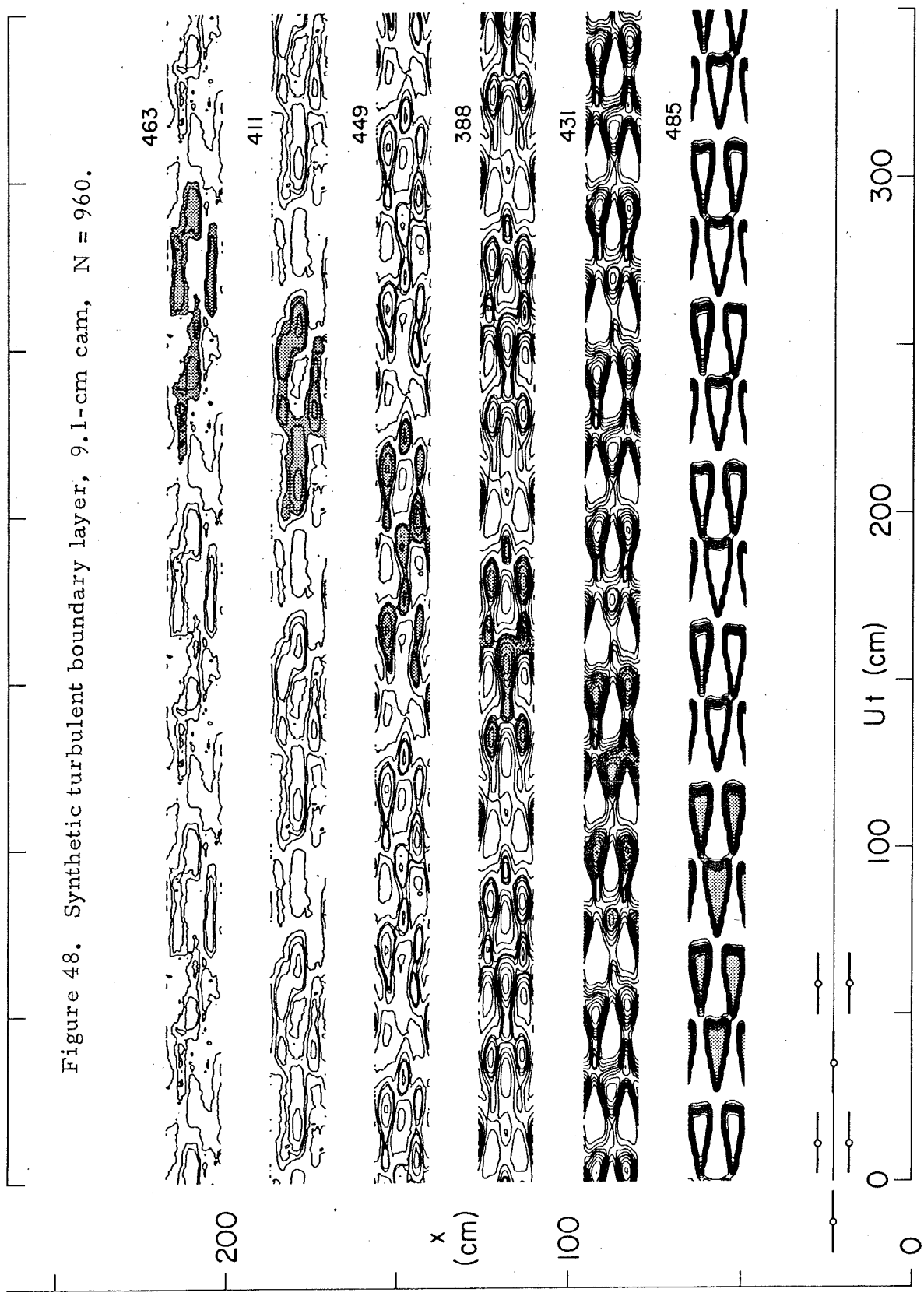

Figure 48. Synthetic turbulent boundary layer, 9.1-cm cam, N = 960.

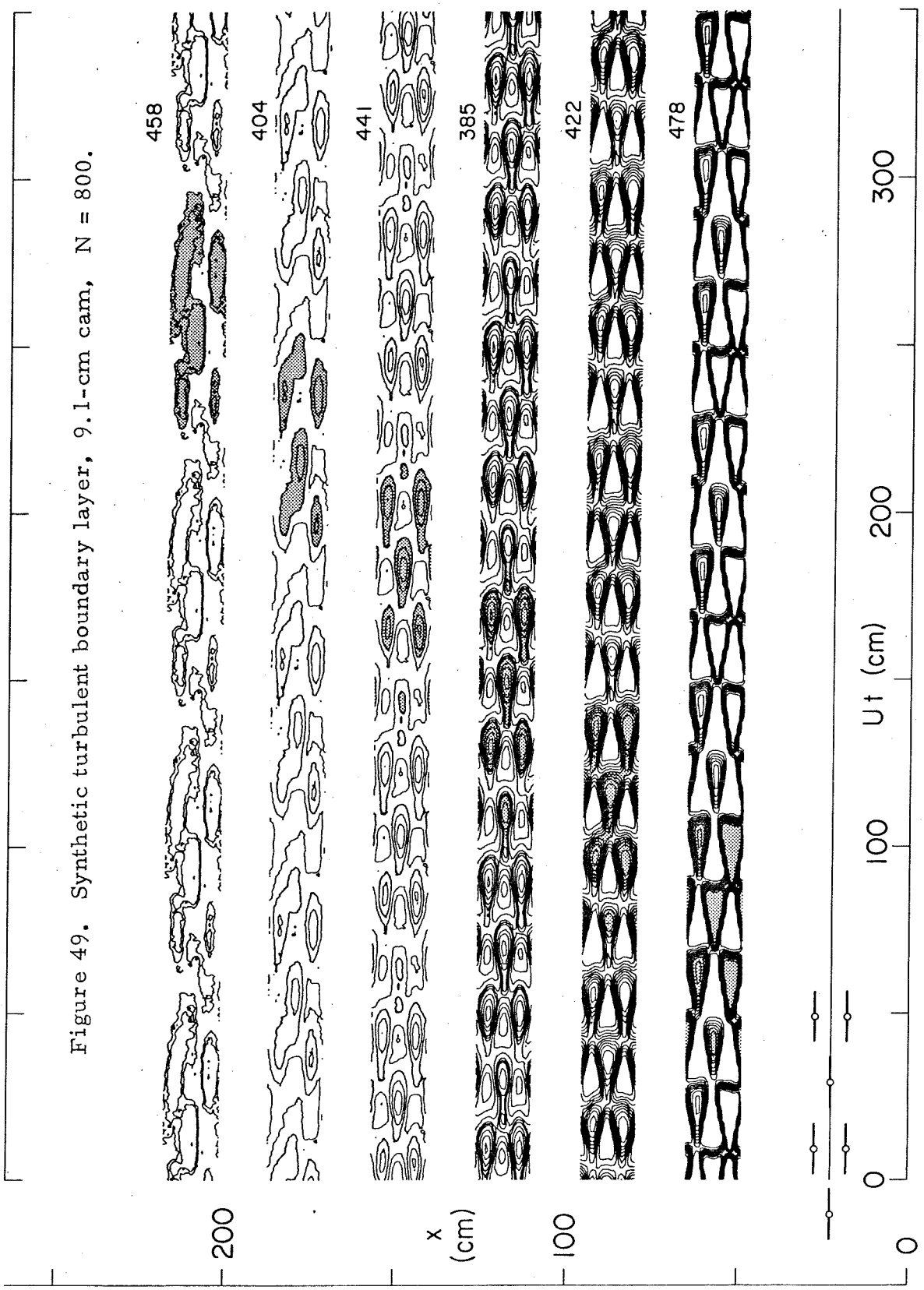

Figure 49. Synthetic turbulent boundary layer, 9.1-cm cam, N = 800.

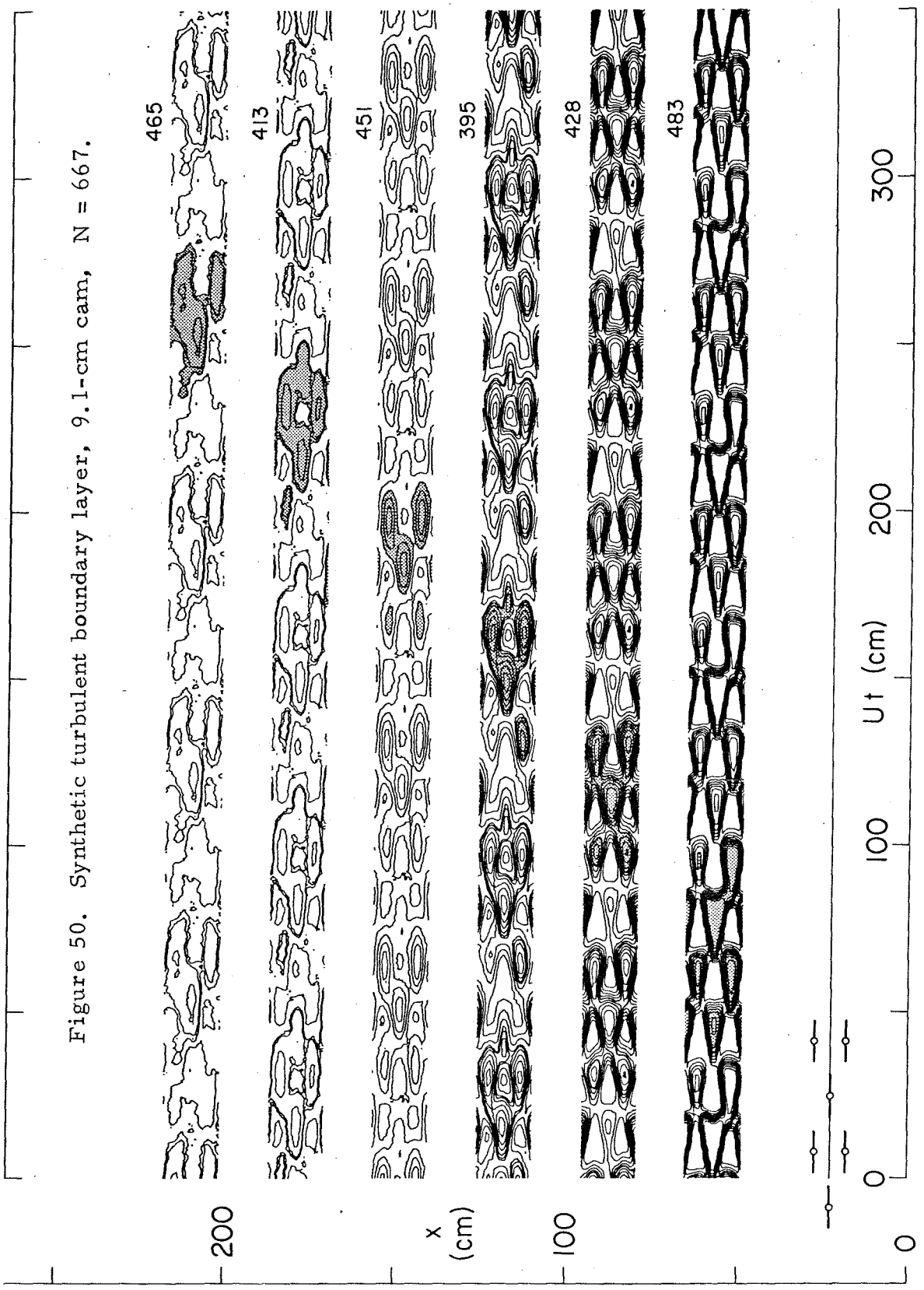

Figure 50. Synthetic turbulent boundary layer, 9.1-cm cam, N = 667.

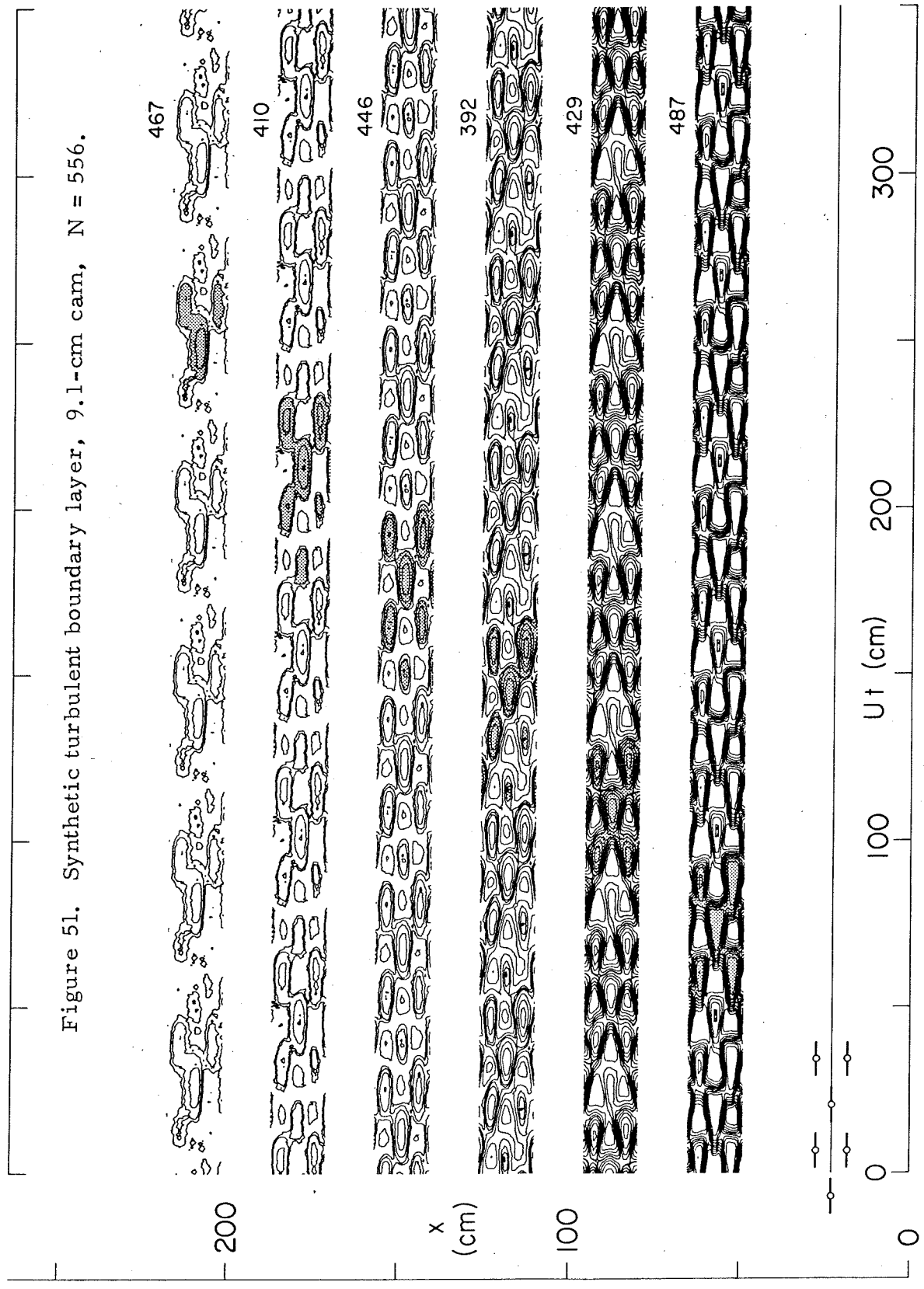

Figure 51. Synthetic turbulent boundary layer, 9.1-cm cam, N = 556.

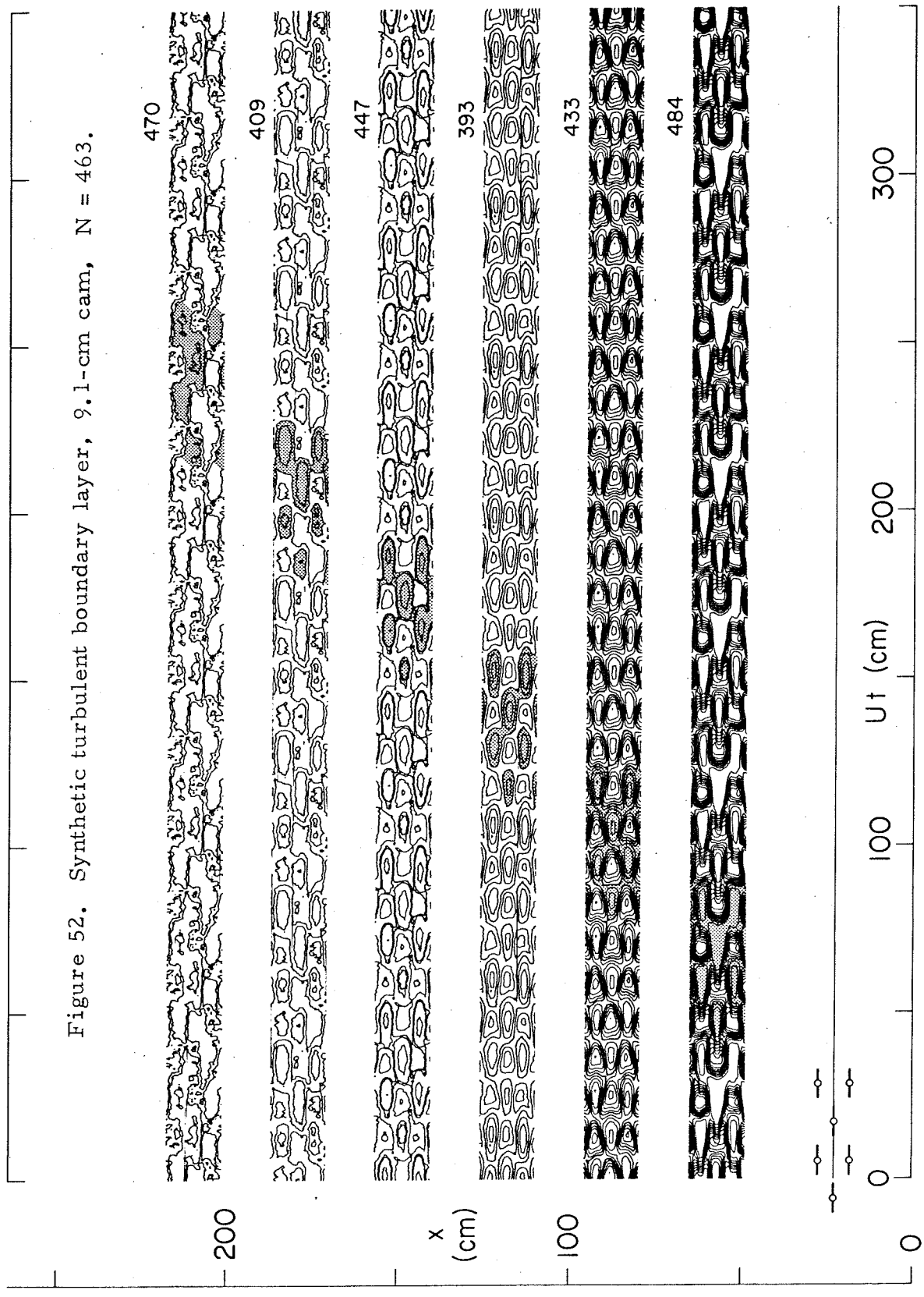

Figure 52. Synthetic turbulent boundary layer, 9.1-cm cam, N = 463.

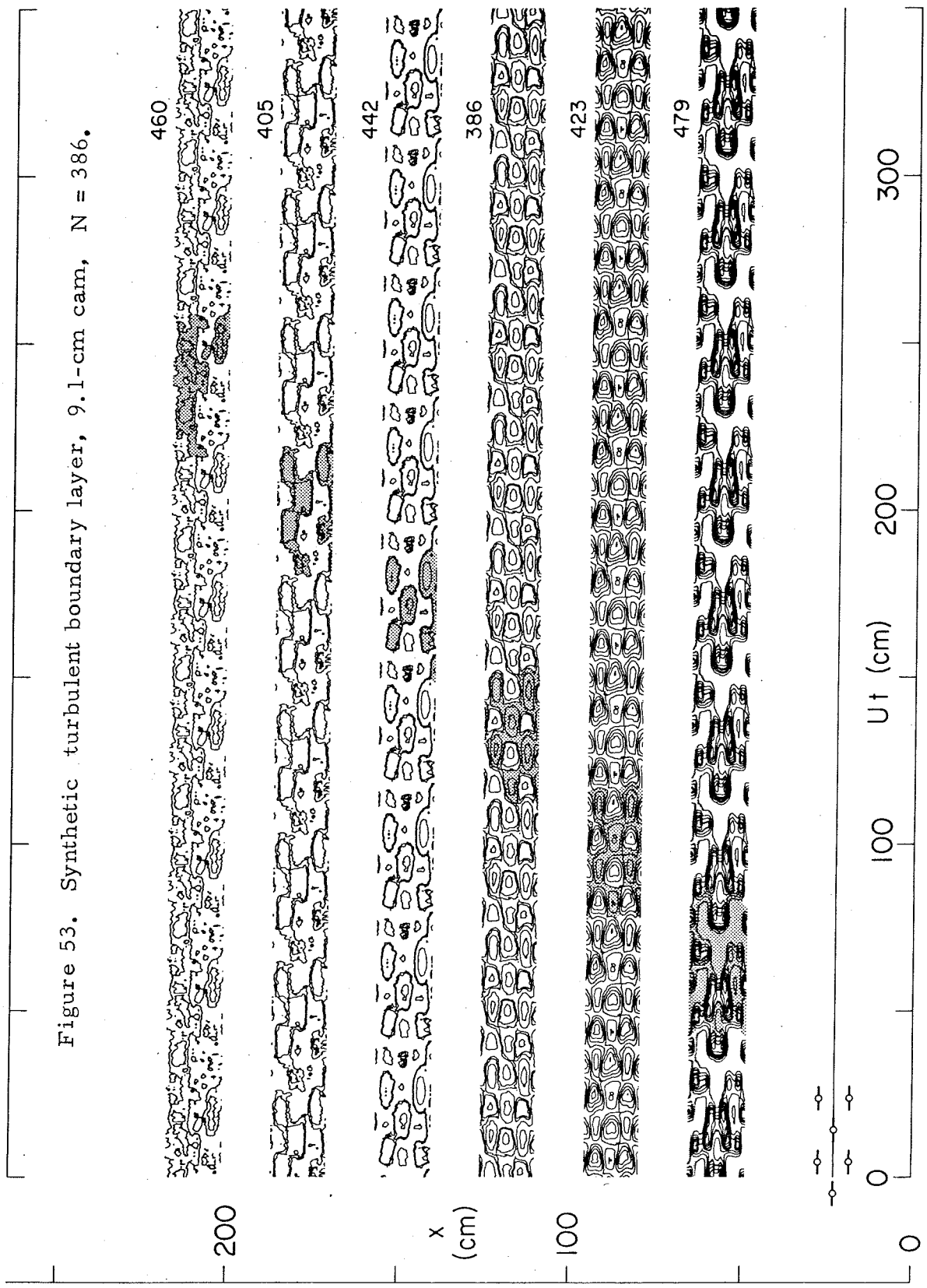

Figure 53. Synthetic turbulent boundary layer, 9.1-cm cam, N = 386.

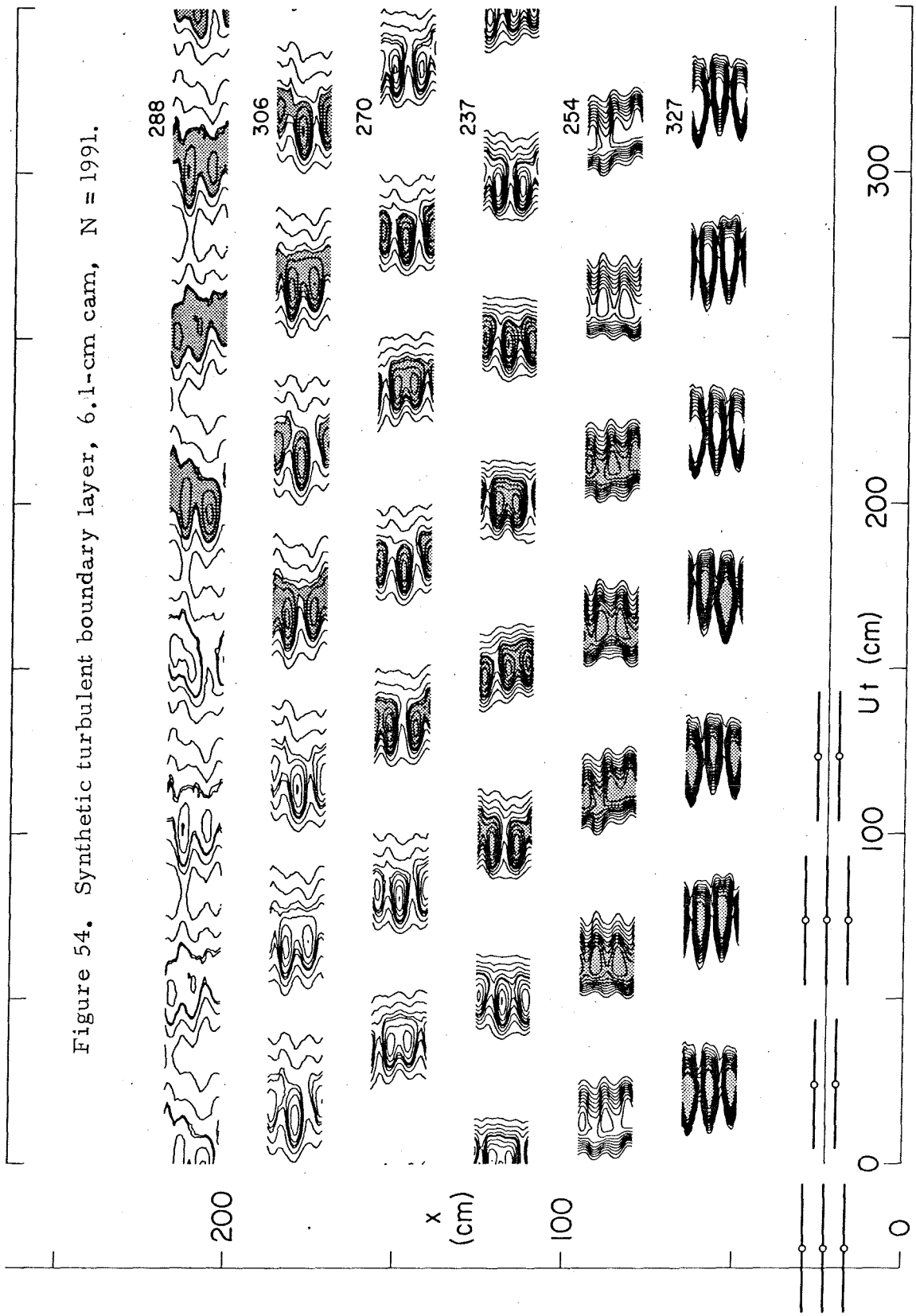

Figure 54. Synthetic turbulent boundary layer, 6.1-cm cam, N = 1991.

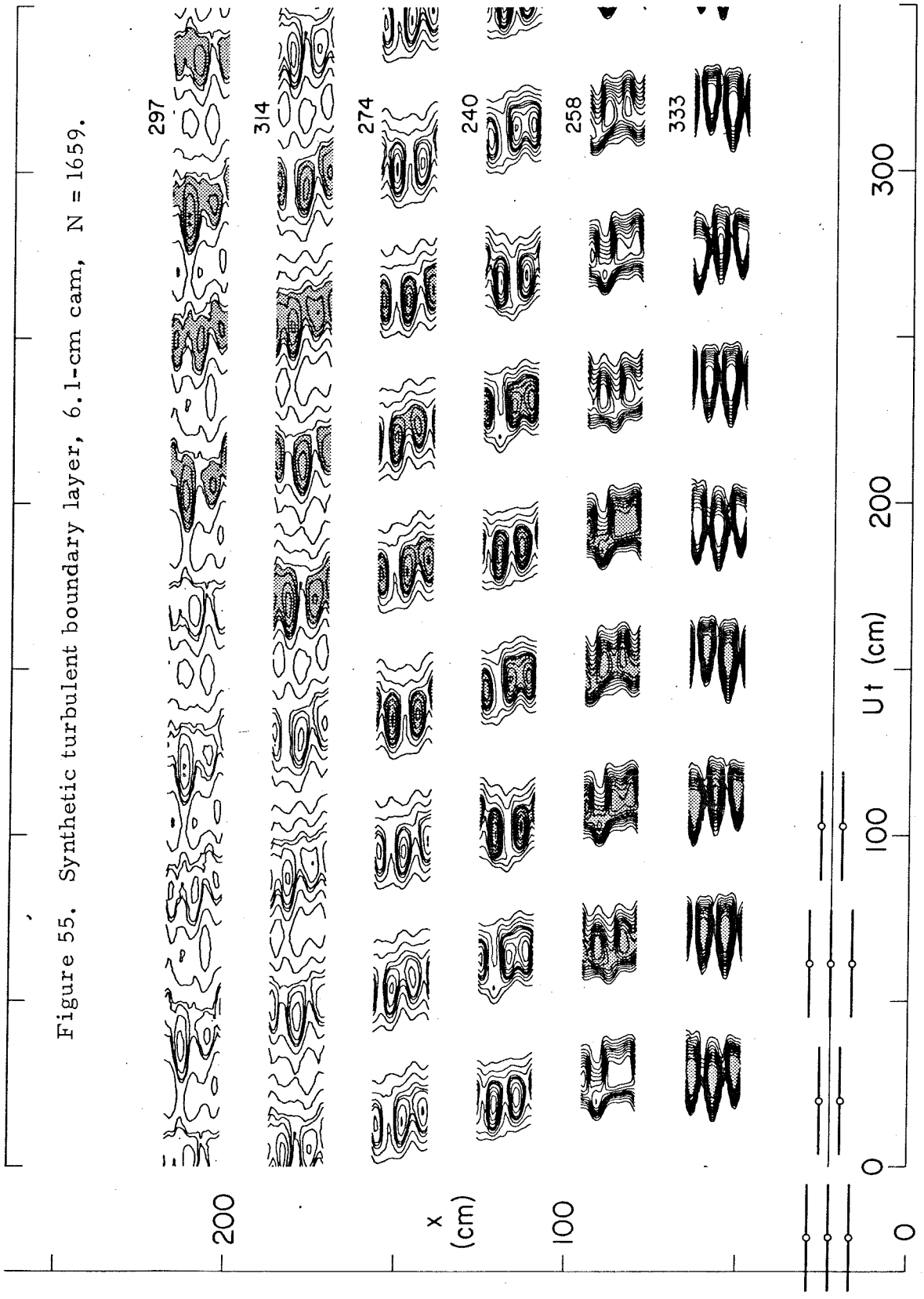

Figure 55. Synthetic turbulent boundary layer, 6.1-cm cam, N = 1659.

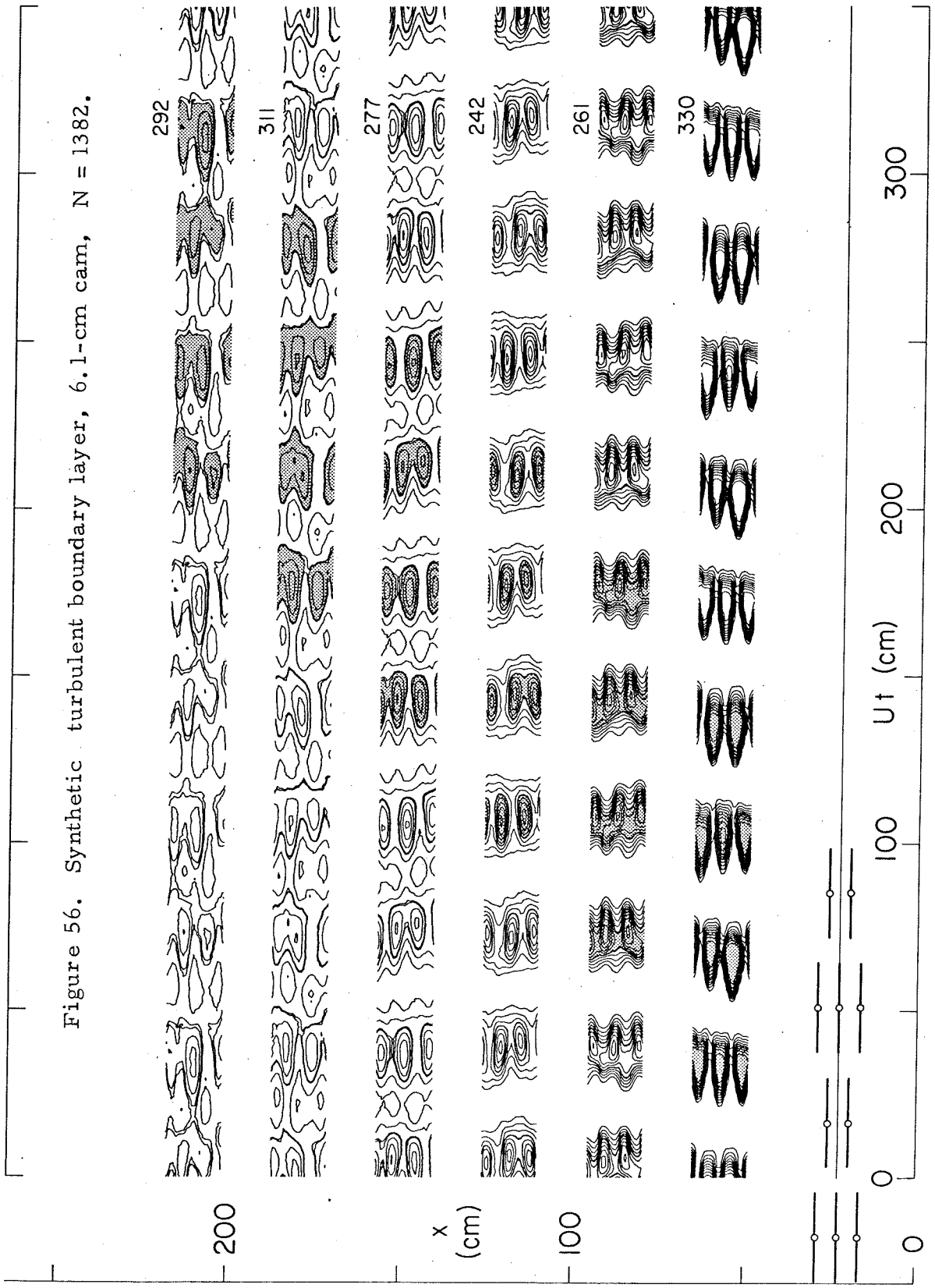

Figure 56. Synthetic turbulent boundary layer, 6.1-cm cam, N = 1382.

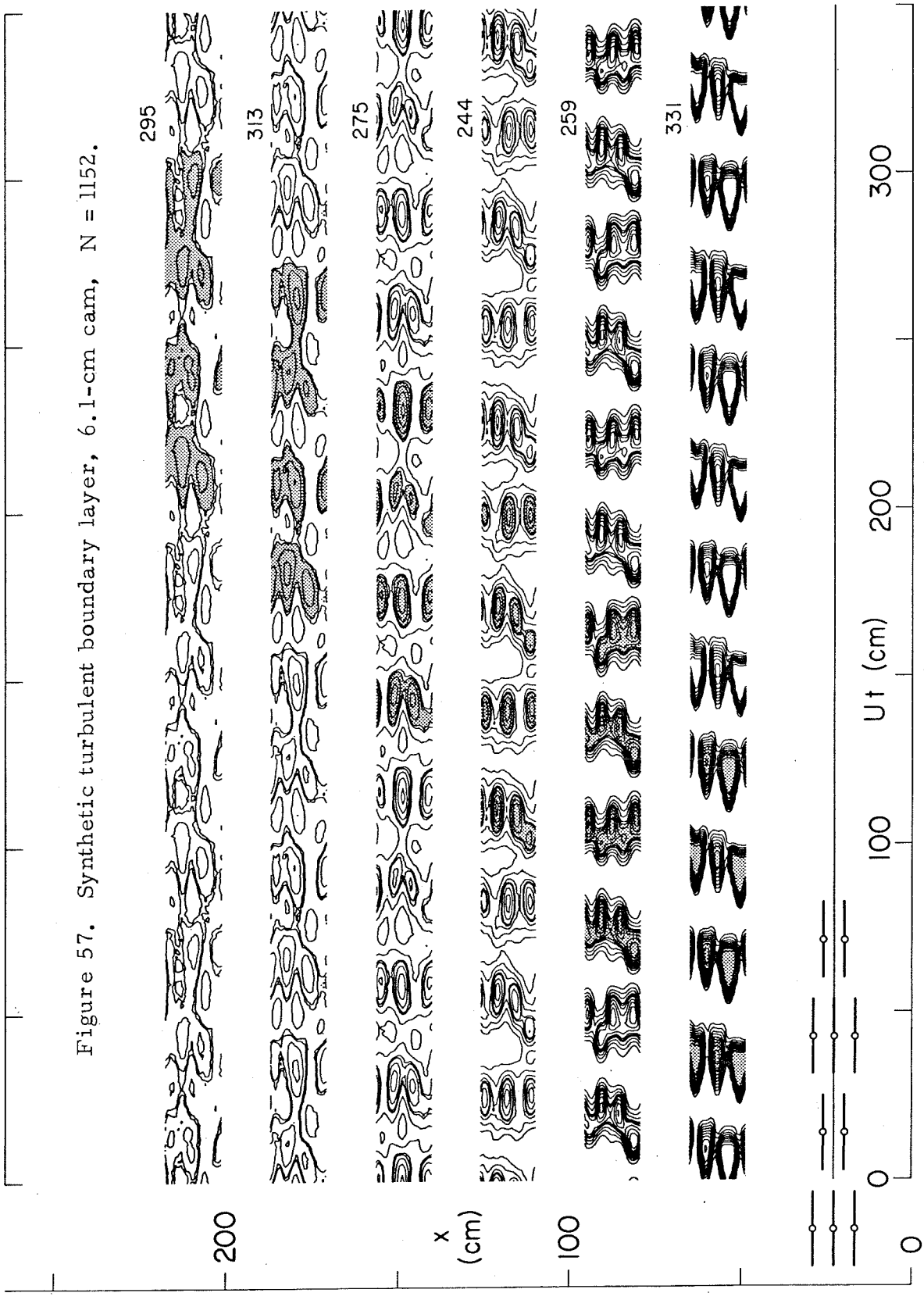

Figure 57. Synthetic turbulent boundary layer, 6.1-cm cam, N = 1152.

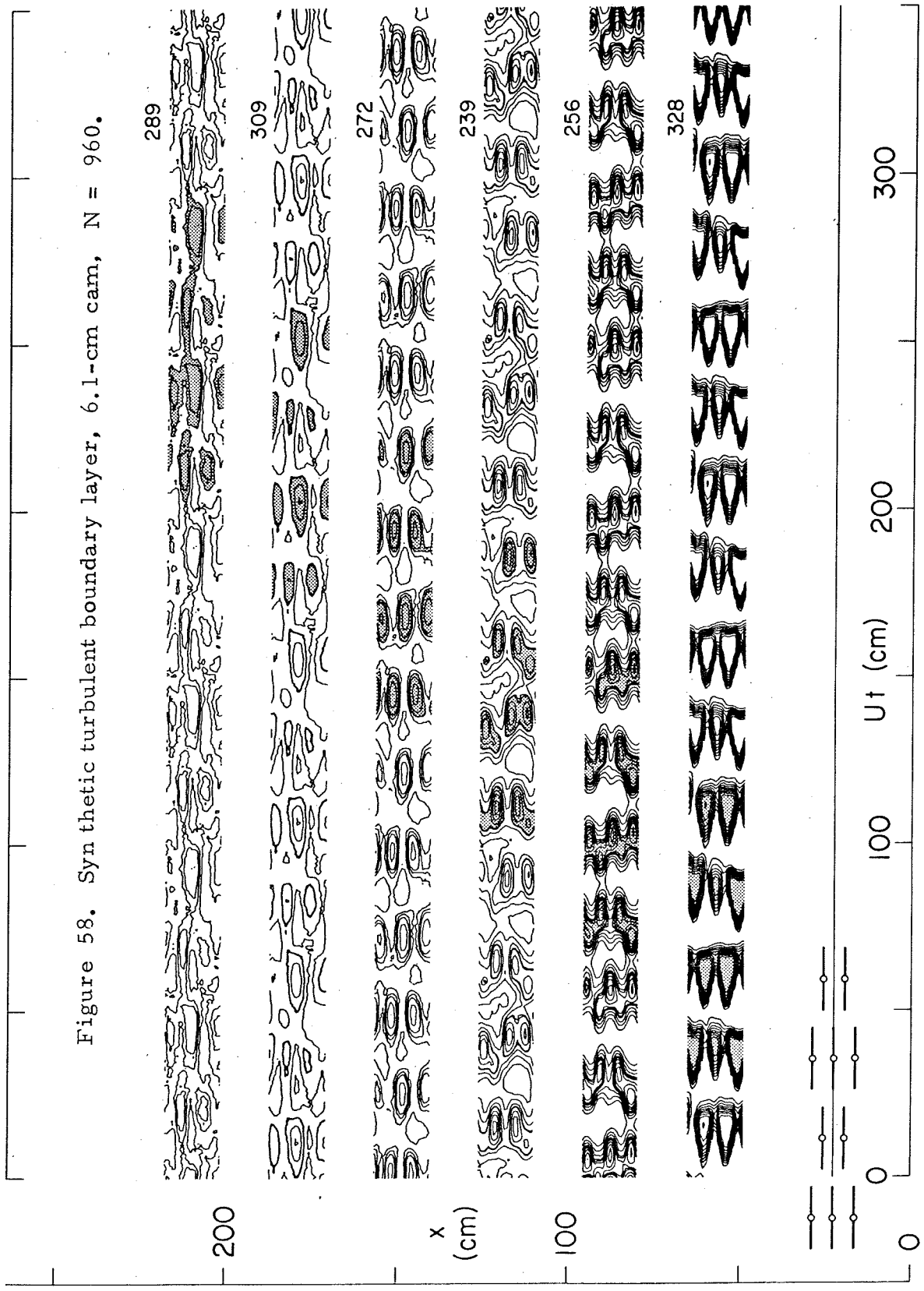

Figure 58. Syn thetic turbulent boundary layer, 6.1-cm cam, N = 960.

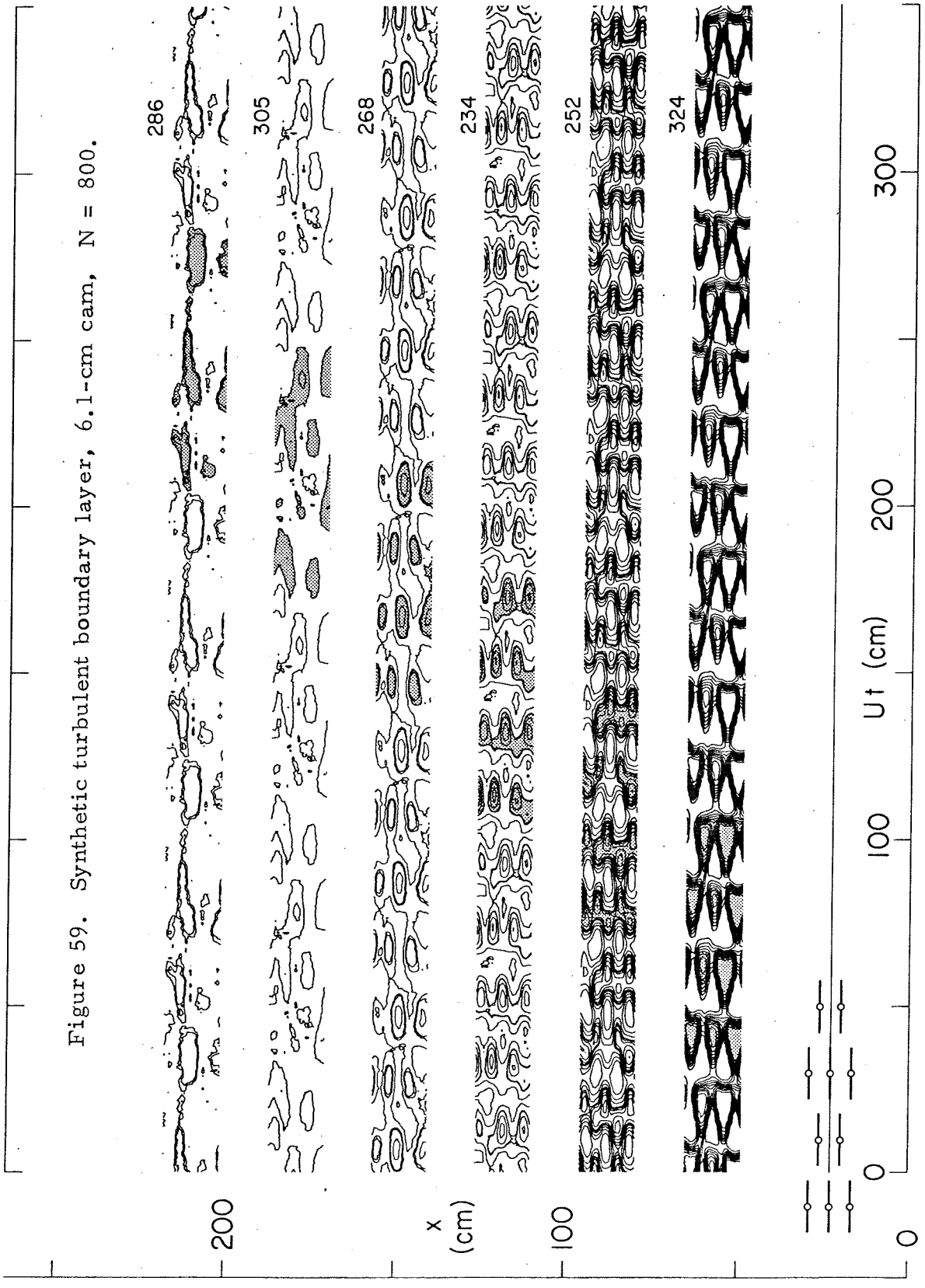

Figure 59. Synthetic turbulent boundary layer, 6.1-cm cam, N = 800.

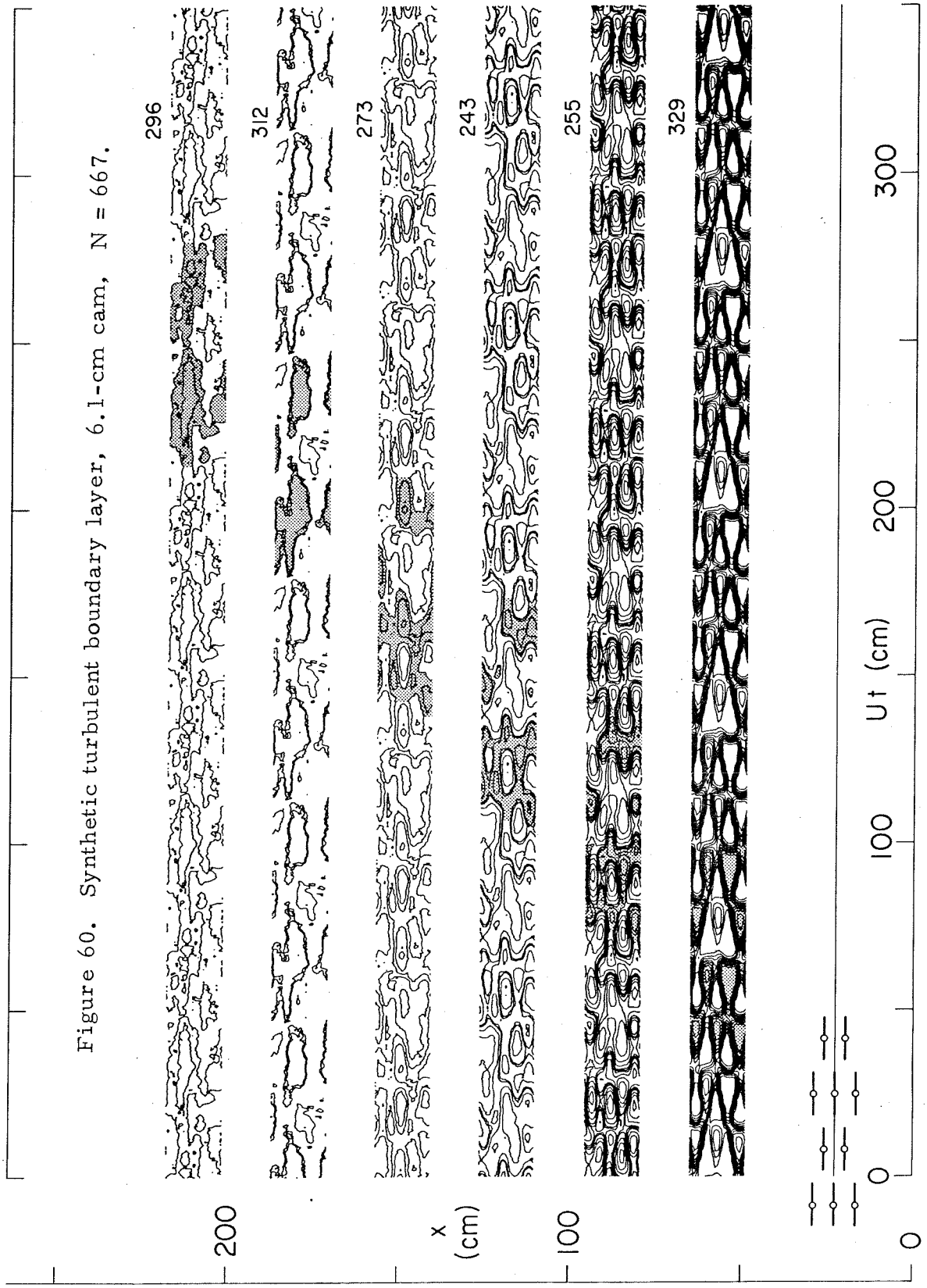

Figure 60. Synthetic turbulent boundary layer, 6.1-cm cam, N = 667.

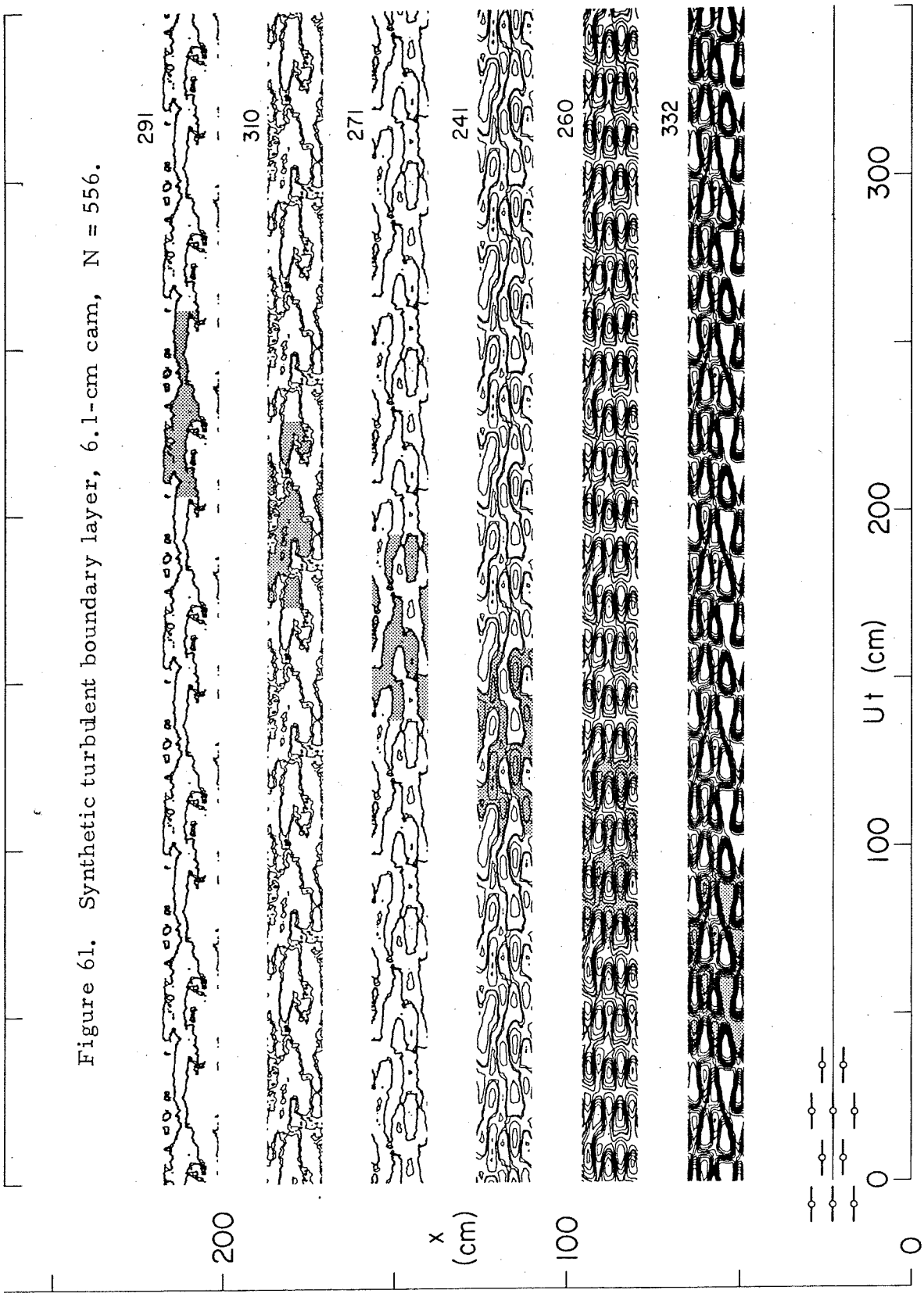

Figure 61. Synthetic turbulent boundary layer, 6.1-cm cam, N = 556.

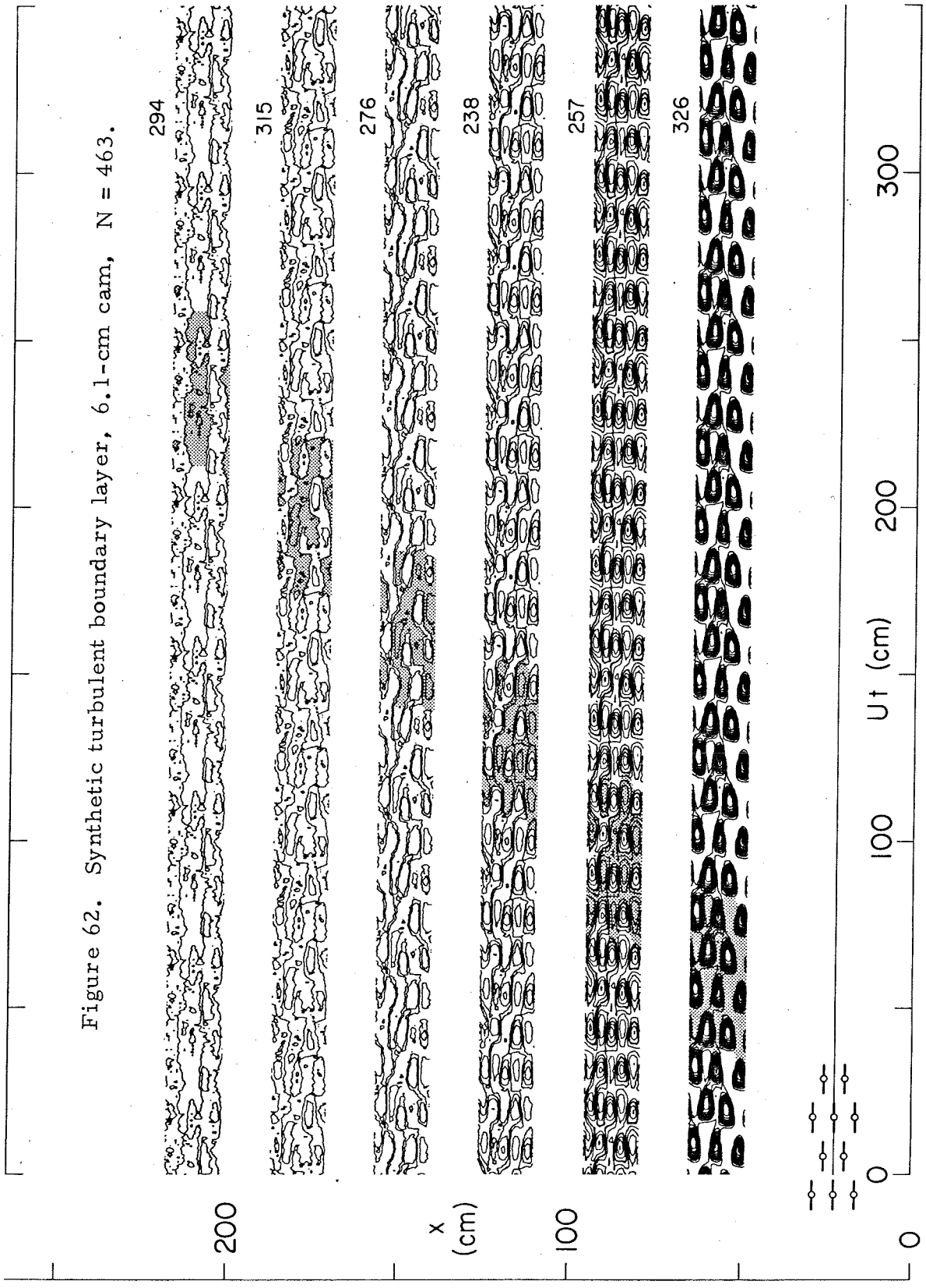

Figure 62. Synthetic turbulent boundary layer, 6.1-cm cam, N = 463.

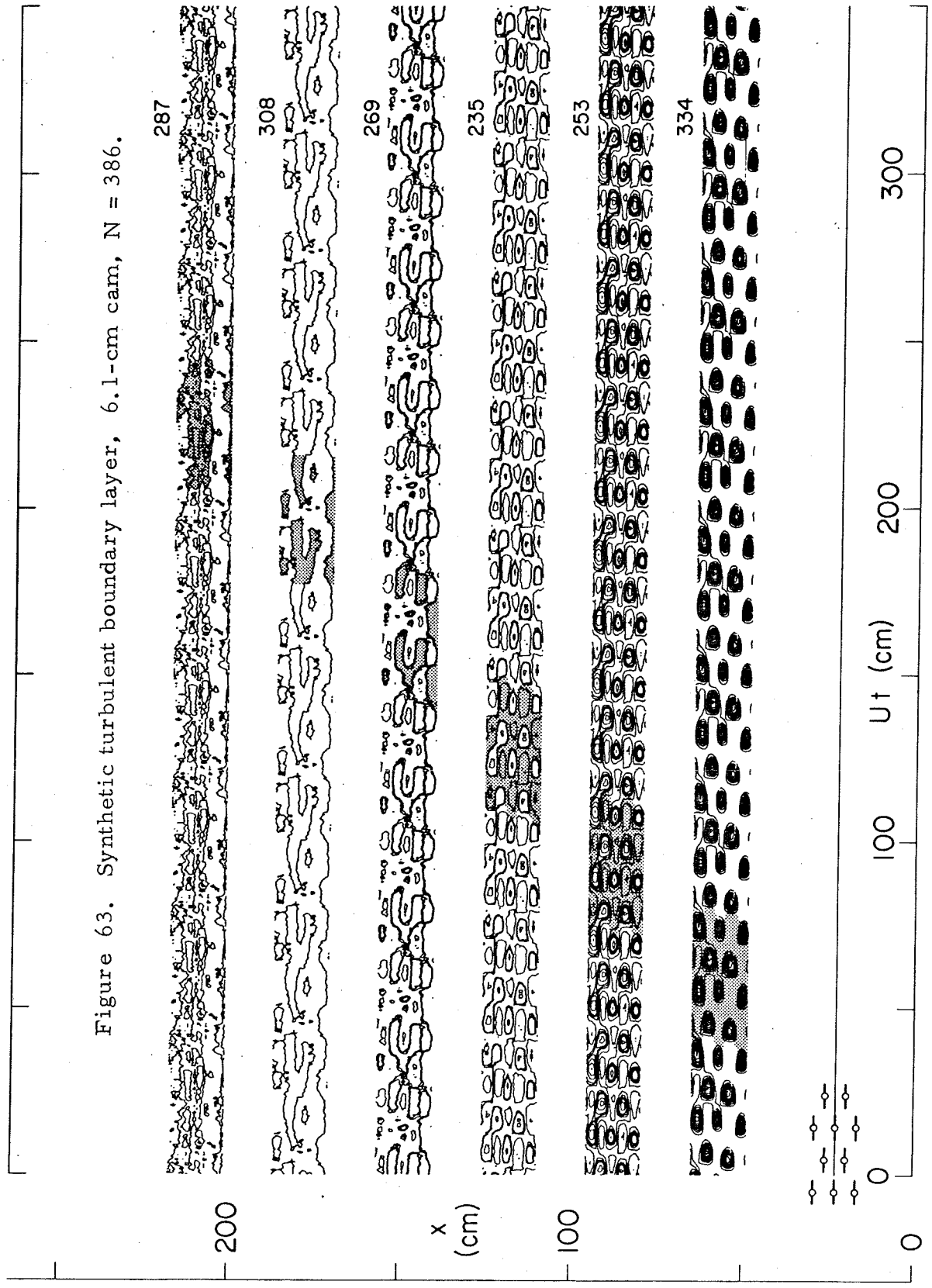

Figure 63. Synthetic turbulent boundary layer, 6.1-cm cam, N = 386.

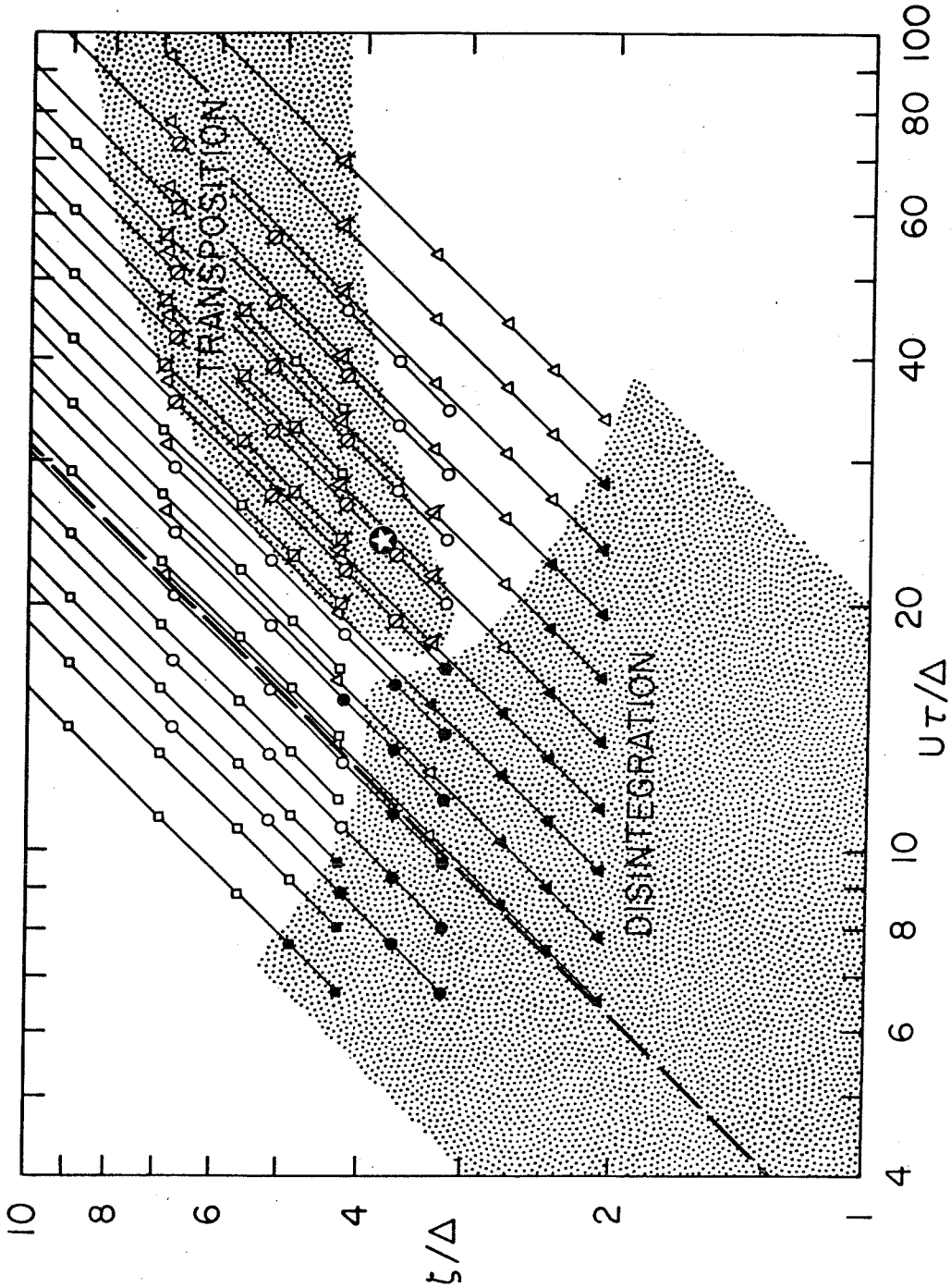

Figure 64. Coherence diagram for synthetic turbulent boundary layer. Open symbols: coherent pattern. Slashed symbols: transposition. Solid symbols: disintegration or loss of coherence. Squares: 12.2-cm cam. Circles: 9.1-cm cam. Triangles: 6.1-cm cam. Dashed line: $\zeta/u_\infty \tau = 0.32$. Star: flow studied by Coles and Barker.